

Di- and Mono- Phenyl Amine Based Sodium Channel Blockers
for the Treatment of Pain

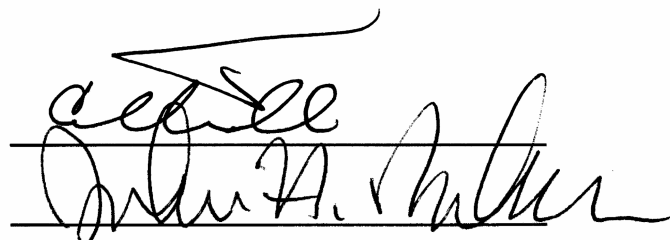
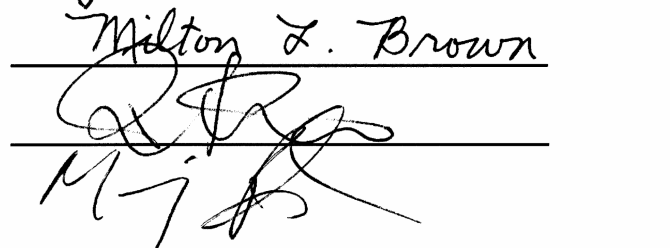
Debjani Patangia Hudgens
Little Rock, AR

B.S., University of Arkansas, 2000

A Dissertation presented to the Graduate Faculty
of the University of Virginia in Candidacy for the Degree of
Doctor of Philosophy

Department of Chemistry

University of Virginia
January, 2007


Milton Z. Brown


Acknowledgements

*I would like to thank the collaborative efforts of several groups who
have made this body of work possible.*

Chapters 2 & 3

All of the [³H]-BTX and [³H]-norepinephrine binding assays were conducted by Novascreen Biosciences, Inc. A great deal of thanks goes to the laboratory of Dr. Manoj K. Patel, particularly Catherine Taylor and Dr. Timothy Batts, for the electrophysiological work conducted on sodium channels. Merck, Division of Ion Channel Research, carried out all of the fluorescence based assay work in collaborative efforts with the Brown lab. The NIH screening program at NINDS was responsible for anticonvulsant and toxicity screening in animal models. I would also like to thank the work of Dr. Steve White's lab, particularly Misty Smith-Yockman, whose efforts in conjunction with NIH has provided for screening in animal models of inflammatory pain.

Chapter 5

I would like to thank my advisor, Dr. Milton Brown, for help with the CoMFA model and prediction of future analogues. All of the [³H]-BTX binding assays were conducted by Novascreen Biosciences, Inc. Electrophysiological screening in calcium channels was conducted in the laboratory of Dr. Yong Kim, with special thanks to Nathan Lewis and Maiko Sakai.

Chapter 6

I would also like to thank Dr. Howard Kutchai and Lisa Geddis for their studies on the Ca²⁺-ATPase activity in cardiac sarcoplasmic reticulum.

Table of Contents

Table of Contents	I
Index of Figures and Schemes	V
Index of Tables and Charts	VII
Abstract	IX
Chapter 1	
Introduction to Sodium Channels	
1.1 The Voltage Gated Sodium Channel (VGSC)	
1.1.1 Structure and Isoforms	1
1.1.2 Function and Channel States	5
1.1.3 Relationship of Structure and Function	7
1.1.4 Binding Sites, Neurotoxin and Local Anesthetic	8
1.2 VGSC and Pain	
1.2.1 Pain Types and Incidence	13
1.2.2 Expression of VGSC in Pain	15
1.2.3 VGSC in Pain Therapeutics	18
1.3 References	20
Chapter 2	
Discovery of Diphenyl Amine Based Sodium Channel Blockers	
2.1 Neuropathic Pain Therapeutics	
2.1.1 Current Therapeutics for Neuropathic Pain	26
2.1.2 Tricyclic Antidepressants as Treatment	29
2.2 Design and Synthesis	
2.2.1 Three Sites of Modification	32
2.2.2 Site 1, Phenyl Ring Modification	32
2.2.3 Site 2, Phenyl Ring Replacement	33
2.2.4 Site 3, Amine Isosteres	34

2.2.5 Optimization of Diphenyl Lead	36
2.3 Results	
2.3.1 Binding Assay	37
2.3.2 Electrophysiological Analysis	41
2.3.3 Fluorescence Based Assay	45
2.3.4 Animal Model of Anticonvulsant Activity	48
2.4 Discussion	50
2.5 Conclusion	53
2.6 Experimental Section	
2.6.1 Chemistry	54
2.6.2 Biology	71
2.7 References	73
Chapter 3	
Second Generation Monophenyl Amines as Anti-Inflammatory Agents	
3.1 Previous Investigations	
3.1.1 Comprehensive Structure Activity Relationship	78
3.1.2 Comparative Molecular Field Analysis Studies	79
3.2 Design	80
3.3 Synthesis and [³ H]-BTX Data	
3.3.1 General Synthetic Methods	81
3.3.2 Chain Length Modification	83
3.3.3 Heterocycle Isosteres	84
3.3.4 Optimization of Monophenyl Lead	85
3.4 Results	
3.4.1 IC ₅₀ of Lead Monophenyl Analogue	87
3.4.2 Functional Block	88
3.4.3 FRET Based Assay	90
3.4.4 Animal Model of Inflammatory Pain	91
3.4.5 Norepinephrine Transport	93
3.5 Discussion and Conclusion	

3.5.1 Discussion	94
3.5.2 Conclusion	96
3.6 Experimental Section	
3.6.1 Chemistry	97
3.6.2 Biology	119
3.7 References	122

Chapter 4

Introduction to Calcium Channels

4.1 The Voltage Gated Calcium Channel (VGCC)	
4.1.1 Structure	123
4.1.2 Subtypes	125
4.1.3 Function	126
4.1.4 Antagonists and Binding Sites	128
4.2 References	130

Chapter 5

Dual Calcium/Sodium Channel Blocker Derived from a Verapamil Scaffold

5.1 Calcium Antagonists and Therapeutic Use	
5.1.1 Verapamil	132
5.1.2 Clinical Relevance of Dual Inhibitors	133
5.2 Design and Synthesis	134
5.3 Results	
5.3.1 Binding Assay	137
5.3.2 Electrophysiological Methods	138
5.4 Discussion	142
5.5 Conclusion	143
5.6 Experimental Section	
5.6.1 Molecular Modeling	144
5.6.2 Chemistry	146
5.6.3 Biology	150
5.7 References	153

Chapter 6**Agonists of Calcium-ATPase Activity**

6.1 Ca^{2+} -ATPase Pump	
6.1.1 Structure and Function	156
6.1.2 Stimulants of Activity	157
6.2 Design and Synthesis	158
6.3 Results	160
6.4 Discussion and Conclusion	
6.4.1 Discussion	161
6.4.2 Conclusion	162
6.5 Experimental Section	
6.5.1 Chemistry	162
6.5.2 Biology	165
6.6 References	166

Figures and Schemes

Figure 1-1 Structural Overview of the VGSC	2
Figure 1-2 IFM Motif of the Inactivation Loop	3
Figure 1-3 Inner Pore of the VGSC	4
Figure 1-4 Action Potential of a Neuron	6
Figure 1-5 States of Sodium Channel Gating	7
Figure 1-6 Neurotoxin Binding Sites	11
Figure 1-7 Local Anesthetic Binding Site	12
Figure 1-8 Structure of a Neuron	16
Figure 1-9 Location of the Dorsal Root Ganglion	17
Figure 2-1 Neuropathic Pain Therapeutics	27
Figure 2-2 Class of Tricyclic Antidepressants	29
Figure 2-3 Major Sites of Scaffold Modification	32
Scheme 2-1 Modification at Site 1, Phenyl Ring Orientation	33
Scheme 2-2 Modification at Site 2, Phenyl Replacement	34
Scheme 2-3 Modification at Site 3, Amine Isosteres	35
Scheme 2-4 Optimization of Lead Compound (2.6)	36
Figure 2-4 Structure of Batrachotoxin and Tritiated Analogue	37
Figure 2-5 [³ H]-BTX Displacement Assay	38
Figure 2-6 Patch Clamp Electrophysiology	41
Figure 2-7 Comparing Sample Current Traces of Amitriptyline and Compound (2.6)	44
Figure 2-8 FRET Based Assay for Determining Membrane Potential	45

Figure 3-1 Previous CoMFA Studies of the VGSC	80
Figure 3-2 Design and Strategies	81
Scheme 3-1 General Synthetic Pathways	82
Figure 3-3 Dose Response Curve for Functional Block of hNa _v 1.2	90
Figure 4-1 Structural Overview of the VGCC	123
Figure 4-2 Ball and Chain Model of Inactivation	126
Figure 4-3 Three Drug Classes of the VGCCs	127
Figure 4-4 Binding Sites of VGCC Antagonists	128
Figure 5-1 Electrostatic and Steric CoMFA Fields	133
Figure 5-2 Potential Sodium Channel Blockers Based on Previous CoMFA	134
Scheme 5-1 α -Hydroxy Amide and Hydantoin Analogues of Verapamil	135
Figure 5-3 Test Set Analogues Used in CoMFA Model	143
Figure 6-1 Mechanism of Ca ²⁺ -ATPase Function	156
Figure 6-2 Structure of Gingerol	156
Figure 6-3 Agonists of Calcium-ATPase Activity	157
Scheme 6-1 Synthesis of Agonists of Ca ²⁺ -ATPase Activity	158

Tables and Charts

Table 1-1 Voltage Gated Sodium Channel Isoforms	5
Table 1-2 Neurotoxin and Insecticide Binding Sites of the Voltage Gated Sodium Channel	9
Table 1-3 Sodium Channel Blockers as Therapeutics	12
Table 2-1 Inhibition of [3H]-BTX Binding to Brain Vesicular Preparations	30
Table 2-2 [3H]-BTX Displacement of Analogues	39
Table 2-3 Optimization of Lead Compound (2.6)	40
Table 2-4 Percent Block of hNa _v 1.2 Current at 10 μ M	42
Table 2-5 Inhibition Based of FRET Modified Assay	47
Table 2-6 Phase I Rat Anticonvulsant Data	50
Chart 2-1 Functional Block of hNa _v 1.2 upon Compound Administration	52
Table 3-1 Chain Length Optimization	83
Table 3-2 Heterocyclic Isosteres of Compound (3.4)	85
Table 3-3 Optimization of Compound (3.4)	86
Table 3-4 IC ₅₀ of Lead Monophenyl Analogue	87
Table 3-5 Percent Block of hNa _v 1.2 Current at 10 μ M	88
Table 3-6 Inhibition Based on FRET Modified Assay	91
Chart 3-1 Effects of (3.4) in Animal Models of Inflammatory Pain	92
Table 3-7 [3H]-Norepinephrine Binding Displacement	93
Chart 3-2 Norepinephrine Activity and Chain Length	94
Table 4-1 Subtypes of the VGCCs	124
Table 5-1 Predicted and Actual NVGSC Activity of Verapamil Analogues	136

Chart 5-1 Effects of Verapamil on P/Q-Type VGCCs	137
Chart 5-2 Effects of Verapamil on N-Type VGCCs	138
Chart 5-3 Effects of Verapamil on L-type VGCCs	138
Chart 5-4 Effects on (5.5) on P/Q-Type VGCCs	139
Chart 5-5 Effects on (5.5) on N-Type VGCCs	140
Chart 5-6 Effects on (5.5) on L-Type VGCCs	141

Abstract

Ion channels play a major role in the cellular signaling and control processes required within living systems. The voltage gated sodium channel (VGSC) belongs to this superfamily of ion channels and is known to have a critical function in electrically excitable cells, such as those found in neuronal, muscular and cardiac tissue. Ectopic firing of action potentials within neuronal systems can result in chronic pain syndromes, such as neuropathic pain. Therefore, VGSCs are central to the development of pain therapeutics.

Tricyclic antidepressants (TCAs), such as amitriptyline, serve as the best treatment of neuropathic pain syndromes, to date and are thought to function by potently blocking sodium channel current. Although TCAs have wide therapeutic use, they do suffer from some adverse side effects which have led to patient withdrawal. We have therefore chosen to develop novel compounds from an amitriptyline scaffold, in order to obtain a more well tolerated and potent therapeutic. From our investigations, we have been able to identify two potent classes of amitriptyline analogues, which are di- and mono- phenyl amine. We have also determined that the tricyclic moiety is unnecessary for effective inhibition of both channel binding and sodium currents of hNa_v1.2. Additionally, modification to the amine functionality has been found to be detrimental to block. Thus far, our most potent compound containing a monophenyl amine structure provides 94.6% functional block of sodium channels at 10 μ M, which is a three-fold increase in current block in comparison to amitriptyline. Further evaluation of this analogue in animal models of inflammatory pain has shown promising results.

Chapter 1

Introduction to Sodium Channels

Voltage gated sodium channels (VGSCs) are ubiquitous to mammalian systems and are essential for proper cellular signaling and control processes, particularly in cardiac and nerve function. The VGSC is an integral membrane protein which selectively allows for flux of Na^+ ions from one side of the membrane to the other and functions by utilizing an electrochemical gradient. Separation of the extracellular and cytoplasmic contents by the plasma membrane allows for divergent ionic concentrations, thereby creating an electrical potential difference. Activation of the sodium channel occurs and allows a flux of sodium ions for a period of a few to hundreds of milliseconds, thereby relieving this potential. This phenomenon occurs repeatedly in order to transmit crucial information within living systems.

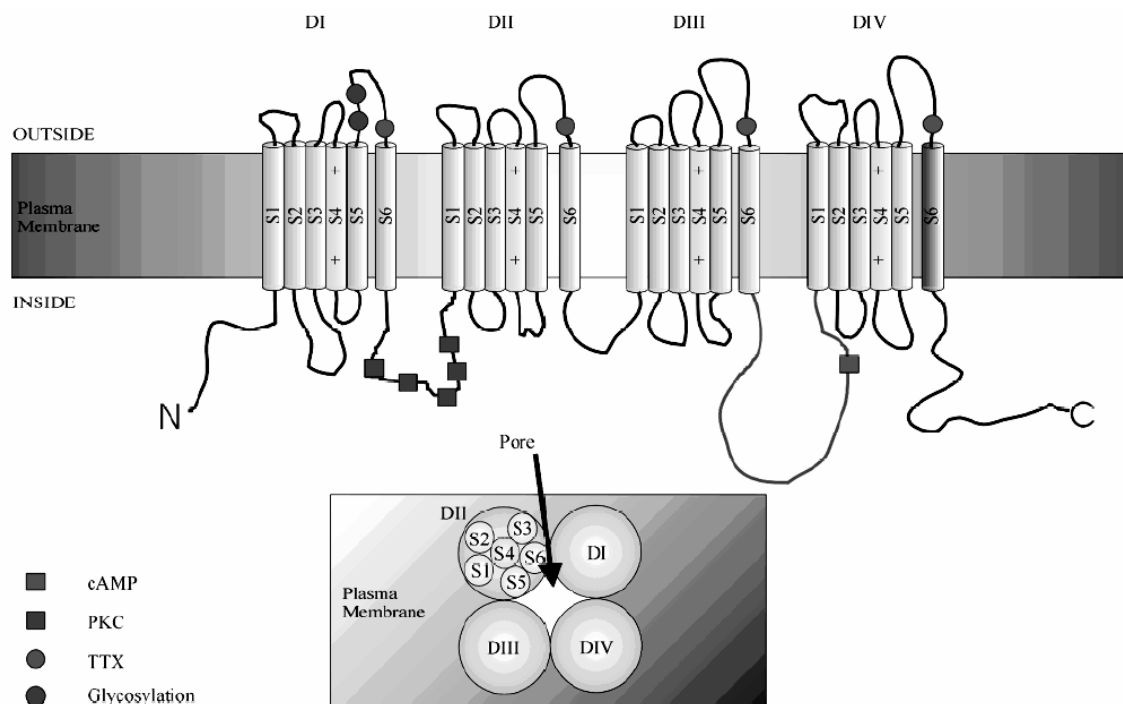
1.1 The Voltage Gated Sodium Channel (VGSC)

1.1.1 Structure and Isoforms

Early biochemical experiments utilizing radio-labelled toxins have identified the major component of sodium channels, isolated from rat brain, to be a 260 kDa α subunit.¹ This α subunit is accompanied by auxiliary $\beta 1$ - $\beta 4$ subunits which are approximately 30-40 kDa, thereby forming a heteromeric protein complex. Studies have shown that depletion of the $\beta 2$ subunit has no apparent effect on function of the sodium channel, whereas removal of the $\beta 1$ subunit results in loss of all functional properties.² It has since then been determined that the $\beta 1$ subunit is essential in maintaining the appropriate kinetics and voltage-dependence of the gating process.³

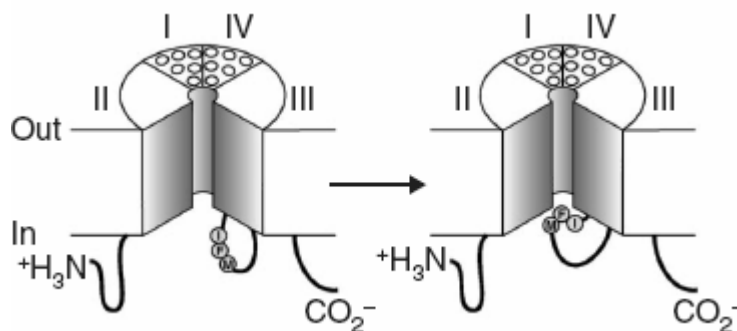
However, the α subunit alone contains all the key pharmacological and physiological properties of the channel, with all known drug interactions occurring within this site.⁴ Based on sequence data, it has been predicted that the α subunit consists of four homologous domains (I-IV), each with six transmembrane segments (S1-S6) (Figure 1-1).⁵ These domains orient in a manner allowing for formation of a central pore, with the S5 and S6 segments permeating the central lining. Intracellular and extracellular loops connect the domains and contain multiple receptor sites for ligand binding. Within each domain, the fourth segment contains a highly conserved region of positively charged arginine or lysine residues, which is thought to behave as the channel's voltage sensor.

Figure 1-1 Structural Overview of the VGSC



To date, no three-dimensional structure of the sodium channel has been obtained, which is due to both the size and hydrophobic nature of the protein. However some limited information has been obtained through NMR analysis, such as identification of an inactivation loop, located between S6 of D(III) and S1 of D(IV), that is responsible for inactivating the channel upon opening.⁶ Solution structure analysis depicts a rigid α helical structure, followed by two twists, that lead to a specifically positioned hydrophobic region of isoleucine-phenylalanine-methionine (IFM). In the hinged lid model of inactivation, the IFM residues of the inactivation loop are able to swing inward thereby placing phenylalanine in occlusion of the ion pore (Figure 1-2).⁷

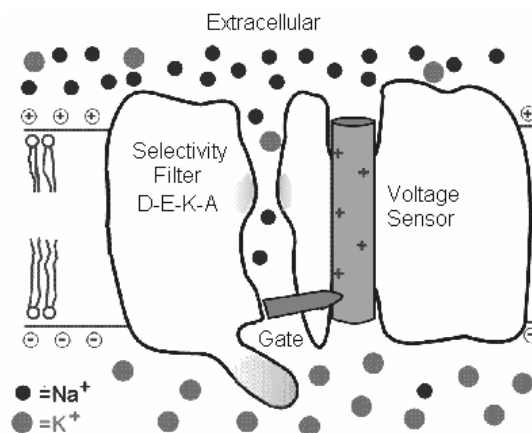
Figure 1-2 IFM Motif of the Inactivation Loop



Permeation studies have also been conducted to predict the channel's relative cross-sectional size,⁸ which was later corroborated by molecular modeling techniques.⁹ The ion pore is believed to contain a large aqueous cavity with a gate towards the interior of the cell and a selectivity filter, comprised of reentrant loops between S5 and S6 that are embedded in the transmembrane region (Figure 1-3). The mouth of the channel is 1.2 nm followed by a narrowing to 0.3-0.5 nm, which corresponds to the selectivity filter.

The narrowest portion of this filter is marked by a conserved sequence of amino acid residues that follow, aspartic acid-glycine-lysine-alanine (DEKA).

Figure 1-3 Inner pore of the VGSC



Nine α subunits ($\text{Na}_v1.1$ - $\text{Na}_v1.9$) have been characterized within mammalian systems and a tenth possible subtype, Na_x may also exist. Expression of each isoform is regulated in a tissue-specific manner (Table 1-1), with variations occurring during separate developmental stages.¹⁰ All isoforms show at least 50% conservation of their amino acid sequence.¹¹ From an evolutionary perspective, each subunit can be classified into one of four groups based upon the chromosomal segment to which they map.^{12,13} The following list corresponds to each subtype's classification: $\text{Na}_v1.1$, $\text{Na}_v1.2$, $\text{Na}_v1.3$, and $\text{Na}_v1.7$ map to chromosome 2; $\text{Na}_v1.5$, $\text{Na}_v1.8$, and $\text{Na}_v1.9$ map to chromosome 3; $\text{Na}_v1.4$ maps to chromosome 11; $\text{Na}_v1.6$ maps to chromosome 15. Characterization of each isoform can also be assessed, in part by their sensitivity to tetrodotoxin (TTX). Interestingly, alteration of a single amino acid residue of the α -subunit can create substantial difference in levels of TTX sensitivity. For instance, $\text{Na}_v1.5$ undergoes a 200-fold decrease in sensitivity to TTX, in comparison to the chromosome 2 subfamily, when

a phenylalanine residue is converted to cysteine.¹⁴ It is also thought the tenth isoform, Na_x, is quite divergent from the other existing subunits and may serve as a salt sensor rather than a voltage-gated channel.¹⁵

Table 1-1 Voltage Gated Sodium Channel Isoforms

Channel name	Variant	TTX IC ₅₀	Tissue Location*
Na _v 1.1	Na _v 1.1a	10 nM	CNS
Na _v 1.2	Na _v 1.2b	10 nM	CNS
Na _v 1.3	Na _v 1.3a,b	2 nM	CNS
Na _v 1.4	-	5 nM	skeletal muscle
Na _v 1.5	-	2 μM	Heart
Na _v 1.6	Na _v 1.6a	1 nM	CNS
Na _v 1.7	-	4 nM	PNS
Na _v 1.8	-	60 μM	PNS (DRG)
Na _v 1.9	Na _v 1.9a	1 μM	PNS
Na _x	-	-	PNS (DRG)

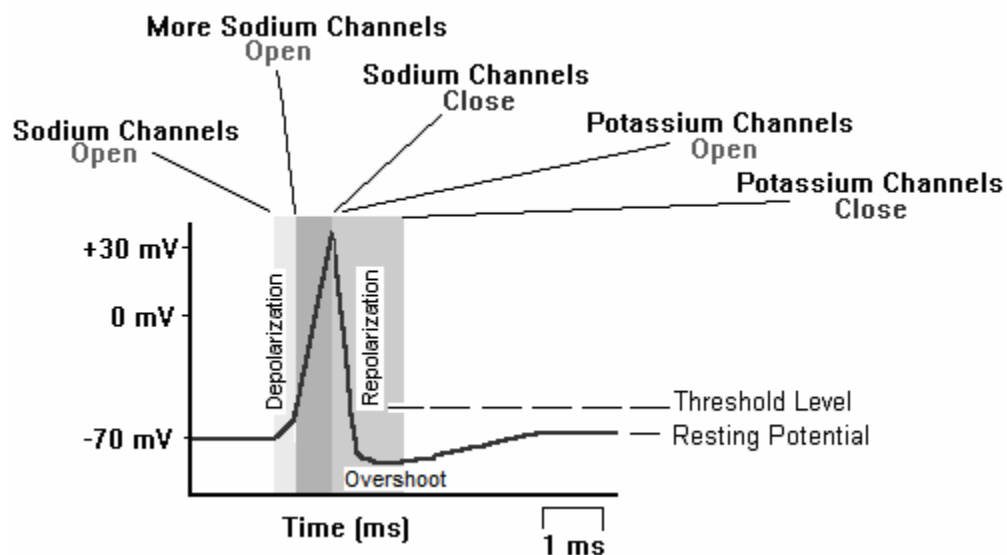
*CNS=central nervous system, PNS=peripheral nervous system, DRG=dorsal root ganglion

1.1.2 Function and Channel States

Voltage gated sodium channels play a critical function in electrically excitable cells, such as those found in neuronal, muscular and cardiac tissue. Activity of these cells relies on generation of an action potential by the VGSCs, which rapidly propagates electrical messages throughout the system. The action potential of a typical neuron is depicted below (Figure 1-4). Initially the membrane potential is at a resting state of -70

mV, meaning that the cytoplasm is 70 mV less than the external membrane. A brief period of depolarization occurs to -55 mV. Once the cell has reached this critical threshold level, an action potential is imminent. Further depolarization then leads to activation of more sodium channels, thus creating a positive internal cellular potential. As a consequence, the sodium channel closes and rapid repolarization occurs by the conductance of potassium ions. An overshoot, or hyperpolarization, takes place past -70 mV but the cell is quickly restored back to its resting potential.

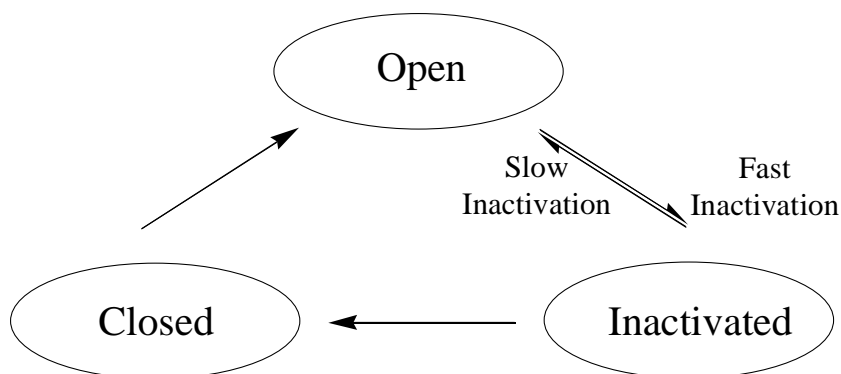
Figure 1-4 Action Potential of a Neuron



Much of the understanding of the sodium channel's structure and function has come about from the work of Hodgkin and Huxley, who were awarded the Nobel Prize in physiology in 1963 based on this work.¹⁶ From their findings, Hodgkin and Huxley were able to develop an empirical model (HH model) that could accurately predict sodium current kinetics and voltage dependence and provide an understanding of sodium channel gating. The HH model accounts for three possible states being involved in gating: closed,

open, and inactivated (Figure 1-5). The probability of finding the channels in a particular state is based on membrane potential, time and interconversion rates.

Figure 1-5 States of Sodium Channel Gating



1.1.3 Relationship of Structure and Function

Gating is the change between conducting and non-conducting states of the channel caused by an alteration in voltage. The VGSC undergo conformational changes as a response to this shift. The voltage sensor, consisting of positively charged arginine and lysine residue in the S4 segment of each domain, is essential in both activation and inactivation of the channel.¹⁷ The S4 segment resides internally to each domain allowing it to have a good voltage sensing capacity.¹⁸

The channel is initially in a closed, or resting, state of -70 mV and is nonconducting. Stimulation of the voltage sensor allows for opening of the channel causing an increase in membrane potential, which is known as activation. This increase in potential raises the probability that the channels are in an open, or conducting, state. Once the critical threshold hold of -55 mV is reached, an action potential will occur. These open channels are then able to convert to an inactivated state that is nonconducting and unavailable for reopening until after membrane repolarization.

Inactivation can occur through either a slow inactivation, which occurs over seconds to minutes, or a fast inactivation, which occurs in milliseconds. Little is known about the slow inactivation process, but it is believed that both fast and slow processes are essential to differing physiological and pathological events.¹⁹ Fast inactivation has been well studied and central to this is the inactivation gate, an intracellular loop located between domains D(III) and D(IV). As previously mentioned, NMR studies have revealed a hinged lid model of fast inactivation involving a series of hydrophobic residues isoleucine-phenylalanine-methionine (IFM). It is believed that this IFM motif binds to a series of amino acid residues in the intracellular mouth of the pore, known as the inactivation receptor, and thereby causes occlusion of the pore resulting in inactivation.

Reactivation of the inactivated state must occur by first entering a closed, or resting, state of the channel. This process is dependent on membrane potential and is often delayed by the occurrence of repeated depolarizations. Once in the closed state, the channel is again available to reopen by stimulation of the voltage sensor. This process occurs repeatedly within mammalian systems in order to transmit crucial information.

1.1.4 Binding Sites, Neurotoxin and Local Anesthetic

Much insight on the structure and function of VGSC has been obtained through the use of toxins. It has been determined that at least eight distinct neurotoxin binding sites and one local anesthetic, or “drug”, binding site occurs within the sodium channel (Table 1-2).²⁰ Typically, VGSC modifiers are able to affect channel function by either occlusion of the pore, or alteration of the voltage dependence of gating.

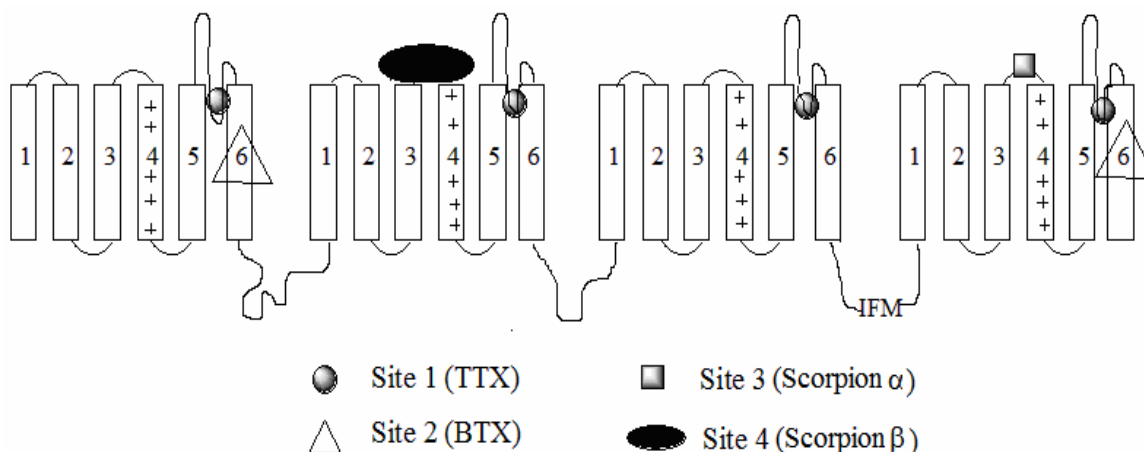
Table 1-2 Neurotoxin and Insecticide Binding Sites of the
Voltage Gated Sodium Channel

Site	Neurotoxin	Physiological effect
1	tetrodotoxin (TTX) saxitotoxin (STX) μ -conotoxin	inhibition of transport
2	batrachotoxin (BTX) veratridine aconitine grayanotoxin (GTX)	persistent activation
3	α -scorpion toxin sea anemone II toxin (ATX) δ -atracotoxins	enhancement of persistent activation; slow sodium current inactivation
4	β -scorpion toxin	shifting of voltage dependence
5	brevetoxins cinguatoxins	repetitive firing shifting of voltage dependence
6	δ -conotoxins	inhibition of activation
7	DDT and analogues pyrethroids	inhibition of activation shifting of voltage dependence
8	goniopora coral toxin	inhibition of activation
9	local anesthetics anticonvulsants dihydropyrazoles	inhibition of ion transport

Site 1 is known to bind water soluble, heterocyclic toxins tetrodotoxin (TTX), saxitoxin (STX) and μ -conotoxin. These channel modifiers are able to bind and cause occlusion of the pore, thereby inhibiting further ion transport. More specifically, they are able to interact with amino acids of the selectivity filter, DEKA. Site 1 binding occurs toward the external side of the membrane, shown by the P-loops of D(I)-D(IV) (Figure 1-6). Site 2 binds lipid soluble alkaloids batrachotoxin (BTX), grayanotoxin (GTX), veratridine and aconitine which lead to persistent activation of the channel. This hyperexcitability is attributable to both a shift in voltage dependence of activation, towards a more negative potential, and block of fast inactivation. The lipophilic nature of these compounds allows them to bind to site 2, which is embedded within the plasma membrane. Allosteric effects of neurotoxin binding are common. BTX binding effects can be enhanced by the binding of site 3, 5, and 7 binders and diminished by site 1 binders, as well as drugs binding to the local anesthetic site. Site 3 binders include low molecular weight, polypeptide venoms, scorpion α -toxin and sea anemone toxin which are able to slow or block inactivation. These toxins enhance effects of site 2 binders leading to a greater degree of persistent activation. Site 4 binds β -scorpion toxin which causes a shift of voltage dependence to more negative potential, sometimes as low as -70 mV, but does not effect inactivation. Site 5 binds both brevetoxin and ciguatoxins (CTX) which alter channel function similarly to site 2 binders. These agents bind within the transmembrane region and cause persistent firing, by shifting voltage dependence and blocking inactivation. It has been found that site 6 binds δ -conotoxin and site 8 goniopora coral toxin, both of which cause inhibition of activation or closure of the channel. Site 7, known as the insecticide binding site, binds pyrethroids and DDT which

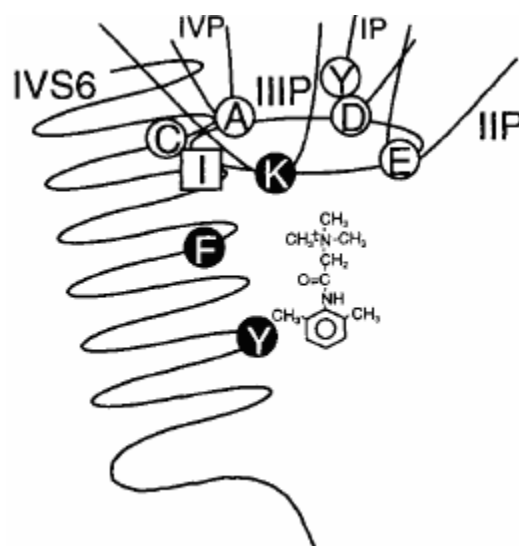
are potent toxins known to cause hyperexcitability and lead to paralysis in vertebrate systems.

Figure 1-6 Neurotoxin Binding Sites



The local anesthetic (LA), or “drug,” binding site is known to overlap site 2 of neurotoxin binding in sodium channels.²¹ Agents binding to this site include local anesthetics, anticonvulsants and antiarrhythmics which function by block of ion transport. It is believed that local anesthetic binders, much like site 2 binders, must be lipid soluble in order to pass through the plasma membrane and reach its associated binding site.²² Numerous site directed mutagenesis studies have been conducted in order to determine the location of this receptor (Figure 1-7).^{23,24} The most compelling mutations occur on the cytosolic side of S6 D(IV), with alteration of phenylalanine 1764 and tyrosine 1771 resulting in a loss of current block by local anesthetics.²⁵ Additionally, lysine 2137 has also been implicated as an essential residue of this site. This current model predicts a location in the pore of the channel that is close to both the selectivity filter (DEKA) and the binding site of the inactivation gate.

Figure 1-7 Local Anesthetic Binding Site



Numerous clinically prescribed drugs function by blocking sodium channel current (Table 1-3).^{26, 27} This includes well known anticonvulsants, phenytoin and carbamazepine, which have made a significant impact in the treatment of epilepsy. Lidocaine has also been extensively utilized for both the treatment of pain and arrhythmias.

Table 1-3 Sodium Channel Blockers as Therapeutics

Disease	Class	Drug
epilepsy	anticonvulsant	phenytoin, lamotrigine, carbamazepine, valproic acid
pain	local anesthetics analgesics	carbamazepine, tricyclic antidepressants, phenytoin, lidocaine, propafol
depression	antidepressants	tricyclic antidepressants
arrhythmia	type 1 anti-arrhythmics	lidocaine, phenytoin, propafenone

Agents that bind to the LA receptor do so in a voltage and frequency dependent manner. Experimental studies have shown that the action of local anesthetic binders is increased at a more depolarized potential and decreased during more hyperpolarized potentials.²⁸ This indicates a greater affinity for channels that are not in the resting state conformation. Frequency dependent block occurs when LA agents show enhanced effectiveness by binding to open or inactivated states of the channel during hyperexcitability. Understanding the mechanism of drug interaction and residues of the LA receptor allow us to further exploit this towards development of new sodium channel blocking therapeutics.

1.2 VGSC and Pain

1.2.1 Pain Types and Incidence

Somatogenic pain, pain originating from a physiological source, can be classified into two categories nociceptive and neuropathic.²⁹ Nociceptive pain is caused by activation of somatic nerve fibers in the skin and internal organs as a response to external stimuli. However, neuropathic pain originates from a dysfunction within the nervous system. Whatever the type, all pain is sensed through the propagation of action potential by voltage gated sodium channels. Once initial firing occurs, further potentiation allows for the transduction of pain signals throughout the body.

Nociceptive pain is typically caused in response to a mechanical, thermal or chemical stress. The ability to sense and respond to this type of pain is essential in protecting ourselves from harm and disease. Nociception can be associated with free nerve endings that sense pain, known as nociceptors.³⁰ Three types of nociceptors that exist are mechanical, heat, and mixed or polymodal. Mechanical nociception is most

often pronounced in response to sharp objects. Thermal stimulation of pain is typically caused by prolonged exposure to temperatures over 45 °C. Mixed, or polymodal, nociception is a response to a mixture of stimulus. Examples of such nociception include, but are not limited to, cuts, bruises, burns, bone fractures, and post-surgical pain.

Neuropathic pain results from an abnormal somatosensory process within the central or peripheral nervous system, often caused by a neurological disorder. Manifestation of these neuropathies can result in sensory deficits such as partial or complete loss of sensation, or sensory enheightenments such as tingling, shooting or burning types of pain.³¹ These syndromes are often persistent and caused by little to no physical injury, with severity being independent of damage. Conversely, nociceptive pain correlates to the extent of tissue damage, and as healing occurs the pain is able to subside.

Neuropathic pain syndromes are maladaptive in nature and cause a great degree of suffering and distress. Diseases associated with such neuropathic states include postherpetic neuralgia (PHN), diabetic neuropathy, carpal tunnel syndrome, HIV related neuropathy, etc. Postherpetic neuralgia arises from infection by the *Herpes zoster* virus that causes shingles. Infection of this type results in painful inflammation of the dorsal root ganglia, location of many sensory neurons involved in neuropathic pain, and the skin of the associated dermatome. Patients suffering from diabetes can often have numbness or a burning and tingling sensation in their extremities, known as diabetic neuropathy.³²

Most neuropathic pain syndromes involve a peripheral process, meaning that it is unassociated with spinal cord, brain stem, or thalamic damage which proceeds through a separate mechanism. Peripheral neuropathic pain can occur as either spontaneous pain

which is stimulus independent or hypersensitive pain in response to an external stimulus. Stimulus invoked pain occurs in response to a mechanical, chemical or thermal stress, which under normal physiological conditions would be more tolerated or not troublesome at all. This can be further clarified by the two types of stimulus invoked pain, hyperalgesia and allodynia. Hyperalgesia is an exaggerated pain response to a stimulus that would normally be painful. Whereas, allodynia is caused by a stimulus that would not normally be troublesome. Due to the unknown mechanistic pathway of allodynia, diagnosis and mechanism can best be determined by classifying it under hyperalgesia.³³

Pain syndromes involving a neuropathic origin are often chronic, meaning that the symptoms persist or reoccur over a period of three months or longer. Chronic pain syndromes are prominent within the general population, affecting approximately 15% of all people. Within chronic pain syndromes, painful neuropathies affect 1.5% of the US population.³⁴ This can be further distinguished on the basis of disease state, with 2.1 to 4.7 persons per 100,000 being effected by trigeminal neuralgia, 11-16% of Type I and Type II diabetics displaying diabetic neuropathies, and 34 persons per 100,000 suffering from postherpetic neuralgia, or shingles.³⁵ As it can be seen, neuropathic pain syndromes are quite common within the general population, which necessitates the development of suitable therapeutics.

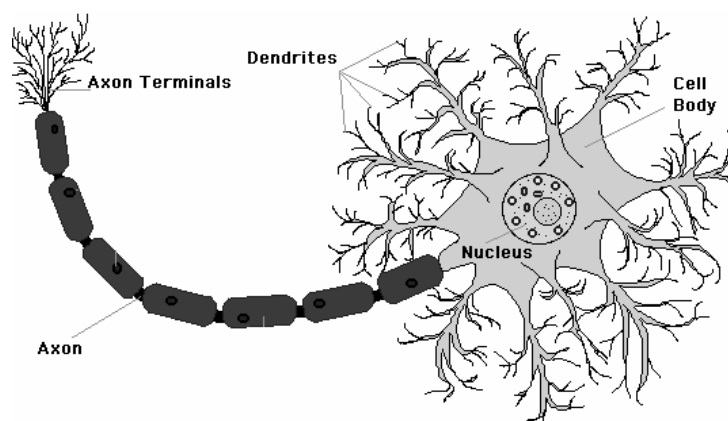
1.2.2 Expression of VGSC in Pain

Central to the development of pain therapeutics is the voltage gated sodium channel. It has been well established that sodium channels are associated with the sensitivity of neuronal firing, especially during a state of injury when hyperexcitability is observed. This hyperexcitability is typically found at both sites of damage and within the

dorsal root ganglion neurons, DRGs.³⁶ In order to fully comprehend this complex system of neuronal signaling that causes hyperexcitability, the structure of the neuron must first be examined.

The neuron is composed of a cell body with two possible types of fibers extending from it, dendrites and axons (Figure 1-8). The dendrite is responsible for receiving information in the form of stimuli from sensory receptors, or other nerve cells. The axon on the other hand, transmits information away from the cell body towards other adjacent nerve cells. Once a stimulus is received by the dendrite or cell body, activation and propagation of nerve impulse is sent down the axon. When this impulse reaches the terminal branches of the axon, neurotransmitters further carry the impulse towards the next cell. In states of damage or injury, exaggeration of this process leads to hyperexcitability which the brain is then able to convey as pain.

Figure 1-8 Structure of a Neuron

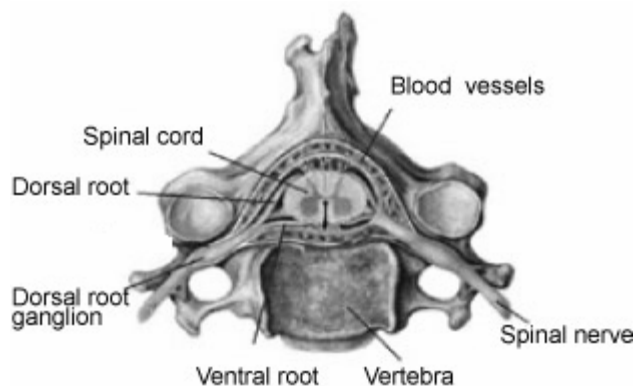


Two types of VGSC are found in neurons, those that are TTX sensitive and others that are TTX insensitive, or resistant. As it should be recalled TTX, tetrodotoxin, is a site 1 binding neurotoxin to which varying channel isoforms can display divergent sensitivity. TTX sensitive channels are found on all sensory neurons and are responsible for the

initiation of an action potential. However TTX insensitive channels are found only in nociceptors, pain receptors found on nerve endings. These channels display a much slower activation and inactivation kinetics and have been implicated in pain states.³⁷ However during a state of trauma both TTX sensitive and insensitive types of channels are upregulated at these sites leading to hyperexcitability.³⁸

Numerous biochemical experiments have shown that this morphological change in sodium channel accumulation upon injury, occurs in dorsal root ganglion (DRG) sensory neurons.^{39,40} The dorsal root ganglion is an extension from the dorsal root that occurs in the posterior of each spinal segment (Figure 1-9). These ganglions contain neuronal cells responsible for relaying vital somatosensory information to the brain and spinal cord.

Figure 1-9 Location of the Dorsal Root Ganglion



Within the DRG, VGSCs play an essential role in the electrogenesis of primary sensory neurons.⁴¹ Expression of multiple sodium channel isoforms occurs within the DRGs, with certain isoforms not being expressed elsewhere in the body. At least six isoform subtypes have been found within DRGs, several of which are known to play a role in the messaging of pain.⁴² Regulation of this expression occurs in a preferential

manner, since differing isoforms are likely to serve varying roles. In states of injury or damage, expression of VGSC within the DRGs becomes a dynamic process. Morphological changes in the upregulation and downregulation of particular channel isoforms occurs during these injured states resulting in a physiological change of hyperexcitability. In fact, electrophysiological methods have been able to show hyperexcitability and spontaneous firing in animal models of sciatic nerve injury.⁴³ Differing types of injuries yield distinct changes in sodium channel expression and one underlying mechanism therefore can not be determined. This increasing knowledge of the VGSC's role in the pain pathway has provided itself as useful therapeutic target for the treatment of pain syndromes.

1.2.3 VGSC in Pain Therapeutics

Currently, sodium channel blockers such as local anesthetics, antiarrhythmics, anticonvulsants, and tricyclic antidepressants serve as the most commonly prescribed therapeutics for the treatment of neuropathic pain syndromes.⁴⁴ However many of these channel blockers suffer from a lack of subtype selectivity, thereby resulting in adverse side effects to the central nervous and cardiovascular systems. Great difficulty lies in the development of isoform specific sodium channel inhibitors and none have been accomplished to date. However the ability to enhance subtype selectivity would allow for the direct targeting of disease states and lower the degree of adverse effects. In particular, sodium channel isoforms $Na_v1.7$, $Na_v1.8$ and $Na_v1.9$ are important to neuropathies occurring in the peripheral nervous system.⁴⁵ $Na_v1.7$ has been shown to have a major role in acute and inflammatory pain through gene ablation studies in mice.⁴⁶ $Na_v1.8$ and $Na_v1.9$ are known to be key to nociception and neuropathic pain syndromes.

Also, recent work has implicated the upregulation of $\text{Na}_v1.3$ in DRGs upon nervous system injury, thereby indicating the importance of $\text{Na}_v1.3$ and the dynamic expression of sodium channels during states of injury.⁴⁷

VGSC drugs interact via the local anesthetic receptor that overlaps neurotoxin binding site 2. Inhibition by these LA drugs typically occurs in a state dependent manner, with relatively weak binding to the resting state, tight and fast binding to the open state, and tight but slower binding to the inactivated state. This enhanced binding affinity for more depolarized potentials helps to ensure blockade is occurring in hyperexcitable neurons. Upon excessive firing the VGSC blocking drug is able to quickly bind to open channels leaving few unbound channels remaining and therefore the action potential can no longer be maintained. Also, differing isoforms have varying state kinetics and display variable inhibition to state dependent blockers.⁴⁸

The development of novel VGSC blocker necessitates the address of two key issues, isoform specificity and state dependence. Knowledge of the distribution of specific channel isoforms to particular tissues and localities of the body, guides us towards the discovery of more selective therapeutics. State dependence of a drug must also be viewed, so that block is not occurring indiscriminately and that hyperexcitable cells are being targeted.

1.3 References

- 1) Noda, M.; Ikeda, T.; Suzuki, H.; Takeshima, H.; Takahashi, T.; Kuno, M.; Numa, S. "Expression of functional sodium channels from cloned cDNA," *Nature*. **1986**, 322, 826-828.
- 2) Messner, D.J.; Feller, D.J.; Scheuer, T.; Catterall, W.A. "Functional properties of rat brain channels lacking the $\beta 1$ and $\beta 2$ subunit," *J. Biol. Chem.* **1986**, 261, 211-215.
- 3) Isom, L.L.; De Jongh, K.S.; Patton, D.E.; Reber, B.F.; Offord, J.; Charbonneau, H.; Walsh, K.; Goldin, A.L.; Catterall, W.A. "Primary structure and functional expression of the beta 1 subunit of the rat brain sodium channel," *Science*. **1992**, 256, 839-842.
- 4) West, J.W.; Scheuer, T.; Machler, L.; Catterall, W.A. "Efficient expression of rat brain type IIA Na^+ channel α subunit in the somatic cell line," *Neuron*. **1992**, 8, 59-70.
- 5) Anger, T.; Madge, D.J.; Mulla, M.; Riddall, D. "Medicinal chemistry of neuronal voltage-gated sodium channel blockers," *J. Med. Chem.* **2001**, 44, 115-137.
- 6) Vassilev, P.M.; Scheuer, T.; Catterall, W.A. "Inhibition of inactivation of single sodium channels by site-directed antibody," *Proc. Natl. Acad. Sci.* **1989**, 86, 8147-8151.
- 7) Rohl, C.A.; Boeckman, F.A.; Baker, C.; Scheuer, T.; Catterall, W.A.; Klevit, R.E. "Solution structure of the sodium channel inactivation gate," *Biochemistry*. **1999**, 38, 855-861.

- 8) Hille, B. "The permeability of the sodium channel to organic cations in myelinated nerve," *Gen. Physiol.* **1971**, 58, 599-619.
- 9) Fozzard, H.A.; Lipkind, G.M. "The guanidinium toxin binding site on the sodium channel," *Jpn. Heart J.* **1996**, 37, 683-692.
- 10) Goldin, A.L. "Resurgence of sodium channel research," *Annu. Rev. Physiol.* **2001**, 63, 871-894.
- 11) Goldin, A.L.; Barchi, R.L.; Caldwell, J.H.; Hofmann, F.; Howe, J.R.; Hunter, J.C.; Kallen, R.G.; Mandel, G.; Messner, M.H.; Netter, Y.B.; Noda, M.; Tamkun, M.M.; Waxman, S.G.; Wood, J.N.; Catterall, W.A. "Nomenclature of the voltage-gated sodium channels," *Neuron.* **2000**, 28, 365-368.
- 12) Plummer, N.W.; Meisler, M.H. "Evolution and diversity of mammalian sodium channel genes," *Genomics.* **1999**, 57, 323-331.
- 13) Yu, F.H.; Catterall, W.A. "Overview of the voltage-gated sodium channel family," *Genome Biology.* **2003**, 4, 207-213.
- 14) Satin, J.; Kyle, J.W.; Chen, M.; Cribs, L.L.; Fozzard, H.A.; Rogart, R.B. "A mutant of TTX-resistant cardiac sodium channels with TTX-sensitive properties," *Science.* **1992**, 256, 1202-1205.
- 15) Hiyama, T.Y.; Watanabe, E.; Ono, K.; Inenaga, K.; Tamkun, M.M.; Yoshida, S.; Noda, M. "Na_x channel involved in CNS sodium-level sensing," *Nat. Neurosci.* **2002**, 5, 511-512.
- 16) Hodgkin, A.L.; Huxley, A.F. "The dual effect of membrane potential on sodium conductance in the giant axon of *Loligo*," *J. Physiol.* **1952**, 116, 497-506.

- 17) Kontis, K.J.; Rounaghi, A.; Goldin, A.L. "Sodium channel activation gating is affected by substitutions of voltage sensor positive charges in all four domains," *J. Gen. Physiol.* **1997**, *110*, 391-401.
- 18) Denac, H.; Mevissen, M.; Scholtysik, G. "Structure, function and pharmacology of voltage-gated sodium channels," *Nauyn-Schmiedeberg's Arch Pharmacol.* **2000**, *362*, 453-479.
- 19) Catterall, W.A. "From ionic currents to molecular mechanisms: the structure and function of voltage-gated sodium channels," *Neuron.* **2000**, *26*, 13-25.
- 20) Cestele, S.; Catterall, W.A. "Molecular mechanisms of neurotoxin action of voltage-gated sodium channels," *Biochimie.* **2000**, *82*, 883-892.
- 21) Linford, N.J.; Cantrell, A.R.; Yusheng, Q.; Scheuer, T.; Catterall, W.A. "Interaction of batrachotoxin with the local anesthetic receptor site in transmembrane segment IVS6 of the voltage-gated sodium channel," *Proc. Natl. Acad. Sci.* **1998**, *95*, 13947-13952.
- 22) Hille, B. "Local anesthetics: hydrophilic and hydrophobic pathways for the drug receptor reaction," *J. Gen. Physiol.* **1977**, *69*, 497-515.
- 23) Sunami, A.; Dudley, S.C.; Fozzard, H.A. "Sodium channel selectivity filter regulates antiarrhythmic drug binding," *Proc. Natl. Acad. Sci.* **1997**, *94*, 14126-14131.
- 24) Bai, C.X.; Glaaser, I.W.; Sawanobori, T.; Sunami, A. "Involvement of local anesthetic binding site on IVS6 of sodium channels in fast and slow inactivation," *Neurosci. Lett.* **2003**, *337*, 41-45.

- 25) Li, H.I.; Galue, A.; Meadows, L.; Ragsdale, D.S. "A molecular basis for the different local anesthetic affinities of resting versus open and inactivated states of the sodium channel," *Mol. Pharmacol.* **1999**, *55*, 134-141.
- 26) Kuo, C.C. "A common anticonvulsant binding site for phenytoin, carbamazepine, and lamotrigine in neuronal Na⁺ channels," *Mol. Pharmacol.* **1998**, *54*, 712-721.
- 27) Ragsdale, D.S.; Scheuer, T.; Catterall, W.A. "Frequency and voltage dependent inhibition of type IIA Na⁺ channels, expressed in a mammalian cell line, by local anesthetic, antiarrhythmic and anticonvulsant drugs," *Mol. Pharmacol.* **1991**, *40*, 756-765.
- 28) Li, H.I.; Galue, A.; Meadows, L.; Ragsdale, D.S. "A molecular basis for the different local anesthetic affinities of resting versus open and inactivated states of the sodium channel," *Mol. Pharmacol.* **1999**, *55*, 134-141.
- 29) Cole, B.E. "Pain management: classifying, understanding, and treating pain," *Clinical Rev.* **2003**, *1*, 23-30.
- 30) Wood, J.N.; Perl, E.R. "Pain," *Curr. Opin. Genet. Dev.* **1999**, *9*, 328-332.
- 31) Stacey, B.R. "Management of peripheral neuropathic pain," *Am. J. Phys. Med. Rehabil.* **2005**, *84*, 4-16.
- 32) Sommer, C. "Painful neuropathies," *Curr. Opin. Neurol.* **2003**, *16*, 623-628.
- 33) Woolf, C.J.; Mannion, R.J. "Neuropathic pain: aetiology, symptoms, mechanisms, and management," *Lancet.* **1999**, *353*, 1959-1964.
- 34) Chong, M.S.; Bajwa, Z.H. "Diagnosis and treatment of neuropathic pain," *J. Pain Sympt. Mgmt.* **2003**, *25*, 4-11.

- 35) Saarto, T.; Wiffen, P.J. "Antidepressants for neuropathic pain (review)," *Cochrane Collab.* **2006**, *1*, 1-48.
- 36) Devor, M.; Govrin-Lippmann, R.; Angelides, K. "Na⁺ channel immunolocalization in peripheral mammalian axons and changes following nerve injury and neuroma formation," *J. Neurosci.* **1993**, *13*, 1976-1992.
- 37) Novakovic, S.D.; Tzoumaka, E.; McGivern, J.G. "Distribution of the tetrodotoxin-resistant sodium channel PN3 in rat sensory neurons in normal and neuropathic conditions," *J. Neurosci.* **1998**, *18*, 2174-2187.
- 38) Akopian, A.N.; Souslova, V.; England, S.; Okuse, K.; Ogata, N.; Ure, J.; Smith, A.; Kerr, B.J.; McMahon, S.B.; Boyce, S.; Hill, R.; Stanfa, L.C.; Dickenson, A.H.; Wood, J.N. "The tetrodotoxin-resistant sodium channel SNS has a specialized function in pain pathways," *Nature Neuroscience.* **1999**, *2*, 541-548.
- 39) Waxman, S.G. "The molecular pathophysiology of pain: abnormal expression of sodium channel genes and its contributions to hyperexcitability of primary sensory neurons," *Pain.* **1999**, *6*, 133-140.
- 40) Black, J.A.; Liu, S.; Tanaka, M.; Cummins, T.R.; Waxman, S.G. "Changes in the expression of tetrodotoxin-sensitive sodium channels within dorsal root ganglia neurons in inflammatory pain," *Pain.* **2004**, *108*, 237-247.
- 41) Waxman, S.G.; Dib-Hajj, S.; Cummins, T.R.; Black, J.A. "Sodium channels and pain," *Proc. Natl. Acad. Sci.* **1999**, *96*, 7635-7639.
- 42) Waxman, S.G.; Cummins, T.R.; Dib-Hajj, S.D.; Black, J.A. "Voltage-gated sodium channels and the molecular pathogenesis of pain: a review," *J. Rehab. Res. Dev.* **2000**, *37*, 517-528.

- 43) Xie, Y.; Zhang, J.; Petersen, M.; LaMotte, R.H. "Functional changes in the dorsal root ganglion cells after chronic nerve constriction in the rat," *J. Neurophysiol.* **1995**, 73, 1811-1820.
- 44) Matzner, O.; Devor, M. " Na^+ conductance and the threshold for repetitive neuronal firing," *Brain Res.* **1992**, 597, 92-98.
- 45) Kalso, E. "Sodium channel blockers in neuropathic pain," *Curr. Pharm. Des.* **2005**, 11, 3005-3011.
- 46) Nassar, M.A.; Stirling, L.C.; Forlani, G.; Baker, M.D.; Matthews, E.A.; Dickenson, A.H.; Wood, J.N. "Nociceptor-specific gene deletion reveals a major role for $\text{Na}_v1.7$ (PN1) in acute and inflammatory pain," *Proc. Natl. Acad. Sci.* **2004**, 10, 12706.
- 47) Hains, B.C.; Klein, J.P.; Saab, C.Y.; Craner, M.J.; Blak, J.A.; Waxman, S.G. "Upregulation of sodium channel $\text{Na}_v1.3$ and functional involvement in neuronal hyperexcitability associated with central neuropathic pain after spinal cord injury," *J. Neurosci.* **2003**, 23, 8881-8892.
- 48) Chevrier, P.; Vijayaragavan, K.; Chahine, M. "Differential modulation of $\text{Na}_v1.7$ and $\text{Na}_v1.8$ peripheral nerve sodium channels by the local anesthetic lidocaine," *Br. J. Pharmacol.* **2004**, 142, 576-584.

Chapter 2

Discovery of Diphenyl Amine Based Sodium Channel Blockers

The development of new therapies for chronic pain is an area of unmet medical need. Central to pathways of chronic pain is the upregulation of voltage gated sodium channels. The use of tricyclic antidepressants, which also have sodium channel activity, in chronic pain therapy prompted us to develop novel compounds from this scaffold. Herein, we show that the tricyclic moiety is not needed for effective inhibition of the [^3H]-BTX binding site and sodium currents of hNa_v1.2. Our lead compound (**2.6**), containing a diphenyl amine motif demonstrated a 53.2% inhibitory block of Na_v1.2 current at 10 μM , which is greater than 50% increase in current block in comparison to the amitriptyline standard. Altogether our study establishes that the tricyclic motif is unnecessary for hNa_v1.2 activity and modification of the amine portion is detrimental to sodium channel block. Further evaluation of several representative analogues has demonstrated the potency of this diphenyl class towards inhibitory effects in Na_v1.7 and Na_v1.8, as well as in animal models of anticonvulsant activity.

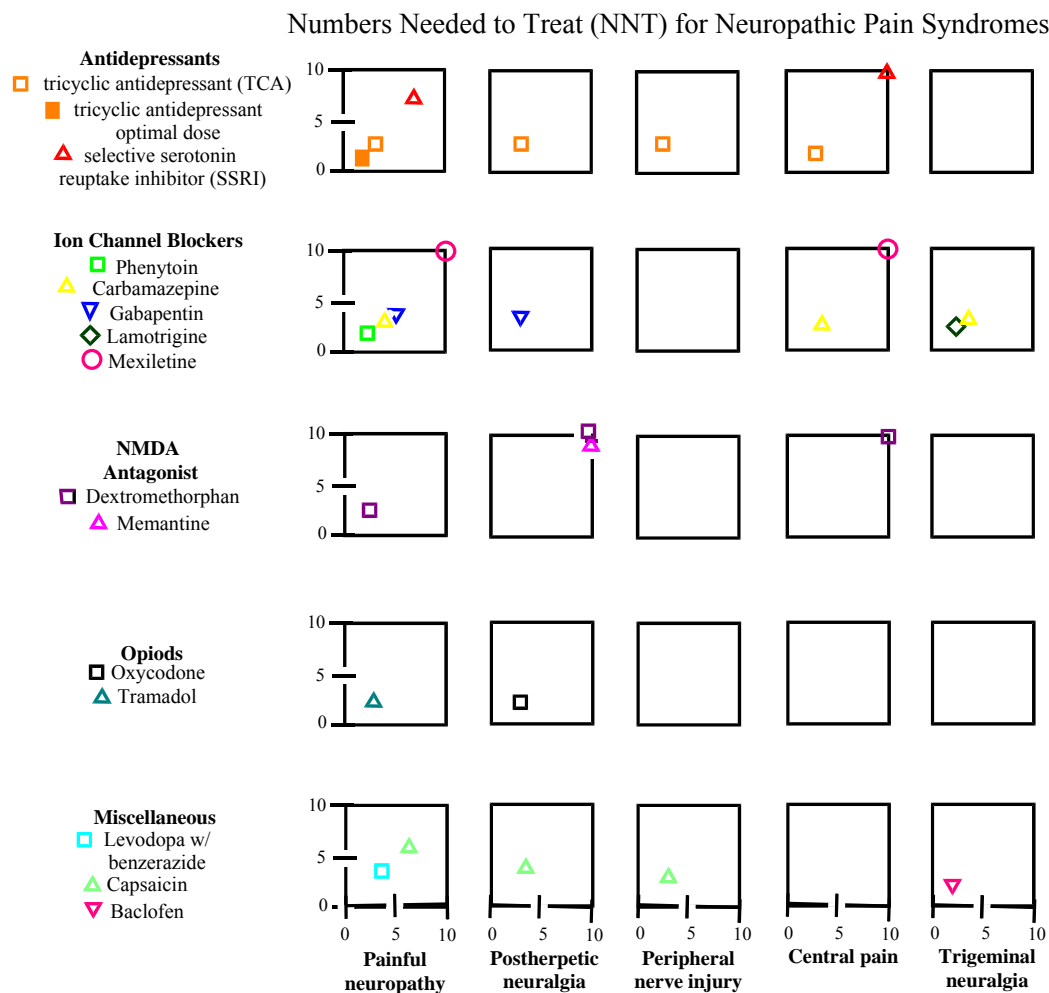
2.1 Neuropathic Pain Therapeutics

2.1.1 Current Therapeutics for Neuropathic Pain

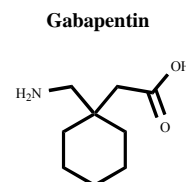
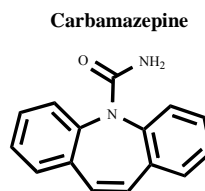
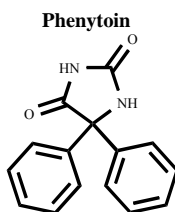
Therapeutics currently available for the treatment of neuropathic pain syndromes include: antidepressants, ion channel blockers, N-methyl-D-aspartate antagonists, opioids and other inhibitors (Figure 2-1).¹ These drug classes can be compared on the basis of their number needed to treat (NNT), which is the amount needed to obtain at least 50% relief of symptoms in a patient upon compound administration. When comparing all drug classes, tricyclic antidepressants (TCAs) show the greatest efficacy in relation to all pain

types, i.e. painful neuropathy, postherpetic neuralgia (shingles), peripheral nerve injury, and central pain. However determination of appropriate therapeutic choice can often be challenging, due to multiple underlying mechanisms often giving rise to a single symptom.²

Figure 2-1 Neuropathic Pain Therapeutics



Ion Channel Blocker Therapeutics



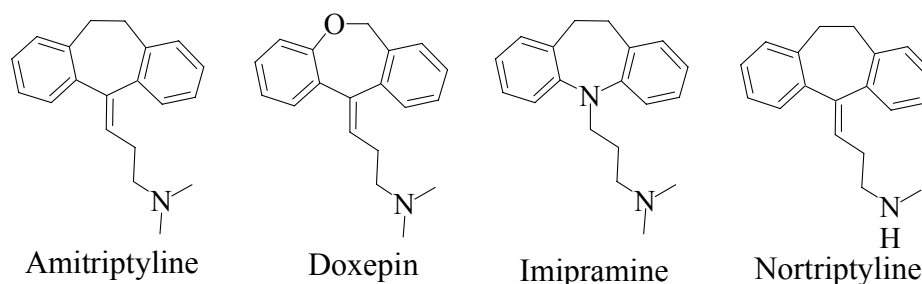
Sodium channel blockers such as anticonvulsants and tricyclic antidepressants have been the most commonly prescribed therapeutics for the treatment of neuropathic pain syndromes. Anticonvulsant gabapentin has been shown to be effective towards postherpetic neuralgia and diabetic neuropathy and carbamazepine towards trigeminal neuralgia.³ Other drug classes which normally function in the treatment of pain, such as non-steroidal anti-inflammatory drugs (NSAIDs) and opiates show less effectiveness towards neuropathic conditions.⁴ Additionally, issues such as tolerance and addictiveness of opiate drugs must also be assessed prior to administration. Utilization of newer antidepressants, selective serotonin reuptake inhibitors (SSRIs) have limited data but show promise for future use.

Although many of the existing sodium channels blocking drugs have been beneficial in treating neuropathies, most suffer from adverse side effects to the central nervous system or cardiovascular system. For example, sodium channel blocker bupivacaine has long been used as a local anesthetic and is known to substantially block nerve activity. However, this drug suffers from a high degree of cardiotoxicity.⁵ Anticonvulsants, phenytoin and carbamazepine also have adverse pharmacokinetic interactions by production of liver enzymes.⁶ TCAs suffer from some side effects as well, and in one particular study 20% of patients withdrew from treatment due to the severity of these effects, which included drowsiness, blurred vision, arrhythmias, and heart attack.⁷ However, TCAs such as amitriptyline serve as one of the best treatments of neuropathic pain to date.⁸

2.1.2 Tricyclic Antidepressants as Treatment

Tricyclic antidepressants (TCAs) have been clinically utilized as mood stabilizing agents since their discovery in the early 1960s.⁹ Mechanistically these drugs function in depressive illness by inhibiting neurotransmitter reuptake. Application of these drugs to patients with chronic pain was serendipitously able to elucidate their clinical efficacy as analgesics. These analgesic properties are known to function separately to antidepressive action and have been utilized in post operative pain therapy.¹⁰ Longer durations of administration have proven well for the treatment of chronic conditions such as diabetic neuropathy. TCAs encompass a vast class of compounds, all of which contain a tricyclic motif. One particular drug of this class, amitriptyline has shown to be a potent therapeutic with clinical effectiveness against certain pain syndromes (Figure 2-2).

Figure 2-2 Class of Tricyclic Antidepressants (TCAs)



Amitriptyline has been clinically utilized in the treatment of migraines,^{11,12} diabetic neuropathy,¹³ postherpetic neuralgia,¹⁴ and chronic lower back pain.¹⁵ The mechanistic pathway by which amitriptyline functions in the treatment of pain has yet to be fully determined. However, it is reasonable to propose that its remarkable capabilities as a sodium channel blocker correlate to these physiological functions (Table 2-1).¹⁶ Literature precedence has shown that amitriptyline behaves as a potent sodium channel

binder with $73.8\% \pm 2.3$ inhibition at $10\ \mu\text{M}$.¹⁷ This astonishingly high ability to bind sodium channels is even greater than the long-acting local anesthetic bupivacaine with $63.6\% \pm 2.4$ inhibition at $10\ \mu\text{M}$. These values of inhibition for various drug classes are based on the displacement of tritiated batrachotoxin ($[^3\text{H}]\text{-BTX}$) from synaptoneuroosomes.

Table 2-1 Inhibition of $[^3\text{H}]\text{-BTX}$ Binding to
Brain Vesicular Preparations

Drug Class	Compound	Percent Inhibition at $10\ \mu\text{M}$
local anesthetics	bupivacaine	63.6 ± 2.4
	lidocaine	9.8 ± 1.1
anticonvulsants	diphenylhydantoin	18.5 ± 1.9
	carbamazepine	1.6 ± 2.1
antidepressants (TCAs)	amitriptyline	73.8 ± 2.3
	imipramine	72.7 ± 1.6
analgesics	dextrophan	38.2 ± 4.1

Site directed mutagenesis studies in rat skeletal muscle $\text{Na}_v1.4$ have shown an overlap of the amitriptyline binding site to the LA receptor with several key amino acid residues, N434 at S6 of DI, L1280 at S6 of DIII, and F1579 of S6 of DIV-S6.¹⁸ It has been proposed that the tricyclic portion is responsible for interaction with these hydrophobic residues of the S6 segments, which permeate the central lining of the pore.¹⁹ Binding within the pore region has further suggested physical occlusion of the channel as a mechanism for current block.²⁰ This mutual binding site of LA drugs and amitriptyline provides further insight into their similar blocking effects on the VGSC.

Amitriptyline and LA drugs have both been shown to have similar state dependent block, with preferential binding to inactivated states over resting states. Interestingly mutation of L1280 at S6 of DIII in inactivated states shows a greater effect in amitriptyline binding, than in resting states with the same mutation. This establishes the importance of the L1280 residue for binding and the preference for inactivated states when compared to resting state channels. Further examination of amitriptyline's effects to open states has been conducted through the use of inactivation deficient mutant channels, due to the short duration of channel opening.²¹ Application of amitriptyline to these mutant channels demonstrated block in a concentration dependent fashion with preferential binding to open states over resting states. However the greatest affinity of amitriptyline binding has been shown for open states of the channel, which may occur through either physical occlusion of the pore or by modulation of sodium channel gating to more hyperpolarizing currents.²²

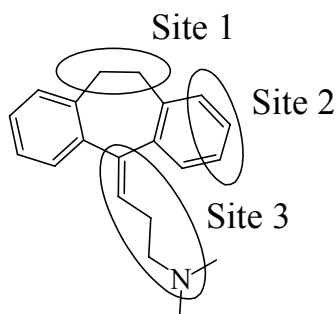
Amitriptyline has proven to be a potent inhibitor of sodium channel current in a state dependent manner. Such state dependent block allows for the targeting of hyperexcitable neurons and ectopic firing associated with neuropathic conditions. Conservation of amitriptyline's mutual binding site with the LA receptor occurs in numerous channel isoforms found in sensory neurons, $Na_v1.3$, $Na_v1.6$, $Na_v1.7$, $Na_v1.8$, and $Na_v1.9$. These factors display the clinical relevancy of amitriptyline as a therapeutic for neuropathic conditions.^{23, 24}

2.2 Design and Synthesis

2.2.1 Three Sites of Modification

In this study, we propose to further develop analogues of amitriptyline in order to create a more potent and well-tolerated therapeutic for the potential treatment of neuropathic pain syndromes. We have been able to design, synthesize and evaluate novel compounds designed from a common amitriptyline scaffold. Modification at three major sites (Figure 2-3) was ensued in order to elucidate structural and electronic requirements necessary for enhanced sodium channel inhibition.

Figure 2-3 Major Sites of Scaffold Modification



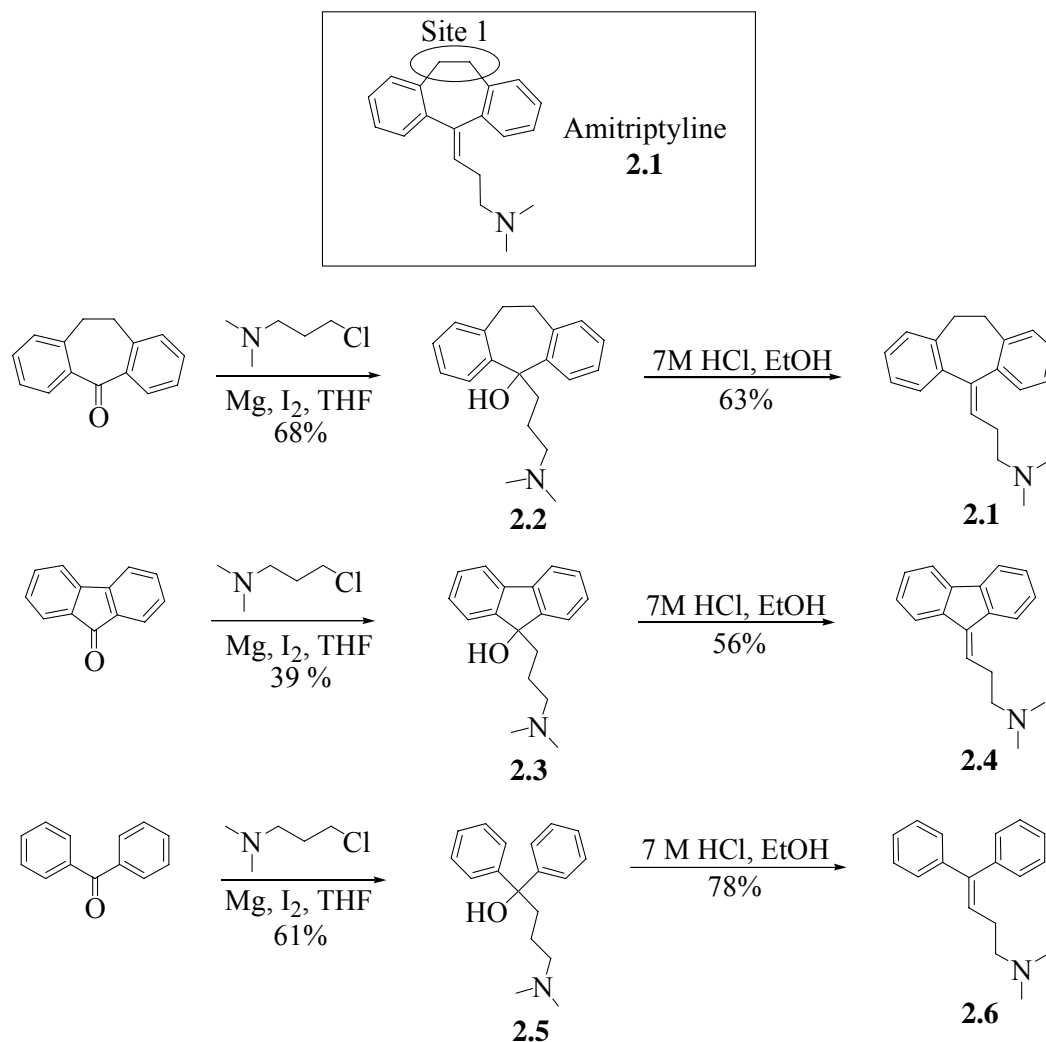
All compounds were initially screened in the [^3H]-BTX displacement assay. Analogues showing substantial binding to the sodium channel protein were further evaluated for inhibitory effects on hNa_v1.2 using patch-clamp electrophysiology. From our findings we have been able to establish key elements for activity, as well as develop a more potent structural class of sodium channel blockers.

2.2.2 Site 1, Phenyl Ring Orientation

Analogues (2.1)-(2.6) were initiated by Grignard addition of the dimethylaminopropylmagnesium chloride (DMP-Cl) complex to the commercially available starting ketones. Tertiary alcohols (2.2), (2.3), and (2.5) were subsequently

dehydrated to their corresponding alkenes by refluxing in a 7M HCl/EtOH solution (Scheme 2-1).

Scheme 2-1 Modification at Site 1, Phenyl Ring Orientation

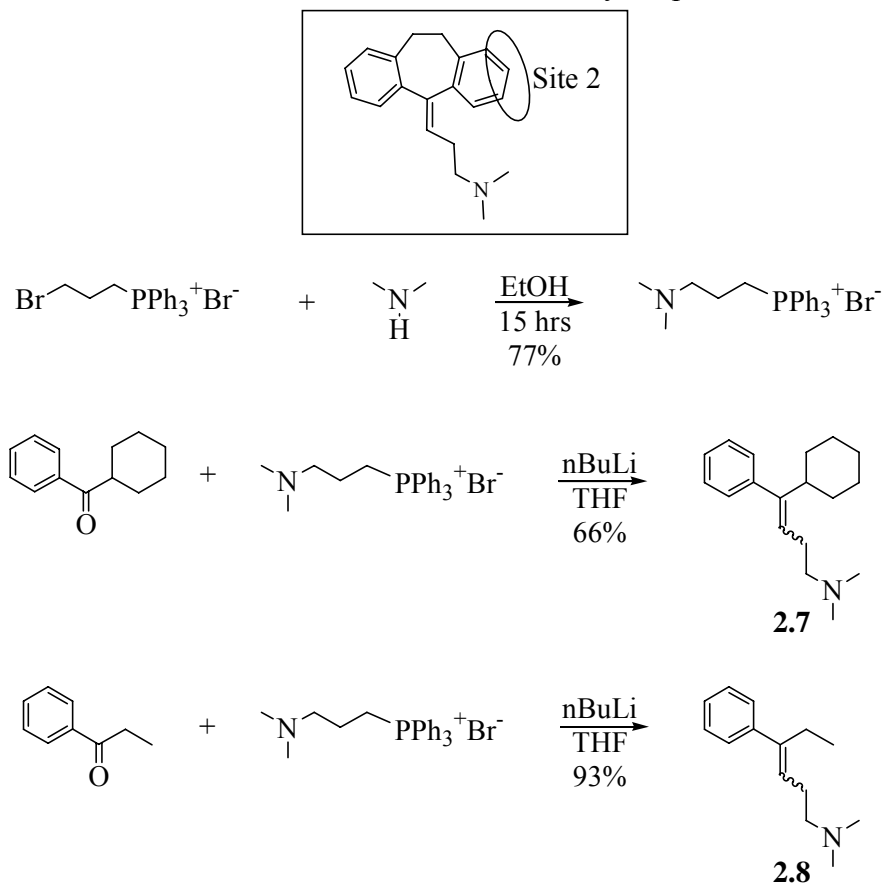


2.2.3 Site 2, Phenyl Ring Replacement

Addition of these organomagnesium complexes proved to be low yielding, in accordance with previously reported studies.²⁵ Herein we have found that a higher yielding and more direct route to these analogues was achieved by formation of the corresponding phosphonium salt for subsequent Wittig addition. Analogues (**2.7**) and

(**2.8**) were synthesized according to these routes in yields of 66% and 93%, respectively (Scheme 2-2).

Scheme 2-2 Modification at Site 2, Phenyl Replacement

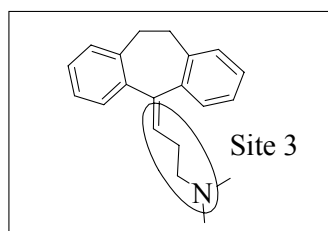


2.2.4 Site 3, Amine Isosteres

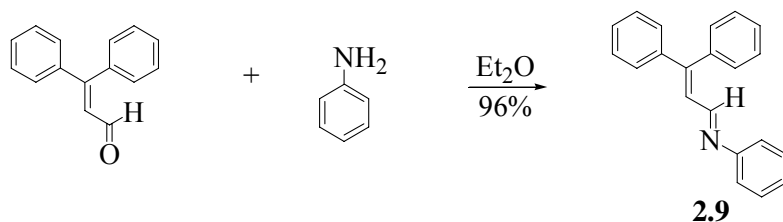
Higher yields were obtained utilizing a freshly distilled THF solution and accurately determining nBuLi concentration through NMR analysis, as previously reported.²⁶ Analogue (**2.9**) was constructed via imine condensation providing the product in 96% yield (Scheme 2-3). Doebner modified-Knoevenagel condensation yielded acid (**2.10**), which was further coupled to dimethylamine using DCC conditions to provide dimethylamide (**2.11**) in 56% yield. Analogue (**2.12**) was achieved by standard Bucherer-Berg conditions to provide the hydantoin in good yield.²⁷ Wittig addition

provided analogues (**2.13**)-(**2.25**) in 43-91% yield (Scheme 2-4). All reactions resulting in a mixture of alkene stereoisomers were used without further separation, so that sufficient quantities for biological testing could be obtained.

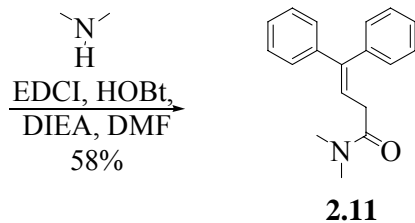
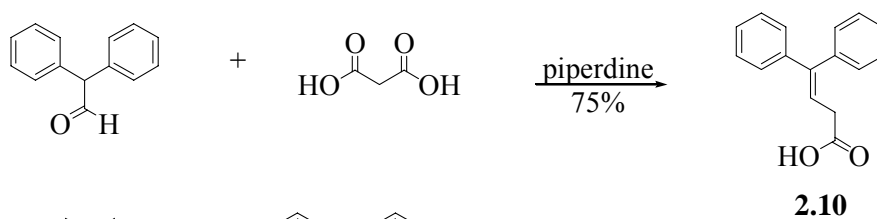
Scheme 2-3 Modification at Site 3, Amine Isosteres



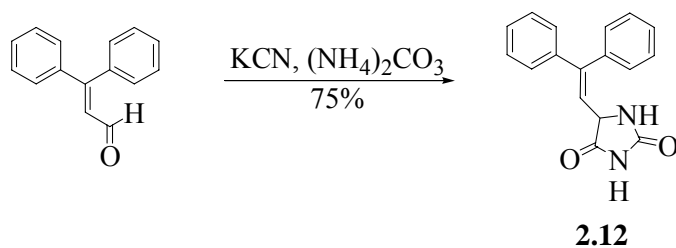
A. Imine Formation



B. Amide Insertion



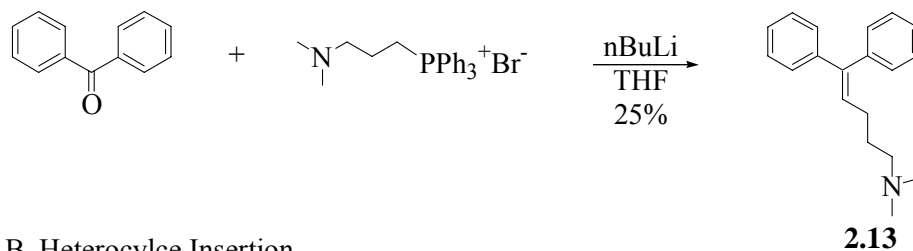
C. Hydantoin Isostere



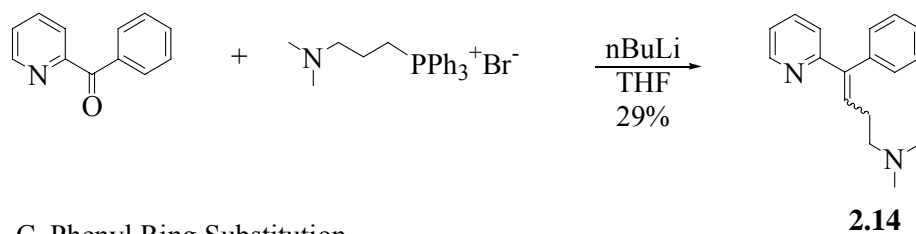
2.2.5 Optimization of Diphenyl Lead

Scheme 2-4 Optimization of Lead Compound (**2.6**)

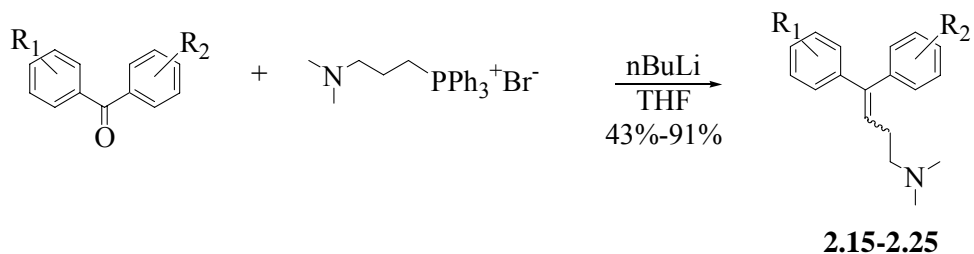
A. Chain Length Modification



B. Heterocycle Insertion



C. Phenyl Ring Substitution



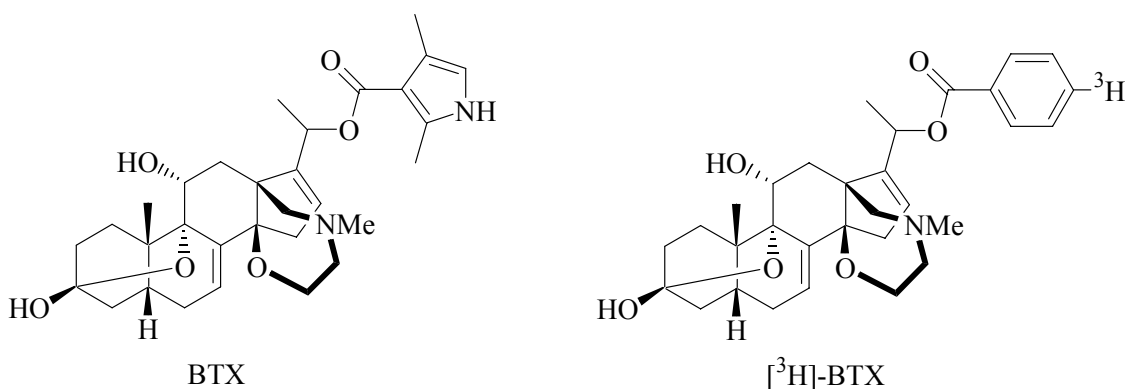
Compound	R_1	R_2	Percent Yield
2.15	2-Cl	H	91%
2.16	3-Cl	H	80%
2.17	4-Cl	H	81%
2.18	2-OMe	H	82%
2.19	3-OMe	H	91%
2.20	4-OMe	H	52%
2.21	2-Me	H	48%
2.22	3-Me	H	43%
2.23	4-Me	H	89%
2.24	2-Cl	2-Cl	68%
2.25	4-Cl	4-Cl	83%

2.3 Results

2.3.1 Binding Assay

The binding affinity of these novel analogues was determined through competitive inhibition assay utilizing [^3H]-BTX, tritiated batrachotoxin (Figure 2-4). Batrachotoxin is a lipid soluble alkaloid released as milky secretions from the granular gland of the poison dart frog, *Phyllobates aurotaenia*, as a defense mechanism.²⁸ The toxin is known to preferentially bind to neurotoxin site 2 of the sodium channel and causes persistent activation of the channel.

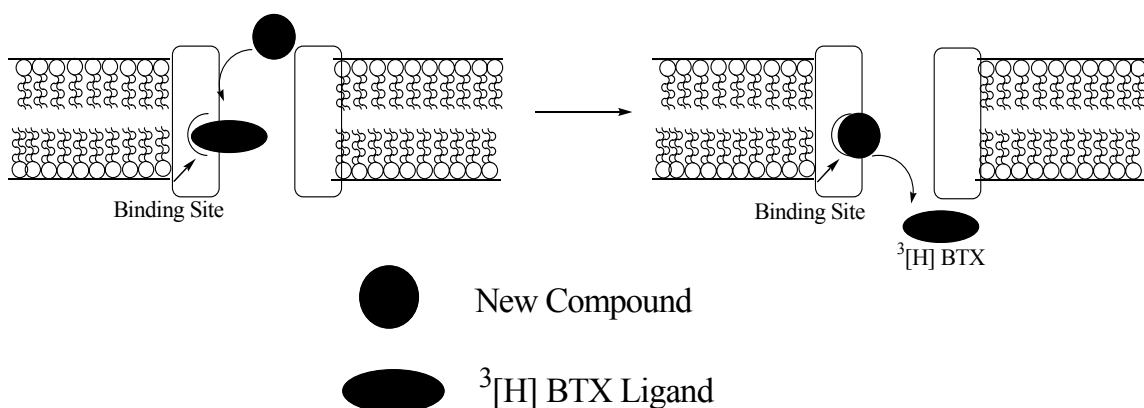
Figure 2-4 Structure of Batrachotoxin and Tritiated Analogue



It has been determined that neurotoxin site 2 overlaps the LA receptor, where numerous sodium channel blocking drugs bind. These include drugs such as local anesthetics, anticonvulsants and antiarrhythmics. Therefore utilization of radiolabelled BTX could provide a facile displacement assay capable of measuring a compound's binding affinity for the sodium channel protein and determine its potential as a local anesthetics-like drug (Figure 2-5).^{29, 30} Although this assay serves as useful diagnostic tool in order to determine the extent of a compound's affinity for sodium channel

binding, it does not provide any adequate information as to current block or state dependency.

Figure 2-5 [^3H]-BTX Displacement Assay



Novel diphenyl amine analogues, synthesized as previously shown, were evaluated at 10 μM for the ability to displace [^3H]-BTX binding from the neuronal voltage-gated sodium channel (NVSC) in prepared rat synaptosomes. All evaluations were carried out in duplicate. In our study, amitriptyline was used as a standard and found to have 89% inhibition at 10 μM .

Incorporation of a tertiary alcohol into the amitriptyline scaffold, as in analogue (2.2) provided equivalent activity with 82% block. Other analogues, (2.3)-(2.13) and (2.14) provided lower binding affinities than amitriptyline ranging from 7%-71% (Table 2-2). Phenyl ring replacement by cyclohexyl provided analogue (2.7) with 85% inhibition. Modification of the diphenyl amine structural class, by various substitutions led to numerous analogues (2.15)-(2.18) and (2.20)-(2.22) with similar or much higher displacement of [^3H]-BTX than amitriptyline, thereby demonstrating this novel class as better binders of the sodium channel protein (Table 2-3).

Table 2-2 [³H]-BTX Displacement of Analogues

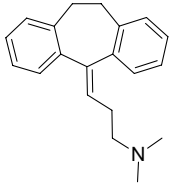
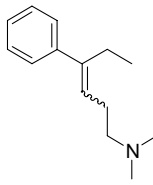
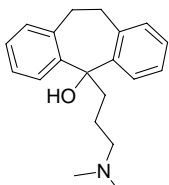
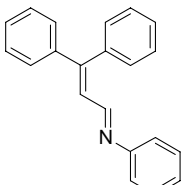
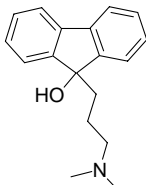
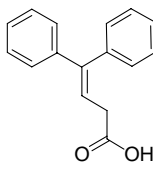
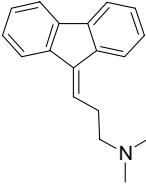
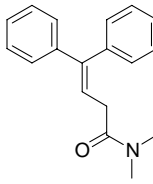
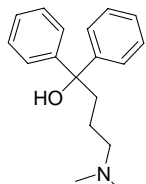
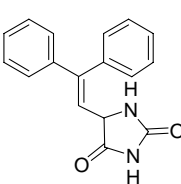
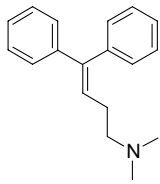
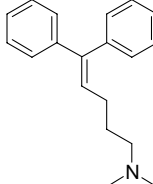
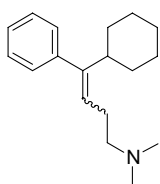
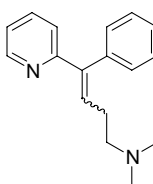
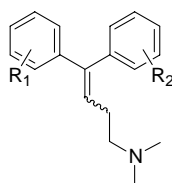
Compound	ID	Percent Inhibition of [³ H]-BTX at 10 μM	Compound	ID	Percent Inhibition of [³ H]-BTX at 10 μM
	2.1	88.73%		2.8	68.75%
	2.2	82.05%		2.9	7.45%
	2.3	19.24%		2.10	27.81%
	2.4	48.70%		2.11	25.93%
	2.5	71.10%		2.12	35.92%
	2.6	67.59%		2.13	69.71%
	2.7	85.41%		2.14	34.47%

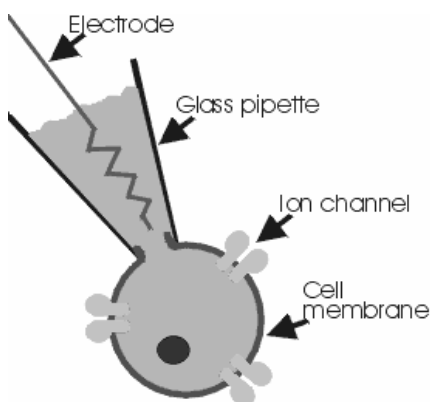
Table 2-3 Optimization of Lead Compound (**2.6**)

Compound	ID	Percent Inhibition of [³ H]-BTX at 10 μ M
R ₁ =2-Cl R ₂ =H	2.15	83.84%
R ₁ =3-Cl R ₂ =H	2.16	79.03%
R ₁ =4-Cl R ₂ =H	2.17	88.09%
R ₁ =2-OMe R ₂ =H	2.18	99.35%
R ₁ =3-OMe R ₂ =H	2.19	70.26%
R ₁ =4-OMe R ₂ =H	2.20	85.05%
R ₁ =2-Me R ₂ =H	2.21	85.33%
R ₁ =3-Me R ₂ =H	2.22	76.83%
R ₁ =4-Me R ₂ =H	2.23	41.70%
R ₁ =2-Cl R ₂ =2-Cl	2.24	63.90%
R ₁ =4-Cl R ₂ =4-Cl	2.25	56.26%

2.3.2 Electrophysiological Analysis

Patch clamp electrophysiology allows for the direct studying of ion channel properties, as well as alteration of these properties upon various drug binding. These methods involve use of a fire polished glass electrode, filled with an intracellular solution, which upon interaction with the cell or neuron causes an increase in resistance (Figure 2-6).³¹ Application of suction then creates a tight seal and a gentle disruption of the membrane, or patch, by the electrode tip allows for electrical continuity. The cell can now be held at varying membrane potentials by use of a computer interface, which allows for examination of sodium channel activity at different channel states.

Figure 2-6 Patch Clamp Electrophysiology

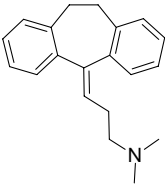
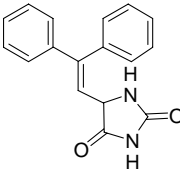
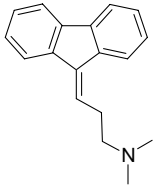
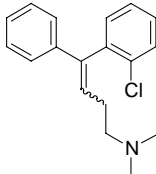


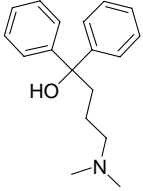
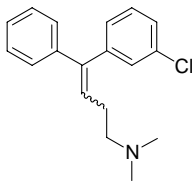
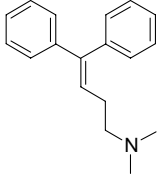
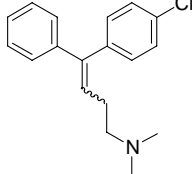
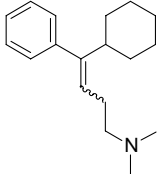
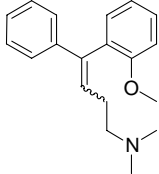
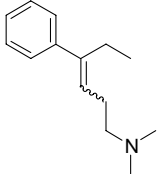
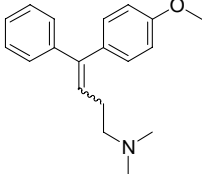
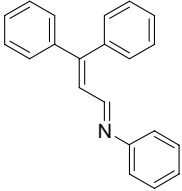
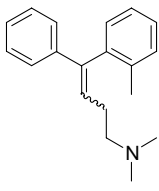
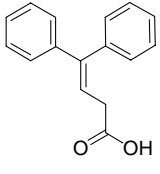
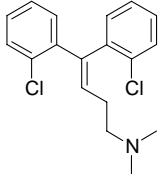
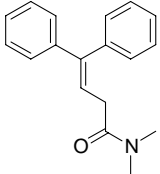
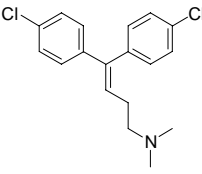
Tonic block is frequently examined by these methods, through the stimulation of a cell or neuron at low frequency. Low frequency protocol often consists of 0.03 Hz application every 30 seconds, at a particular concentration. Use of this protocol allows for a specific block of sodium current and establishes a steady state, or tonic, block. These methods provide key information as to the efficacy of a compound in functionally blocking sodium channel current at a specific concentration. Demonstration of sufficient

tonic block must first be established before subsequent experiments involving state dependency can be conducting, thereby identifying the compound's potential as a therapeutic.

Amitriptyline analogues of this novel class were evaluated for inhibitory tonic effects against firing of hNa_v1.2. These novel diphenyl amine derivatives were able to cause inhibition of sodium current in a range of $10.27\% \pm 2.79$ to $54.33\% \pm 18.85$ at 10 μ M. The currents were elicited using depolarizing pulses from a holding potential of -100 mV to +10 mV, at 15 second intervals. It was found that our standard, amitriptyline, at 10 μ M concentration provided $33.78\% \pm 1.91$ block of the hNa_v1.2 current. Of the eighteen analogues tested, only eight were found to have attenuated block of the sodium current compared with amitriptyline (Table 2-4).

Table 2-4 Percent Block of hNa_v1.2 Current at 10 μ M

Compound	ID	Percent Block of hNa _v 1.2 Current at 10 μ M	Compound	ID	Percent Block of hNa _v 1.2 Current at 10 μ M
	2.1	33.78 ± 1.91 (n=11)		2.12	13.19 ± 2.39 (n=2)
	2.4	48.19 ± 5.87 (n=9)		2.15	36.36 ± 8.43 (n=7)

Compound	ID	Percent Block of hNa _v 1.2 Current at 10μM	Compound	ID	Percent Block of hNa _v 1.2 Current at 10μM
	2.5	18.83 ± 7.95 (n=2)		2.16	49.18 ± 6.54 (n=3)
	2.6	53.24 ± 2.55 (n=6)		2.17	35.78 ± 6.97 (n=3)
	2.7	35.32 ± 3.22 (n=5)		2.18	27.04 ± 4.78 (n=4)
	2.8	10.27 ± 2.79 (n=3)		2.20	22.55 ± 4.36 (n=5)
	2.9	37.49 ± 8.98 (n=3)		2.21	54.33 ± 18.85 (n=2)
	2.10	23.80 ± 2.66 (n=4)		2.24	28.43 ± 4.98 (n=2)
	2.11	15.35 ± 7.98 (n=3)		2.25	39.51 ± 6.03 (n=3)

Evaluation by electrophysiological methods provided data contrary to our initial [^3H]-BTX displacement assay, which yielded few compounds showing substantial activity. However evaluation by patch-clamping has revealed the majority of analogues to be better functional blockers of the sodium channel current than amitriptyline. Our initial lead, diphenyl analogue (**2.6**) provided $53.24\% \pm 2.55$ block of $\text{hNa}_v1.2$ current, which is a 50% increase of sodium current block when compared to amitriptyline (Figure 2-7). Similar or enhanced activity was found for substituted diphenyl analogues (**2.16**) and (**2.21**).

Figure 2-7 Comparing Sample Current Traces of Amitriptyline & Compound (**2.6**)

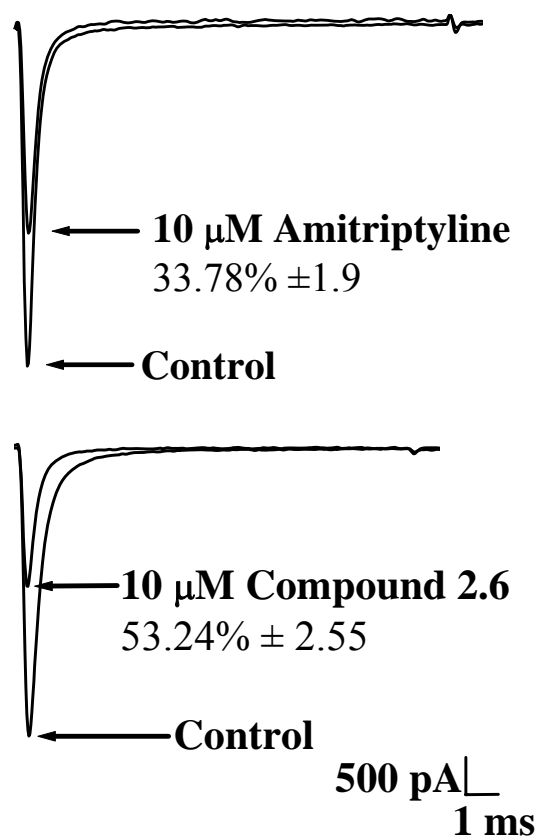
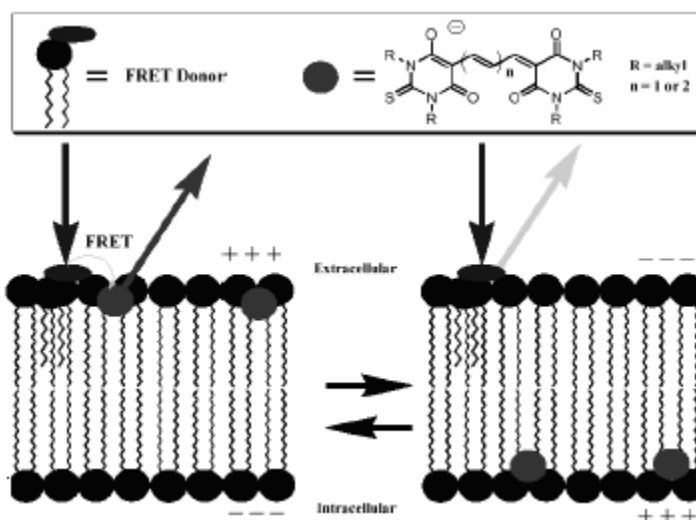


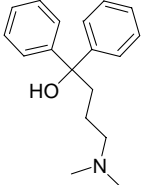
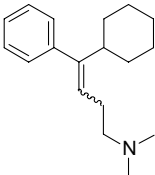
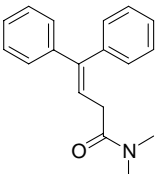
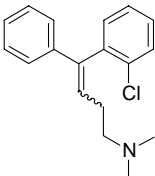
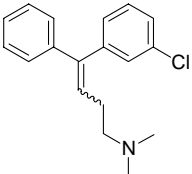
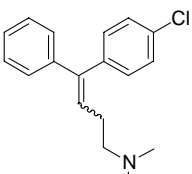
Figure 2-8 FRET Based Assay for Determining Membrane Potential

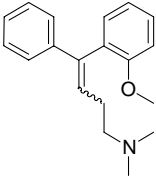
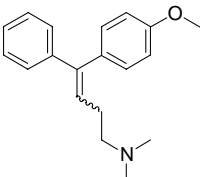
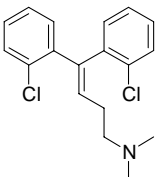
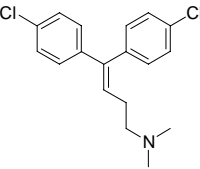


Recent studies have further modified these methods for determining membrane potential by incorporation of an activator, such as brevetoxin or veratridine.³³ These neurotoxins are able to prolong the duration of sodium channel opening, thereby resolving the inherent problem of fast inactivation times. High-throughput screening of potential sodium channel blocking drugs can be conducted by utilization of these methods. Cells are initially incubated with drug and application of an activator allows for channel opening. Membrane depolarization causes sodium ion flux which can be measured by the FRET dye membrane potential-sensing system.³⁴

Several representative analogues of the diphenyl class were evaluated for inhibitory effects in Na_v1.7 and Na_v1.8, by the methods described above. Of the thirteen compounds, ten were found to block sodium current in a non-subtype selective manner (Table 2-5). All effective compounds showed similar effects in both isoforms. Analogues **(2.9)**, **(2.10)** and **(2.12)** had no effect in either isoform which most likely is due to modification of the dimethylamine portion. This may also be attributable to the weak inhibition provided by amide analogue **(2.11)**. Of the ten effective compounds, mono- and di- chloro derivatives proved to be better blockers. These include compounds **(2.15)**, **(2.16)**, **(2.17)**, **(2.24)**, and **(2.25)** which provided inhibition in a range of 81%-100% for both isoforms at 10 μ M. Based on this data, it seems that methoxy analogues, such as **(2.18)** and **(2.20)** are weaker blockers of sodium current than their chloro counterparts.

Table 2-5 Percent Inhibition Based on FRET Modified Assay

Compound	ID	Na _v 1.7				Na _v 1.8			
		0.3 μM	1 μM	3 μM	10 μM	0.3 μM	1 μM	3 μM	10 μM
	2.5	3	0	12	16	-6	6	15	16
	2.7	-2	5	83	101	-1	3	30	88
	2.11	-4	-2	7	26	-2	0	3	17
	2.15	-2	6	40	96	6	9	67	92
	2.16	-6	0	62	100	-5	-3	46	85
	2.17	-6	1	5	83	-12	-15	17	81

Compound	ID	Na _v 1.7				Na _v 1.8			
		0.3 μM	1 μM	3 μM	10 μM	0.3 μM	1 μM	3 μM	10 μM
	2.18	-6	0	3	60	0	-12	6	49
	2.20	1	2	17	79	5	20	50	78
	2.24	-6	1	34	91	-6	12	55	87
	2.25	-7	1	8	91	-5	9	58	91

2.3.4 Animal Model of Anticonvulsant Activity

Drug screening through National Institute of Health's Anticonvulsant Screening Project of the Antiepileptic Drug Discovery Program (NINDS ADDS program) was conducted for anticonvulsant activity in phase I animal trials. Administration of the drug was through oral (p.o.) or intraperitoneal (i.p) methods in healthy animals, those not normally experiencing seizures. Maximum electroshock (MES) was conducted by placing corneal electrode implants and stimulating electric shock every 0.2 seconds in

order to elicit psychomotor based seizures. These methods were used to evaluate a drug's efficacy in impeding further seizures.

Toxicity issues of a drug must also be addressed in correlation to its neuroprotective properties. For this evaluation, the mice were placed on a spinning rod for varying durations to check for loss of reflex or other toxic effects. Those mice capable of walking on the rod for indefinite amounts of time were considered normal, and those falling off within one minute were considered to exhibit signs of neurotoxicity.

Several representative analogues of this class were sent to NINDS for evaluation by these methods. Based on the five analogues tested, **(2.15)**, **(2.16)** and **(2.20)** displayed substantial neuroprotection but suffered greatly from high levels of toxicity (Table 2-6). Compound **(2.9)** showed no protection or toxicity, which is most likely due to the detrimental effects of altering the amine functionality. Only compound **(2.12)** provided moderate protection with little to no harmful effects and is currently undergoing more extensive evaluation by NINDS. From these findings we have been able to determine that the diphenyl class is quite potent in animal models and that determining appropriate dosing regimens will be essential for effective administration of these compounds in *in vivo* studies.

Table 2-6 Phase I Rat Anticonvulsant Data

Compound	Maximum electroshock		Rotorod (Toxicity)	
	300 mg/kg		300 mg/kg	
	0.5 hrs	4.0 hrs	0.5 hrs	4.0 hrs
2.9	0/1	0/1	0/4	0/2
2.12	0/1	1/1	0/4	0/2
2.15	3/3	0/3	4/4	0/0
2.16	3/3	1/3	4/4	0/0
2.20	1/1	0/0	4/4	0/0

2.4 Discussion

The demand for a highly effective treatment of chronic pain without the toxicities associated with most has led us to pursue this area of unmet medical need. In this investigation, we have successfully made analogues of amitriptyline, the most commonly utilized therapeutic for neuropathic pain syndromes. Design and synthesis of analogues was ensued in order to develop more potent therapeutics and to determine essential structural and electronic properties of amitriptyline and its analogues for binding to the sodium channel protein. Modification at three major sites consisting of: alteration of the phenyl ring orientation, replacement of the phenyl ring, and variation of the amine functional group were carried out.

Alteration of the tricyclic portion by either ring contraction or removal of the internal ring resulted in better blockers of hNa_v1.2 current. [³H]-BTX evaluation of the intermediate tertiary alcohols (**2.2**) and (**2.5**) showed similar binding affinities as

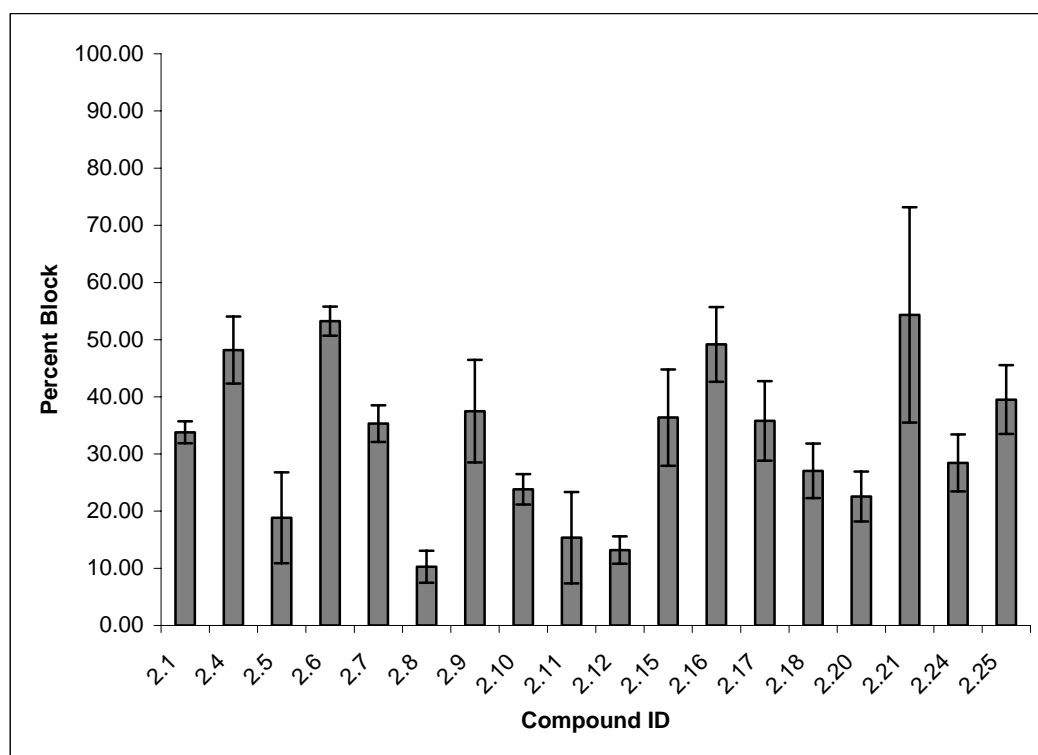
amitriptyline, whereas alcohol (**2.3**) provided substantially less binding and was therefore not pursued for inhibition of Na_v1.2. Dehydration of these analogues led to (**2.4**) and (**2.6**), which had lower binding in the [³H]-BTX evaluation, but functional block revealed that these analogues were better inhibitors of hNa_v1.2 current than amitriptyline. Particularly compound (**2.6**), which provided 53% ± 2.55 inhibition at 10 μM in comparison to amitriptyline with 33% ± 1.91 at 10 μM. From these initial findings, we have been able to develop an inhibitor with over 50% more activity than amitriptyline and provide evidence against current design, by revealing that the tricyclic portion is not essential for inhibition of sodium channel current.^{35, 36}

Analogues were also constructed by replacement of one phenyl ring, by either a cyclohexyl ring (**2.7**) or an ethyl chain (**2.8**). Both (**2.7**) and (**2.8**) showed poor results in the [³H]-BTX assay, and (**2.7**) provided similar functional block to amitriptyline, whereas (**2.8**) was substantially lower. This indicates a degree of steric bulk is required upon phenyl ring replacement for activity.

Analogues consisting of amine isosteres, through modification to a phenyl imine (**2.9**), replacement by a carboxylic acid (**2.10**), conversion to the dimethyl amide (**2.11**), and insertion of a hydantoin ring (**2.12**) were evaluated for [³H]-BTX inhibition. Analogue (**2.9**) afforded very low binding affinity with only 7% inhibition of [³H]-BTX, but had slightly better block of sodium current than amitriptyline. This may indicate that analogue (**2.9**) is blocking the sodium channel by means of an alternate site from the BTX site. Analogues (**2.10**)-(b2.12) were poor inhibitors of both [³H]-BTX and hNa_v1.2 sodium current, indicating that modification of the amine functionality is detrimental to sodium channel activity.

Analogue (**2.6**) demonstrated to be the most potent diphenyl analogue, and we therefore were interested in conducting an optimization of the phenyl ring portion of this lead compound. Modifications incorporating ortho, meta, and para substitutions of the diphenyl structure by -Cl, -OMe, and -Me groups were designed and synthesized. The 2,2-dichloro and 4,4-dichloro analogues were also constructed by similar methods. Substituted analogues (**2.15**)-(**2.18**) and (**2.20**)-(**2.22**) provided similar or higher displacement of [^3H]-BTX than amitriptyline, and substantial block of $\text{hNa}_v1.2$ current by analogues (**2.16**) and (**2.21**) was shown with equal or enhanced activity when compared to lead analogue (**2.6**) (Chart 2-1).

Chart 2-1 Functional Block of $\text{hNa}_v1.2$ upon Compound Administration



We have been able to determine that the [^3H]-BTX displacement assay does not sufficiently explain the functional effects on sodium channel current. This is consistent with site directed mutagenesis studies suggesting the TCA binding site overlaps with only a portion of the local anesthetic site in the channel. The dogma that the tricyclic portion is essential for sodium activity has been disproven, and we have thereby introduced a new class of diphenyl amitriptyline analogues.

More extensive evaluation of this diphenyl class has further proven its potent effects. Several representative diphenyl analogues were also found to substantially block $\text{Na}_v1.7$ and $\text{Na}_v1.8$ currents in a range of 81%-100% for both isoforms at 10 μM . Additionally, NINDS examination of several analogues for anticonvulsant activity in animal model has shown that this class exhibits neuroprotective properties but suffers greatly from toxicity issues due to its high potency. However these adverse effects may be alleviated by future determination of appropriate administration conditions, as well as rational development of additional inhibitors not suffering from such unwanted effects.

2.5 Conclusion

There is a great need for the discovery and development of new analgesics. Herein, we have been able to successfully design and synthesize analogues derived from an amitriptyline scaffold, thereby revealing a potent new class of diphenyl amine sodium channel blockers. We have also been able to prove that the tricyclic portion is unnecessary for block of neuronal sodium channel current, as previously reported. Also, alteration of the amine portion was shown to be detrimental to both binding of the sodium channel protein and block of sodium channel current.

2.6 Experimental Section

2.6.1 Chemistry

All syntheses requiring anhydrous conditions were kept under inert gas, N₂, and conducted in flame-dried glassware. Solvents were obtained from activated alumina stills or were of commercial grade quality. THF obtained directly from the alumina still was further dried by distillation over CaH₂. N-Butyllithium concentrations were determined by NMR methods. Reactions resulting in a mixture of alkene stereoisomers were used without further separation. Melting points were recorded from an Electrothermal Mel-Temp™ melting point apparatus and are uncorrected. ¹H and ¹³C NMRs were conducted on a Varian 300 MHz NMR in CDCl₃ at ambient temperature. High resolution mass spectral (HRMS) data was determined at the University of Illinois Urbana-Champaign School of Chemical Sciences.

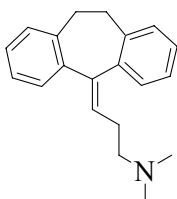
General Procedure A.1: A flame dried flask equipped with condenser, stir bar, and drying tube was kept under N₂. Magnesium shavings (1.5 equiv), finely ground with a mortar and pestle, were placed in the flask along with one small crystal of I₂. Mild heat was applied until an atmosphere of iodine could be visualized. THF, freshly distilled over CaH₂, was now added along with a small amount of MeI (0.001 equiv). The solution was refluxed vigorously for several minutes, after which a freshly distilled solution of dimethylaminopropyl chloride (DMAP-Cl) (1.5 equiv) was added. The solution was refluxed approximately 2-3 hrs, or until disappearance of all magnesium shavings. A separate flame dried flask containing the ketone (1.0 equiv) in THF was obtained and kept at 0 °C, while under an atmosphere of N₂. The Grignard solution was added dropwise to the flask, while trying to decant any remaining magnesium solid. The

reaction was allowed to slowly warm to room temperature overnight and was later quenched by addition of a saturated NH_4Cl solution. The crude product was extracted into CH_2Cl_2 (3 x 50 mL), washed with brine (1 x 20 mL), dried over MgSO_4 , filtered, and evaporated to provide the crude product material. Flash column chromatography was carried out using a CH_2Cl_2 : MeOH system from (100:0)-(9:1).

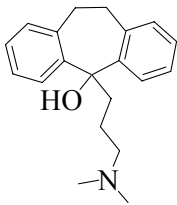
General Procedure A.2: In a flask equipped with stir bar and condenser was added the tertiary alcohol (1.0 equiv) obtained from Procedure A.1. Dehydration was then carried out by refluxing in an ethanolic solution of 7M HCl (> 25 equiv) for 3-4 hrs. The solution was now evaporated, dissolved in water, and basified to a pH=10 with K_2CO_3 . The material was taken up in CH_2Cl_2 and extracted (3 x 50 mL), dried over MgSO_4 , filtered, and evaporated. Flash column chromatography of the crude material was carried out using a CH_2Cl_2 : MeOH system from (100:0)-(10:1).

General Procedure B.1: (3-Bromopropyl) triphenylphosphonium bromide (1.0 equiv) was added to a flame dried flask under N_2 . The salt was then stirred in absolute EtOH at 0 °C and a dimethylamine solution in THF (1.5 equiv) was added dropwise. The solution was stirred with warming to room temperature for over 15 hrs. The solvent was then evaporated and the salt used directly without further purification. Note: (4-Dimethylaminobutyl) triphenylphosphonium bromide was made similarly for analogue **(13)**.

General Procedure B.2: (3-Dimethylaminopropyl) triphenylphosphonium bromide (1.5-2.0 equiv) obtained from Procedure B.1 was placed in a flame dried flask containing freshly distilled THF and kept under N₂. The mixture was cooled to 0 °C and a solution of 2.5 M nBuLi in hexane (1.5-2.0 equiv) was added dropwise. Stirring was continued for several minutes, after which the ketone (1.0 equiv) was added slowly. The reaction was allowed to continue stirring overnight with warming to room temperature and was later quenched by addition of a saturated NH₄Cl solution. The crude material was then extracted into CH₂Cl₂ (3 x 50 mL), washed with brine (1 x 20 mL), dried over MgSO₄, filtered, and evaporated to provide the crude product. Flash column chromatography was carried out using a CH₂Cl₂: MeOH system from (100:0)-(9:1).

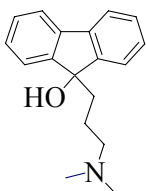


[3-(10,11-Dihydro-dibenzo[a,d]cyclohepten-5-ylidene)-propyl]-dimethyl-amine hydrochloride (**2.1**). Procedure A.2 was carried out using the tertiary alcohol (0.5 g, 1.7 mmol) and 7M HCl/EtOH (15 mL). The product was obtained in 0.29 g as an off-white solid in 63% yield. TLC: CH₂Cl₂: MeOH (10:1), R_f=0.431. ¹H NMR (CDCl₃, 300 MHz) δ 7.27-7.03 (m, 8H), 5.78-5.73 (t, 3H, *J*=7.5 Hz), 3.30-3.26 (m, 2H), 3.12-3.10 (m, 1H), 2.97-2.88 (m, 2H), 2.80-2.76 (m, 1H), 2.66 (br s, 8H); ¹³C NMR (CDCl₃, 75.5 MHz) δ 146.55, 139.39, 138.57, 138.34, 136.42, 129.58, 127.85, 127.57, 127.09, 126.95, 125.65, 125.56, 122.89, 56.27, 42.40, 41.65, 33.02, 31.35, 23.69. ESIMS: 278 (M+H). Lit mp=193-194 °C, mp=175-182°C.

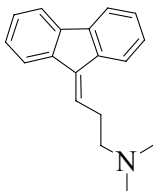


5-(3-Dimethylamino-propyl)-10,11-dihydro-5H-dibenzo[a,d]cyclohepten-5-ol **(2.2)**.

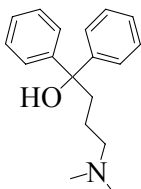
Procedure A.1 was carried out using DMAP-Cl (1.25 g, 10.25 mmol), Mg^0 (0.25 g, 10.25 mmol), dibenzosuberone (1.6 g, 7.6 mmol), and THF (5 mL). The product was obtained in 1.5 g as a white solid in 68% yield. TLC: CH_2Cl_2 : MeOH (10:1), $R_f=0.24$. ^1H NMR (CDCl_3 , 300 MHz) δ 8.13-8.11 (appt d, 2H, $J=7.5$ Hz), 7.28-7.11 (m, 6H), 3.56-3.48 (m, 2H), 3.07-3.02 (m, 2H), 2.57-2.53 (m, 2H), 2.24 (br s, 8H), 1.40 (br s, 2H); ^{13}C NMR (CDCl_3 , 75.5 MHz) δ 146.63, 137.99, 130.91, 127.55, 127.44, 126.61, 77.01, 60.37, 45.89, 45.06, 34.47, 23.06. APCIMS: 296 (M+H). Lit mp=118-120°C, mp=119-120°C.



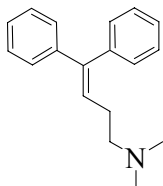
9-(3-Dimethylamino-propyl)-9H-fluoren-9-ol **(2.3)**. Procedure A.1 was carried out using DMAP-Cl (0.91 g, 7.5 mmol), Mg^0 (0.18 g, 7.5 mmol), fluorenone (0.9 g, 5.0 mmol), and THF (15 mL). The product was obtained in 0.25 g as a yellow solid in 39% yield. TLC: CH_2Cl_2 : MeOH (10:1), $R_f=0.18$. ^1H NMR (CDCl_3 , 300 MHz) δ 7.60-7.58 (d, 2H, $J=6.0$ Hz), 7.45-7.42 (d, 2H, $J=9.0$ Hz), 7.38-7.10 (m, 4H), 4.80 (br s, 1H), 2.05-1.91 (m, 4H), 1.85 (s, 6H), 1.21-1.09 (m, 2H); ^{13}C NMR (CDCl_3 , 75.5 MHz) δ 149.62, 139.24, 128.29, 127.54, 123.53, 119.56, 81.31, 59.39, 44.51, 38.03, 21.62. ESIMS: 268 (M+H). Lit mp=101-103°C, mp=78-82°C.



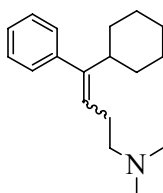
(3-Fluoren-9-ylidene-propyl)-dimethyl-amine (**2.4**). Procedure A.2 was carried out using the tertiary alcohol (0.1 g, 0.37 mmol) and 7M HCl/EtOH (10 mL). The product was obtained in 54 mg as an orange solid in 56% yield. TLC: CH₂Cl₂: MeOH (10:1), R_f=0.30. ¹H NMR (CDCl₃, 300 MHz) δ 7.88-7.65 (m, 4H), 7.22-7.45 (m, 4H), 6.78-6.73 (t, 1H, *J*=7.5 Hz), 3.15-2.95 (m, 2H), 2.68-2.63 (t, 2H, *J*=7.2 Hz), 2.35 (s, 6H); ¹³C NMR (CDCl₃, 75.5 MHz) δ 148.76, 132.16, 131.83, 130.85, 128.94, 128.70, 127.93, 127.07, 119.97, 59.20, 44.85, 27.48. ESIMS: 250 (M+H). mp=110–115°C.



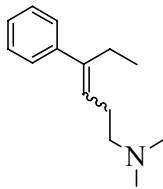
(3-Fluoren-9-ylidene-propyl)-dimethyl-amine (**2.5**). Procedure A.1 was carried out using DMAP-Cl (0.77 g, 6.2 mmol), Mg⁰ (0.15 g, 6.2 mmol), benzophenone (0.73 g, 4.0 mmol), and THF (10 mL). The product was obtained in 0.65 g as a white solid in 61% yield. TLC: CH₂Cl₂: MeOH (10:1), R_f=0.19. ¹H NMR (CDCl₃, 300 MHz) δ 7.55-7.49 (m, 4H), 7.34-7.27 (m, 5H), 7.23-7.18 (m, 1H), 2.57-2.51 (m, 4H), 2.24 (s, 6H), 1.68-1.61 (m, 2H). ESIMS: 270 (M+H). Lit mp=120-123°C, mp=118–120°C.



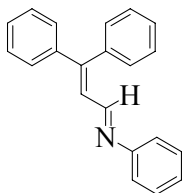
(4,4-Diphenyl-but-3-enyl)-dimethyl-amine (**2.6**). Procedure A.2 was carried out using the tertiary alcohol (0.25 g, 0.93 mmol) and 7M HCl/EtOH (10 mL). The product was obtained in 0.18 g as a pale yellow oil in 78% yield. TLC: CH₂Cl₂: MeOH (10:1), R_f=0.36. ¹H NMR (CDCl₃, 300 MHz) δ 7.37-7.18 (m, 10H), 6.13-6.08 (t, 1H, *J*=7.2 Hz), 2.45-2.41 (t, 2H, *J*=6.6 Hz), 2.34-2.30 (t, 2H, *J*=7.1 Hz), 2.22 (s, 6H); ¹³C NMR (CDCl₃, 75.5 MHz) δ 142.67, 142.43, 139.98, 132.04, 131.96, 131.86, 129.71, 128.49, 128.40, 128.17, 128.00, 127.15, 126.95, 126.87, 59.48, 45.22, 28.09. ESIMS: 252 (M+H).



(4-Cyclohexyl-4-phenyl-but-3-enyl)-dimethyl-amine (**2.7**). Procedure B.2 was carried out using (3-dimethylaminopropyl) triphenylphosphonium bromide (1.14 g, 2.66 mmol) from procedure B.1, 2.5 M nBuLi/Hex (1 mL, 2.60 mmol), cyclohexyl phenyl ketone (0.25g, 1.33 mmol), and THF (5 mL). The product was obtained in 0.18 g as a pale yellow oil in 66% yield. TLC: CH₂Cl₂: MeOH (10:1), R_f=0.33. ¹H NMR (CDCl₃, 300 MHz) δ 7.35-7.23 (m, 4H), 7.11-7.03 (m, 2H), 5.42-5.34 (m, 0.80H), 5.21-5.19 (br m, 0.17H), 2.42-2.33 (m, 4H), 2.20 (s, 6H) 2.08-2.05 (m, 2H), 1.74-1.65 (br m, 5H), 1.29-1.07 (br m, 5H); ¹³C NMR (CDCl₃, 75.5 MHz) δ 149.05, 141.38, 128.80, 128.00, 127.55, 126.49, 125.90, 121.54, 59.89, 59.68, 46.27, 45.44, 45.00, 32.43, 32.18, 26.83, 26.41. ESIMS: 258 (M+H). HRMS calcd for C₁₈H₂₇N: 258.2216; Found: 258.2222.

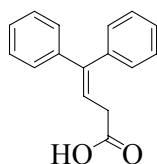


Dimethyl-(4-phenyl-hex-3-enyl)-amine (**2.8**). Procedure B.2 was carried out using (3-dimethylaminopropyl) triphenylphosphonium bromide (1.6 g, 3.73 mmol) from procedure B.1, 2.5 M nBuLi/Hex (1.5 mL, 3.73 mmol), propiophenone (0.25g, 1.86 mmol), and THF (5 mL). The product was obtained in 0.70 g as a white solid in 93% yield. TLC: CH₂Cl₂: MeOH (10:1), R_f=0.6. ¹H NMR (CDCl₃, 300 MHz) δ 7.32-7.18 (m, 4H), 7.18-7.08 (appt d, 1H, *J*=8.4 Hz), 5.58-5.54 (t, 0.41H, *J*=6.8 Hz), 5.41-5.36 (t, 0.58H, *J*=7.2 Hz), 2.52-2.44 (m, 4H), 2.38 (s, 3H), 2.27 (s, 3H), 2.21-2.14 (appt q, 2H, *J*=7.6 Hz), 0.98-0.90 (m, 3H); ¹³C NMR (CDCl₃, 75.5 MHz) δ 146.01, 143.97, 142.52, 140.91, 128.28, 128.18, 126.86, 126.39, 123.63, 120.91, 59.02, 58.77, 44.73, 44.15, 32.26, 26.03, 25.68, 23.21, 13.67, 12.97. ESIMS: 204 (M+H). HRMS calc for C₁₄H₂₁N: 204.1747. Found: 204.1752. mp=104-110°C.

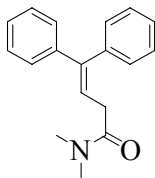


Dimethyl-(4-phenyl-hex-3-enyl)-amine (**2.9**). In a flame dried flask under N₂, β-phenyl cinnamaldehyde (0.25 g, 1.2 mmol) was stirred in dry ether and kept at room temperature. Aniline (0.11 mL, 1.2 mmol) was now added dropwise and allowed to stir for an additional 30 min. The solution was evaporated to provide the product in 0.33 g as a yellow solid in 96% yield. TLC: Hex: EtOAc (5:1), R_f=0.32. ¹H NMR (CDCl₃, 300 MHz) δ 8.17-8.14 (m, 1H), 7.46-7.07 (m, 15H), 6.80-6.69 (m, 1H); ¹³C NMR (CDCl₃,

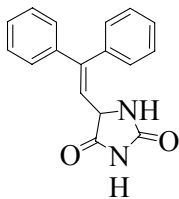
75.5 MHz) δ 160.73, 141.04, 138.53, 130.77, 129.46, 129.38, 128.81, 128.75, 128.67, 128.44, 127.53, 126.31, 121.29, 118.82, 115.37. ESIMS 284 (M+H). Lit mp=99°C, mp=98-100°C.



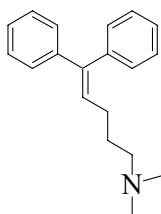
4,4-Diphenyl-but-3-enoic acid (**2.10**). Diphenyl acetaldehyde (0.91 mL, 5.1 mmol), malonic acid (0.54 g, 5.1 mmol), and piperidine (0.5 mL, 5.1 mmol) were added to a flame dried flask and kept under inert conditions. The mixture was heated to 85 °C for 3 hrs. The solution was then cooled to room temperature, evaporated, and taken up in water to be acidified to pH=2 with HCl. Extraction was carried out by addition of EtOAc (3 x 50 mL) and dried by washing with brine (1 x 20 mL). The organic layers were combined, dried over MgSO₄, filtered, and evaporated to provide the product in 0.9 g as an off-white solid in 75% yield. TLC: Hex: EtOAc (1:1), R_f=0.30. ¹H NMR (CDCl₃, 300 MHz) δ 7.28-7.07 (m, 10H), 6.16-6.12 (t, 1H, *J*=7.1 Hz), 3.11-3.09 (d, 2H, *J*=7.2 Hz); ¹³C NMR (CDCl₃, 75.5 MHz) δ 178.29, 145.36, 141.95, 139.22, 129.88, 128.60, 128.33, 127.66, 119.74, 35.37. APCIMS: 239 (M+H). Lit mp=117-118°C, mp=105-108°C.



4,4-Diphenyl-but-3-enoic acid dimethylamide (**2.11**). Under anhydrous conditions, 4,4-diphenyl-but-3-enoic acid (0.47 g, 1.96 mmol), EDCI (0.6 g, 3.06 mmol), HOBT (0.34 g, 2.51 mmol), and 2.0 M dimethylamine in THF (4.2 mL, 8.4 mmol) were added to a flask containing dry DMF (30 mL). DIEA (1.83 mL, 10.5 mmol) was added and the mixture was allowed to stir for 48 hr at room temperature. After this time the DMF was removed by evaporation under reduced pressure, and the resulting orange residue was taken up in CH₂Cl₂. The material was extracted with water (6 x 50 mL) to remove any remaining DMF solvent. The organic layer was then washed with 1 M NaOH (3 x 50 mL), 10% citric acid (3 x 50 mL), water (1 x 50 mL), and brine (1 x 50 mL). The organic layer was dried over MgSO₄, filtered, and evaporated to provide 0.3 g of a brownish-red oil. Flash column chromatography was conducted using a CH₂Cl₂:MeOH system from (100:1)-(10:1). The product was obtained in 0.30 g as a pale orange solid in 58% yield. TLC: CH₂Cl₂: MeOH (32:1), R_f=0.27. ¹H NMR (CDCl₃, 300 MHz) δ 7.39-7.21 (m, 10H), 6.35-6.30 (t, 1H, *J*=7.2 Hz), 3.19-3.17 (d, 2H, *J*=7.2 Hz), 2.94 (s, 3H), 2.83 (s, 3H); ¹³C NMR (CDCl₃, 75.5 MHz) δ 170.61, 143.20, 141.45, 139.00, 131.53, 131.38, 129.20, 127.76, 127.47, 126.81, 126.74, 126.63, 121.57, 36.60, 34.90, 34.22. mp=67-72°C.

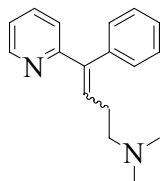


5-(2, 2-Diphenyl-vinyl)-imidazolidine-2,4-dione (**2.12**). To a solution of β -phenyl cinnamaldehyde (1.0 g, 4.8 mmol) in 50% aq. EtOH (10 mL) was added KCN (0.95 g, 14.4 mmol) and $(\text{NH}_4)_2\text{CO}_3$ (3.0 g, 28.8 mmol). The reaction was heated to 65 °C for 1 day, after which the solution was cooled to room temperature and extracted with CH_2Cl_2 (3 x 50 mL). The organic layers were combined, dried over MgSO_4 , filtered, and evaporated to provide a crude brown solid. Purification by flash chromatography was carried out in a system of CH_2Cl_2 : MeOH from (40:1)-(10:1). The product was obtained as an off-brown solid in 75% yield. TLC: Hex: EtOAc (1:1) R_f =0.23. ^1H NMR (CDCl_3 , 300 MHz) δ 7.50-7.23 (m, 12H), 6.22-6.19 (m, 1H), 4.87 (br s, 1H); ^{13}C NMR (CDCl_3 , 75.5 MHz) δ 177.64, 169.23, 162.38, 159.43, 146.49, 144.84, 144.71, 143.05, 133.47, 132.91, 132.49, 132.27, 131.59, 131.48, 131.31, 130.38, 117.94, 61.47. APCIMS: 279 (M+H). HRMS calcd for $\text{C}_{17}\text{H}_{14}\text{N}_2\text{O}_2$: 279.1123; Found: 279.1134. mp=135-138°C.

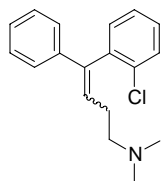


(5, 5-Diphenyl-pent-4-enyl)-dimethyl-amine (**2.13**). Procedure B.2 was carried out using (4-dimethylaminobutyl) triphenylphosphonium bromide (1.0 g, 2.3 mmol) from procedure B.1, 2.5 M $n\text{BuLi}$ /Hex (0.96 mL, 2.3 mmol), benzophenone (0.3 g, 1.50 mmol), and THF (15 mL). The product was obtained in 0.44 g as a pale yellow oil in 25% yield. TLC: CH_2Cl_2 : MeOH (10:1), R_f =0.23. ^1H NMR (CDCl_3 , 300 MHz) δ 7.75-

7.63 (m, 2H), 7.31-7.05 (m, 8H), 5.99-5.94 (m, 1H), 2.65-2.60 (m, 2H), 2.48 (s, 6H), 2.16-2.05 (m, 2H), 1.82-1.74 (m, 2H); ^{13}C NMR (CDCl_3 , 75.5 MHz) δ 142.78, 142.03, 139.56, 135.12, 133.53, 133.41, 130.50, 129.59, 128.16, 127.97, 127.41, 127.04, 126.97, 58.01, 43.72, 26.95, 25.82. ESIMS: 266 (M+H). HRMS calcd for $\text{C}_{19}\text{H}_{23}\text{N}$: 266.1913; Found: 266.1909.

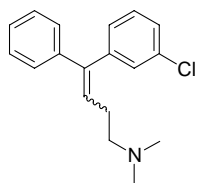


Dimethyl-(4-phenyl-4-pyridin-2-yl-but-3-enyl)-amine (**2.14**). Procedure B.2 was carried out using (3-dimethylaminopropyl) triphenylphosphonium bromide (1.74 g, 4.0 mmol) from procedure B.1, 2.5 M nBuLi/Hex (1.6 mL, 4.0 mmol), 2-pyridinyl phenyl ketone (0.5 g, 2.7 mmol), and THF (5 mL). The product was obtained in 0.68 g as a brown oil in 29% yield. TLC: CH_2Cl_2 : MeOH (10:1), R_f =0.55. ^1H NMR (CDCl_3 , 300 MHz) δ 8.53-8.49 (m, 1H), 7.42-7.25 (m, 4H), 7.16-7.13 (m, 2H), 7.01-6.98 (m, 1H), 6.88-6.77 (m, 2H), 2.41-2.36 (appt t, 2H, J =6.9 Hz), 2.27-2.22 (appt t, 2H, J =7.7 Hz), 2.11 (s, 6H); ^{13}C NMR (CDCl_3 , 75.5 MHz) δ 158.45, 149.21, 141.82, 138.83, 136.36, 131.11, 129.94, 128.62, 127.41, 122.26, 121.81, 59.30, 45.32, 28.06. ESIMS: 253 (M+H). HRMS calcd for $\text{C}_{17}\text{H}_{20}\text{N}_2$: 253.1701; Found: 253.1705.

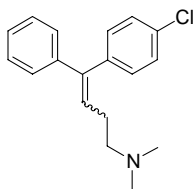


[4-(2-Chloro-phenyl)-4-phenyl-but-3-enyl]-dimethyl-amine (**2.15**). Procedure B.2 was carried out using (3-dimethylaminopropyl) triphenylphosphonium bromide (1.5 g, 3.5

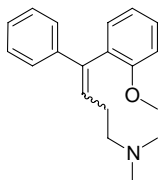
mmol) from procedure B.1, 2.5 M nBuLi/Hex (1.4 mL, 3.5 mmol), 2-chlorobenzophenone (0.5 g, 2.3 mmol), and THF (5 mL). The product was obtained in 0.6 g as a clear oil in 91% yield. TLC: CH₂Cl₂: MeOH (10:1), R_f=0.22. ¹H NMR (CDCl₃, 300 MHz) δ 7.71-7.20 (m, 9H), 6.28-6.23 (t, 1H, *J*=7.4 Hz), 2.65-2.63 (m, 2H), 2.37 (s, 6H), 2.33-2.25 (m, 2H); ¹³C NMR (CDCl₃, 75.5 MHz) δ 141.24, 140.18, 138.45, 132.34, 132.21, 131.74, 130.04, 129.16, 128.74, 128.61, 127.64, 127.61, 127.23, 126.49, 126.25, 58.24, 44.43, 27.17, 27.08. APCIMS: 285 (M), 287(M+2). HRMS calcd for C₁₈H₂₀ClN: 286.1355; Found: 286.1363.



[4-(3-Chloro-phenyl)-4-phenyl-but-3-enyl]-dimethyl-amine (**2.16**). Procedure B.2 was carried out using (3-dimethylaminopropyl) triphenylphosphonium bromide (1.5 g, 3.5 mmol) from procedure B.1, 2.5 M nBuLi/Hex (1.4 mL, 3.5 mmol), 3-chlorobenzophenone (0.5 g, 2.3 mmol), and THF (5 mL). The product was obtained in 0.5 g as a pale yellow oil in 80% yield. TLC: CH₂Cl₂: MeOH (10:1), R_f=0.22. ¹H NMR (CDCl₃, 300 MHz) δ 7.39-7.09 (m, 9H), 6.12-6.07 (m, 1H), 2.51-2.46 (appt t, 2H, *J*=7.4 Hz), 2.37-2.33 (m, 2 H), 2.27 (br s, 6H); ¹³C NMR (CDCl₃, 75.5 MHz) δ 144.58, 142.00, 139.48, 134.35, 134.31, 132.39, 132.25, 132..18, 129.90, 129.49, 128.81, 128.65, 128.43, 128.25, 127.98, 127.43, 127.16, 125.69, 59.58, 45.46, 45.42, 28.30, 28.25. APCIMS: 285 (M), 287(M+2).

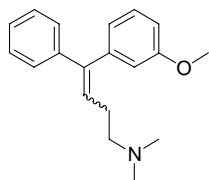


[4-(4-Chloro-phenyl)-4-phenyl-but-3-enyl]-dimethyl-amine (**2.17**). Procedure B.2 was carried out using (3-dimethylaminopropyl) triphenylphosphonium bromide (1.5 g, 3.5 mmol) from procedure B.1, 2.5 M nBuLi/Hex (1.4 mL, 3.5 mmol), 4-chlorobenzophenone (0.5 g, 2.3 mmol), and THF (5 mL). The product was obtained in 0.54 g as an off-white semisolid in 81% yield. TLC: CH₂Cl₂: MeOH (10:1), R_f=0.22. ¹H NMR (CDCl₃, 300 MHz) δ 7.70-7.10 (m, 9H), 6.12-6.07 (m, 1H), 2.42-2.37 (m, 2H), 2.32-2.26 (m, 2H), 2.19 (s, 6H); ¹³C NMR (CDCl₃, 75.5 MHz) δ 142.18, 141.74, 139.65, 138.58, 132.25, 132.12, 132.05, 131.29, 129.80, 128.68, 128.58, 128.45, 128.26, 127.83, 127.73, 127.31, 127.29, 59.57, 45.44, 28.35, 28.27. APCIMS: 285 (M), 287(M+2).

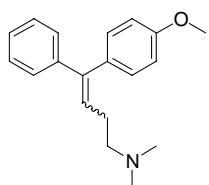


[4-(2-Methoxy-phenyl)-4-phenyl-but-3-enyl]-dimethyl-amine (**2.18**). Procedure B.2 was carried out using (3-dimethylaminopropyl) triphenylphosphonium bromide (1.5 g, 3.6 mmol) from procedure B.1, 2.5 M nBuLi/Hex (1.4 mL, 3.6 mmol), 2-methoxy benzophenone (0.5 g, 2.4 mmol), and THF (5 mL). The product was obtained in 0.54 g as a white semisolid in 82% yield. TLC: CH₂Cl₂: MeOH (10:1), R_f=0.19. ¹H NMR (CDCl₃, 300 MHz) δ 7.32-6.95 (m, 9H), 6.24-6.19 (t, 1H, *J*=7.4 Hz), 3.71 (s, 3H), 2.50-2.45 (m, 2H), 2.25-2.18 (br s, 8H); ¹³C NMR (CDCl₃, 75.5 MHz) δ 157.19, 141.77, 139.01,

131.43, 128.76, 128.14, 127.62, 126.78, 126.34, 120.71, 111.26, 59.31, 55.64, 45.38, 28.40. ESIMS: 282 (M+H). HRMS calc for C₁₉H₂₃NO: 282.1847; Found: 282.1858.

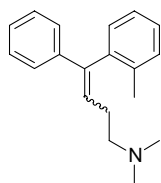


[4-(3-Methoxy-phenyl)-4-phenyl-but-3-enyl]-dimethyl-amine (**2.19**). Procedure B.2 was carried out using (3-dimethylaminopropyl) triphenylphosphonium bromide (2.4 g, 5.6 mmol) from procedure B.1, 2.5 M nBuLi/Hex (2.2 mL, 5.6 mmol), 3-methoxybenzophenone (0.6 g, 2.8 mmol), and THF (15 mL). The product was obtained in 0.75 g as a pale yellow oil in 91% yield. TLC: CH₂Cl₂: MeOH (10:1), R_f=0.19. ¹H NMR (CDCl₃, 300 MHz) δ 7.80-7.60 (m, 7 H), 7.27-7.16 (m, 2H), 6.56-6.50 (m, 1H), 4.23 (s, 1H), 4.19 (s, 2H), 2.92-2.87 (m, 2H), 2.78-2.74 (m, 2H), 2.67 (s, 6H); ¹³C NMR (CDCl₃, 75.5 MHz) δ 159.65, 159.54, 144.09, 142.75, 141.52, 140.00, 129.84, 129.11, 128.35, 127.23, 122.34, 120.00, 115.46, 113.34, 112.62, 112.28, 59.60, 59.56, 55.24, 45.35, 28.23, 28.18. ESIMS: 282 (M+H). HRMS calcd for C₁₉H₂₃NO: 282.1851; Found: 282.1858.

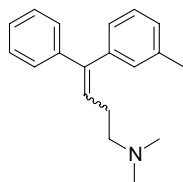


[4-(4-Methoxy-phenyl)-4-phenyl-but-3-enyl]-dimethyl-amine (**2.20**). Procedure B.2 was carried out using (3-dimethylaminopropyl) triphenylphosphonium bromide (1.5 g, 3.6 mmol) from procedure B.1, 2.5 M nBuLi/Hex (1.4 mL, 3.6 mmol), 4-methoxybenzophenone (0.5 g, 2.4 mmol), and THF (10 mL). The product was obtained

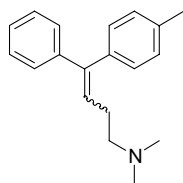
in 0.34 g as a yellow-orange oil in 52% yield. TLC: CH₂Cl₂: MeOH (10:1), R_f=0.22. ¹H NMR (CDCl₃, 300 MHz) δ 7.52-7.15 (m, 7H), 6.97-6.95 (d, 1H, *J*=8.1 Hz), 6.86-6.83 (d, 1H, *J*=8.4 Hz), 6.11-6.03 (m, 1H), 3.89 (s, 1.5H), 3.84 (s, 1.5H), 2.50-2.47 (m, 2H), 2.41-2.33 (m, 2H), 2.28 (s, 6H); ¹³C NMR (CDCl₃, 75.5 MHz) δ 158.95, 158.79, 143.03, 142.57, 140.38, 135.31, 132.12, 131.08, 129.88, 128.40, 128.21, 127.48, 127.11, 124.96, 113.61, 59.64, 55.38, 45.29, 28.20, 28.03. ESIMS: 282 (M+H).



Dimethyl-(4-phenyl-4-o-tolyl-but-3-enyl)-amine (**2.21**). Procedure B.2 was carried out using (3-dimethylaminopropyl) triphenylphosphonium bromide (1.9 g, 4.6 mmol) from procedure B.1, 2.5 M nBuLi/Hex (1.8 mL, 4.6 mmol), 2-methylbenzophenone (0.6 g, 3.1 mmol), and THF (10 mL). The product was obtained in 0.4 g as a pale beige semisolid in 48% yield. TLC: CH₂Cl₂: MeOH (10:1), R_f=0.17. ¹H NMR (CDCl₃, 300 MHz) δ 7.25-7.16 (m, 8H), 7.12-7.10 (m, 1H), 6.25-6.20 (t, 0.82H, *J*=7.4 Hz), 5.68-5.64 (t, 0.16H, *J*=6.8 Hz), 2.55-2.49 (m, 0.38H), 2.45-2.40 (appt t, 1.65H, *J*=7.8 Hz), 2.27 (s, 1H), 2.21 (s, 5H), 2.16 (br s, 1.6H), 2.13 (br s, 0.32H), 2.07 (s, 2.49H), 2.04 (s, 0.5H); ¹³C NMR (CDCl₃, 75.5 MHz) δ 141.95, 140.79, 139.02, 136.31, 130.10, 129.82, 129.08, 128.86, 128.15, 127.90, 127.23, 127.03, 126.82, 126.68, 126.20, 126.08, 125.65, 125.43, 59.49, 58.96, 45.13, 44.99, 27.71, 27.53, 20.36, 19.54. ESIMS: 266 (M+H). HRMS calcd for C₁₉H₂₃N: 266.1904; Found: 266.1909.

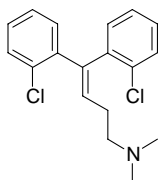


Dimethyl-(4-phenyl-4-m-tolyl-but-3-enyl)-amine (**2.22**). Procedure B.2 was carried out using (3-dimethylaminopropyl) triphenylphosphonium bromide (1.9 g, 4.6 mmol) from procedure B.1, 2.5 M nBuLi/Hex (1.8 mL, 4.6 mmol), 3-methylbenzophenone (0.6 g, 3.1 mmol), and THF (10 mL). The product was obtained in 0.35 g as a pale beige semisolid in 43% yield. TLC: CH₂Cl₂: MeOH (10:1), R_f=0.17. ¹H NMR (CDCl₃, 300 MHz) δ 7.37-6.99 (m, 9H), 6.08-6.03 (m, 1H), 2.52-2.47 (m, 2H), 2.35 (br s, 2H), 2.30 (br s, 2H), 2.27 (br s, 4H), 2.17 (s, 3H); ¹³C NMR (CDCl₃, 75.5 MHz) δ 143.22, 142.61, 140.23, 140.05, 137.95, 137.75, 130.50, 129.91, 128.37, 128.22, 127.94, 127.37, 127.15, 127.09, 126.98, 126.66, 124.64, 59.61, 45.30, 31.10, 28.08, 21.64. ESIMS: 266 (M+H).

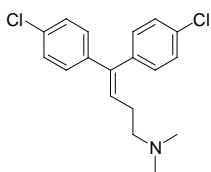


Dimethyl-(4-phenyl-4-p-tolyl-but-3-enyl)-amine (**2.23**). Procedure B.2 was carried out using (3-dimethylaminopropyl) triphenylphosphonium bromide (2.6 g, 6.2 mmol) from procedure B.1, 2.5 M nBuLi/Hex (2.5 mL, 6.2 mmol), 4-methylbenzophenone (0.6 g, 3.1 mmol), and THF (10 mL). The product was obtained in 0.72 g as a pale white semisolid in 89% yield. TLC: CH₂Cl₂: MeOH (10:1), R_f=0.24. ¹H NMR (CDCl₃, 300 MHz) δ 7.42-7.10 (m, 9H), 6.13-6.09 (t, 1H, *J*=7.1 Hz), 2.47-2.40 (m, 2H), 2.39-2.31 (m, 5H), 2.26 (br s, 6H); ¹³C NMR (CDCl₃, 75.5 MHz) δ 142.74, 136.77, 136.71, 129.89, 129.04,

128.90, 128.67, 128.31, 128.15, 127.39, 127.23, 126.98, 126.19, 59.74, 45.40, 28.22, 21.36, 21.18. ESIMS: 266 (M+H).



[4,4-Bis-(2-chloro-phenyl)-but-3-enyl]-dimethyl-amine (**2.24**). Procedure B.2 was carried out using (3-dimethylaminopropyl) triphenylphosphonium bromide (1.3 g, 3.0 mmol) from procedure B.1, 2.5 M nBuLi/Hex (1.2 mL, 3.0 mmol), 2,2-dichlorobenzophenone (0.5 g, 2.0 mmol), and THF (10 mL). The product was obtained in 0.43 g as a yellow oil in 68% yield. TLC: CH₂Cl₂: MeOH (10:1), R_f=0.26. ¹H NMR (CDCl₃, 300 MHz) δ 7.40-7.14 (m, 8H), 6.04-5.99 (t, 1H, *J*= 7.4 Hz), 2.48-2.43 (t, 2H, *J*=7.8 Hz), 2.30-2.25 (t, 2H, *J*=7.5 Hz), 2.22 (s, 6H); ¹³C NMR (CDCl₃, 75.5 MHz) δ 140.94, 138.48, 137.19, 134.64, 134.52, 133.88, 132.99, 132.22, 131.79, 130.27, 129.98, 128.79, 128.38, 126.59, 58.86, 45.44, 28.40. ESIMS: 320 (M+H). HRMS calcd for C₁₈H₁₉Cl₂N: 320.0960; Found: 320.0973.



[4,4-Bis-(4-chloro-phenyl)-but-3-enyl]-dimethyl-amine (**2.25**). Procedure B.2 was carried out using (3-dimethylaminopropyl) triphenylphosphonium bromide (1.3 g, 3.0 mmol) from procedure B.1, 2.5 M nBuLi/Hex (1.2 mL, 3.0 mmol), 4,4-dichlorobenzophenone (0.5 g, 2.0 mmol), and THF (10 mL). The product was obtained in 0.52 g as a yellow oil in 83% yield. TLC: CH₂Cl₂: MeOH (10:1), R_f=0.18. ¹H NMR (CDCl₃, 300 MHz) δ 7.36-7.08 (m, 9H), 6.10-6.06 (t, 1H, *J*=7.2 Hz), 2.46-2.38 (m, 2H),

2.32-2.27 (m, 2H), 2.23 (s, 6H); ^{13}C NMR (CDCl_3 , 75.5 MHz) δ 140.80, 140.63, 138.05, 133.34, 133.13, 132.17, 131.22, 128.77, 128.59, 128.42, 128.10, 59.33, 45.30, 28.16. ESIMS: 320 (M+H). HRMS calcd for $\text{C}_{18}\text{H}_{19}\text{Cl}_2\text{N}$: 320.0957; Found: 320.0973.

2.6.2 Biology

[^3H]-BTX experiment. In the sodium channel evaluation, the IC_{50} , which represents the micromolar concentration of compound required to displace 50% of specifically bound [^3H]-BTX, was determined using rat cerebral cortex synaptoneurosomes. In brief, rat forebrain membranes were incubated with [^3H]-Batrachotoxin (30-60 Ci/mmol). Reactions are carried out in 50 mM HEPES (pH 7.4) containing 130 mM choline chloride at 37 °C for 60 minutes. The reaction was terminated by rapid vacuum filtration of the reaction contents onto glass fiber filters. Radioactivity trapped onto the filters was determined and compared to control values in order to ascertain any interactions of the test compound with the sodium channel site 2 binding site. Aconitine [$1\ \mu\text{M}$] was used as a positive control.

Cell Culture and Electrophysiology. Human embryonic kidney (HEK 293) cells stably expressing $\text{Na}_v1.2$ were grown in DMEM/F12 media (Invitrogen Corp, CA, USA) supplemented with 10% fetal bovine serum, penicillin (100 U/ml), streptomycin (100 $\mu\text{g/ml}$) and geneticin (G418) (500 $\mu\text{g/ml}$; Sigma, MO, USA). Cells were grown in a humidified atmosphere of 5% CO_2 and 95% air at 37 °C.

Sodium currents were recorded using the whole-cell configuration of the patch clamp technique with an Axopatch 200B amplifier (Axon Instruments, Foster City, CA). All voltage protocols were applied using pCLAMP 8 software (Axon, USA) and a Digidata 1322 (Axon, USA). Currents were amplified and low pass filtered (2 kHz) and

sampled at 33 kHz. Cells were plated on glass coverslips and superfused with the following solution: 130 mM NaCl, 4 mM KCl, 1 mM Ca_2Cl , 5 mM MgCl_2 , 5 mM HEPES, and 5 mM glucose (pH adjusted to 7.4 with NaOH). Compounds were prepared as 100 mM stock solutions in dimethylsulfoxide (DMSO) and diluted to desired concentration in perfusion solution. The maximum DMSO concentration of 0.3% had no effect on current amplitude. Borosilicate glass pipettes were pulled using a Brown-Flaming puller (model P87, Sutter Instruments Co, Novato, CA) and heat polished to produce electrode resistances of 0.8-2.6 M Ω when filled with the following electrode solution: 130 mM CsCl, 1 mM MgCl_2 , 5 mM MgATP, 10 mM HEPES, and 10 mM BAPTA (pH adjusted to 7.4 with NaOH). Experiments were performed at room temperature (20-22 °C).

Data Analysis. All data analysis was performed using Clampfit 8 software (Axon Instruments, CA, USA), Excel (Microsoft), and Origin 6.0 (Microcal Software, MA, USA). Statistical analyses were performed using a *t* test for normally distributed data, or the Wilcoxon signed rank test for non-normalized data (Sigma Stat, Jandel). Averaged data were presented as means \pm standard error of the mean (S.E.M.). Significance values of $p < 0.05$ were considered.

2.7 References

- 1) Sindrup, S.H.; Jensen, T.S. "Efficacy of pharmacological treatments of neuropathic pain: an update and effect related to mechanism of drug action," *Pain*. **1999**, 83, 389-400.
- 2) Gordon, D.B.; Love, G. "Pharmacological management of neuropathic pain," *Pain Mgmt. Nursing*. **2004**, 5, 19-33.
- 3) Sindrup, S.H.; Otto, M.; Finnerup, N.B.; Jensen, T.S. "Antidepressants in the treatment of neuropathic pain," *Basic Clin. Pharmacol. Toxicol.* **2005**, 96, 399-409.
- 4) Dellemijn, P. "Are opioids effective in relieving neuropathic pain," *Pain*. **1999**, 80, 453-462.
- 5) Wang, G.K.; Gerner, P. "Tricyclic antidepressants and their analogues as long-acting local anesthetics and analgesics," U.S. Patent 6,545,057 B2, 2003.
- 6) Kalso, E. "Sodium channel blockers in neuropathic pain," *Curr. Pharma. Design*. **2005**, 11, 3005-3011.
- 7) Saarto, T.; Wiffen, P.J. "Antidepressants for neuropathic pain," *Cochrane Collab*. **2006**, 1, 1-48.
- 8) Humber, L.G.; Herr, F.; Charest, M.P. "Chemistry and pharmacology of 5-methylene-4-substituted dibenzo[a,d] cycloheptenes," *J. Med. Chem.* **1971**, 14, 982-985.
- 9) Barbui, C.; Hotopf, M. "Amitriptyline v. the rest: still the leading antidepressants after 40 years of randomized controlled trials," *Br. J. Psych.* **2001**, 178, 129-144.

- 10) Tiengo, M.; Pagnoni, B.; Calmi, A.; Calza, L.; Rigoli, M.; Braga, P.; Panerai, A.E. "Clomipramine compared with pentazocine as a unique treatment in postoperative pain," *Int. J. Clin. Pharmacol. Res.* **1987**, 7, 141-3.
- 11) Cerbo, R.; Barbanti, P.; Fabbrini G.; Pascali, M.P.; Catarci, T. "Amitriptyline is effective in chronic but not episodic tension-type headache: pathogenetic implications," *Headache*. **1998**, 38, 453-457.
- 12) Ashina, S.; Bendtsen, L.; Jensen, R. "Analgesic effect of amitriptyline in chronic tension-type headache is not directly related to serotonin reuptake inhibition," *Pain*. **2004**, 108, 108-114.
- 13) Collins, S.L.; Moore, R.A.; McQuay, H.J.; Wiffen, P. "Antidepressants and anticonvulsants for diabetic neuropathy and postherpetic neuralgia: a quantitative systematic review," *J. Pain & Symp. Manage.* **2000**, 6, 449-458.
- 14) Bowsher, D. "Factors influencing the features of postherpetic neuralgia and outcome when treated with tricyclics," *Euro. J. Pain*. **2003**, 7, 1-7.
- 15) Atkinson, J.H.; Slater, M.A.; Williams, R.A.; Zisook, S.; Patterson, T.L.; Grant, I.; Wahlgren, D.R.; Abramson, I.; Garfin, S.R. "A placebo-controlled randomized clinical trial of nortriptyline for chronic low back pain," *Pain*. **1998**, 76, 287-296.
- 16) Sudoh, Y.; Cahoon, E.E.; Gerner, P.; Wang, G.K. "Tricyclic antidepressants as long-acting local anesthetics," *Pain*. **2003**, 103, 49-55.
- 17) McNeal, E.T.; Lewandowski, G.A.; Daly, J.W.; Creveling, C.R. "[³H]Batrachotoxin A 20 α - benzoate binding to voltage-sensitive sodium channels: a rapid and quantitative assay for local anesthetic activity in a variety of drugs," *J. Med. Chem.* **1985**, 28, 381-388.

- 18) Wang, K.G.; Russell, C.; Wang, S.Y. "State-dependent block of voltage-gated Na⁺ channels by amitriptyline via local anesthetic receptor and its implications for neuropathic pain," *Pain*. **2004**, *110*, 166-174.
- 19) Lipkind, G.M.; Fozzard, H.A. "KscA crystal structure as framework for a molecular model of the Na⁺ channel pore," *Biochemistry*. **2000**, *39*, 8161-8170.
- 20) Hardman, J.G., Limbird, L.E., Molinoff, P.B., Ruddon, R.W., Gilman, A.G., Eds. *Local anesthetics*; In Goodman and Gilman's the pharmacological basis of therapeutics; MacMillan; New York, 2001.
- 21) Aldrich, R.W.; Corey, D.P.; Stevens, C.F. "A reinterpretation of mammalian sodium channel gating based on single channel recording," *Nature*. **1983**, *306*, 436-441.
- 22) Hondeghem, L.M.; Katzung, B.G. "Antiarrhythmic agents: the modulated receptor mechanism of action of sodium and calcium channel-blocking drugs," *Annu. Rev. Pharmacol. Toxicol.* **1984**, *24*, 387-423.
- 23) Gerner, P. "Tricyclic antidepressants and their local anesthetic properties: from bench to bedside and back again," *Reg. Anesthesia Pain Med.* **2004**, *29*, 286-289.
- 24) Pancrazio, J.J.; Kamatchi, G.L.; Roscoe, A.K.; Lynch, C. "Inhibition of neuronal Na⁺ channels by antidepressant drugs," *J. Pharmacol. Exp. Therap.* **1998**, *284*, 208-214.
- 25) Miodownik, A.; Kreisberger, M.; Nussim, M.; Avnir, D. "One-step grignard reactions with dimethylaminopropyl chloride: application to the synthesis of tricyclic drugs," *Syn. Comm.* **1981**, *11*, 241-246.

- 26) Hoye, T.R.; Eklov, B.M.; Voloshin, M. "No-D NMR spectroscopy as a convenient method for titering organolithium (RLi), RMgX, and LDA solutions," *Org. Lett.* **2004**, *6*, 2567-2570.
- 27) Zha, C.; Brown, G.B.; Brouillette, W.J. "Synthesis and structure-activity relationship studies for hydantoins and analogues as voltage-gated sodium channel ligands," *J. Med. Chem.* **2004**, *47*, 6519-6528.
- 28) Li, H.L.; Hadid, D.; Ragsdale, D.S. "The batrachotoxin receptor on the voltage-gated sodium channel is guarded by the channel activation gate," *Mol. Pharmacol.* **2002**, *61*, 905-912.
- 29) Trainer, V.L.; Moreau, E.; Guedin, D.; Baden, D.G.; Catterall, W.A. "Neurotoxin binding and allosteric modulation at receptor site 2 and 5 on purified and reconstituted rat brain sodium channels," *J. Biol. Chem.* **1993**, *268*, 17114-17119.
- 30) Creveling, C.R.; McNeal, E.T.; Daly, J.W.; Brown, G.B. "Batrachotoxin-induced depolarization and [³H]Batrachotoxin-A 20 α - benzoate binding in a vesicular preparation from guinea pig cerebral cortex," *Mol. Pharmacol.* **1982**, *23*, 350-358.
- 31) Nilius, B. "*Pflugers archiv* and the advent of modern electrophysiology, from the first action potential to patch clamp," *Pflugers Arch. Eur. J. Physiol.* **2003**, *447*, 267-271.
- 32) Gonzalez, J.E.; Tsien, R.Y. "Voltage sensing by fluorescence resonance energy transfer in single cells," *Biphs. J.* **1995**, *69*, 1272-1280.
- 33) Felix, J.P.; Williams, B.S.; Priest, B.T.; Brochu, R.M.; Dick, I.E.; Warren, V.A.; Yan, L.; Slaughter, R.S.; Kaczorowski, G.J.; Smith, M.M.; Garcia, M.L.

“Functional assay of voltage-gated sodium channels using membrane potential sensitive dyes,” *Assay Drug Dev. Tech.* **2004**, *2*, 260-268.

- 34) Liu, C.J.; Priest, B.T.; Bugianesi, R.M.; Dulski, P.M.; Felix, J.P.; Dick, I.E.; Brochu, R.M.; Knaus, H.G.; Middleton, R.E.; Kaczorowski, G.J.; Slaughter, R.S.; Garcia, M.L.; Kohler, M.G. “A high-capacity membrane potential FRET-based assay for Na_v1.8 channels,” *Assay Drug Dev. Tech.* **2006**, *4*, 37-48.
- 35) Galantay, E.E.; Simpson, R.; Corriveau, G.; Denzer, M.; Knorr, D.C.; Strohschein, R.J. Paolella, N.A.; Uike, Y.; Gogherty, J.H.; Ryan, E.A.; Iorio, L.C. “Novel tricyclic systems, oxazole, thiazole, and imidazole analogs of the amitriptyline type,” *J. Med. Chem.* **1974**, *17*, 1316-1327.
- 36) Dorsett, M.T.; Grisar, J.M.; Hickey, K.R.; Pohl, R.L. “Aminoalkenyl benzenesulfonamides with hypotensive and histamine-releasing properties,” *J. Med. Chem.* **1970**, *13*, 895-899.

Chapter 3

Second Generation Monophenyl Amines as Anti-Inflammatory Agents

The demand for a highly effective treatment of chronic pain syndromes without significant toxicities has led us to continue our investigations within this area. Initial structure activity relationship of amitriptyline analogues revealed that the tricyclic motif was unnecessary for activity. From this SAR, a first generation diphenyl lead analogue (**2.6**) was found to have 53.2% inhibitory block of hNa_v1.2 current at 10 μ M, which is greater than 50% increase in current block in comparison to amitriptyline. We have chosen to further modify this structural class by creation of a monophenyl series, with optimization of chain length, incorporation of heterocyclic isosteres, and monosubstitutions of the phenyl ring. Evaluation of these analogues through [³H]-BTX binding assay and electrophysiological methods have identified a potent monophenyl amine analogue (**3.4**). This compound was found to have 94.6% functional block of hNa_v1.2 at 10 μ M, which is a three-fold increase in current block in comparison to amitriptyline. Animal models of inflammatory pain have further corroborated these findings.

3.1 Previous Investigations

3.1.1 Comprehensive Structure Activity Relationship

In our continuing efforts to develop potent sodium channel blockers for the treatment of chronic pain syndromes, we have chosen to further investigate analogues derived from an amitriptyline scaffold. Previously a comprehensive structure activity relationship (SAR) of this class was conducted through modifications at three major sites of the scaffold, which included phenyl ring orientation, phenyl replacement and amine

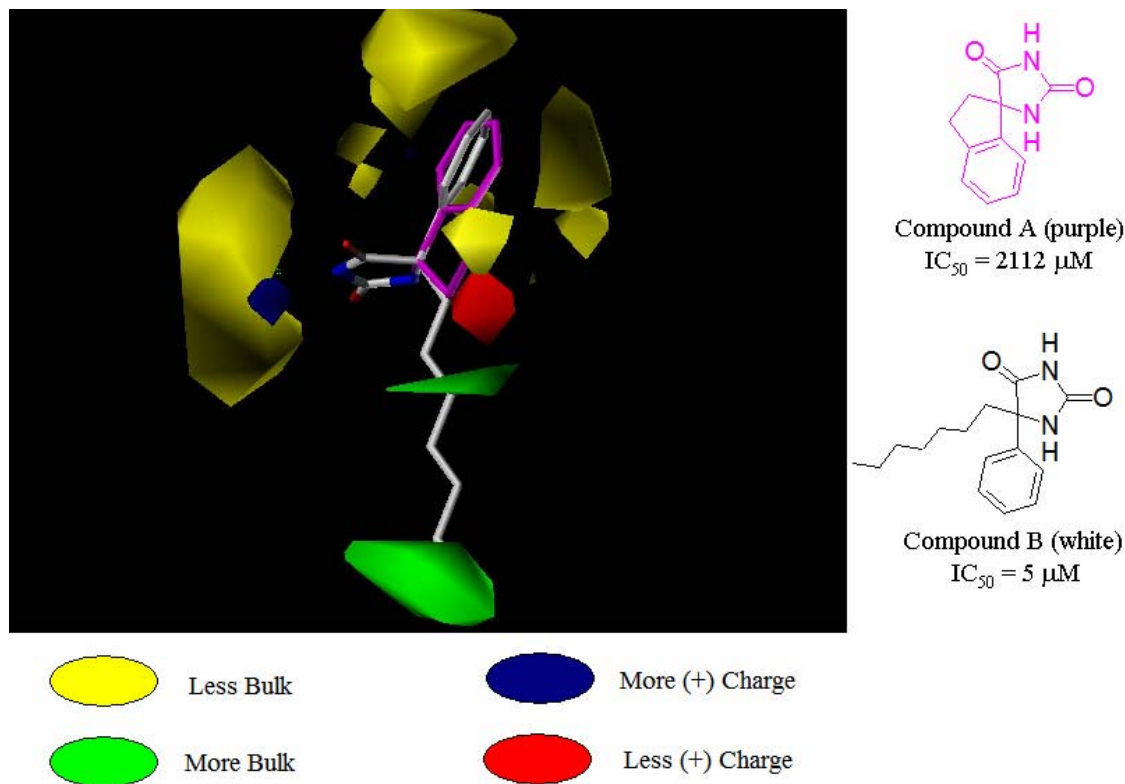
isosteres. Based on these investigations, we were able to determine that the tricyclic moiety is unnecessary for effective inhibition of the [^3H]-BTX binding site and sodium currents of $\text{hNa}_v1.2$. Our lead compound (**2.6**), containing a diphenyl amine motif demonstrated a 53.2% inhibitory block of $\text{Na}_v1.2$ current at 10 μM , which is greater than 50% increase in current block in comparison to the amitriptyline standard. From these findings, we further conducted lead optimizations of analogue (**2.6**) by chain length modification, heterocyclic isosteres and phenyl ring substitutions. Of these additional thirteen compounds, only mono o-Me substitution by compound (**2.21**) provided slightly enhanced functional block of $\text{hNa}_v1.2$ with 54.3% block at 10 μM , in comparison to analogue (**2.6**). This diphenyl class also exhibited potent inhibition of $\text{Na}_v1.7$ and $\text{Na}_v1.8$, with numerous compounds providing 81%-100% inhibition at 10 μM in both isoforms. However we were slightly concerned by toxicity issues arising during NINDS evaluation of several of these compounds in animal models of anticonvulsant activity. Although it is unclear whether the severity of these adverse effects could be eliminated or lessened by appropriate dosing. Therefore, we have chosen to further our studies in the development of a more potent and well-tolerated therapeutic for the treatment of neuropathic syndromes.

3.1.2 Comparative Molecular Field Analysis Studies

Comparative molecular field analysis (CoMFA) is a three-dimensional technique that correlates biological activity with molecular steric and electronic factors. This tool has been greatly utilized in the prediction of novel channel inhibitors, as structural elucidation of the sodium channel protein is currently unavailable. One particular study has employed the use of CoMFA for determination of the hydantoin binding site in

neuronal VGSCs.¹ From their findings, incorporation of an aliphatic long chain was able to significantly decrease the IC_{50} values, or the half maximal inhibitory concentration (Figure 3-1). In this case, CoMFA prediction was confirmed through synthesis and further biological evaluation of these novel inhibitors.

Figure 3-1 Previous CoMFA Studies on the VGSC

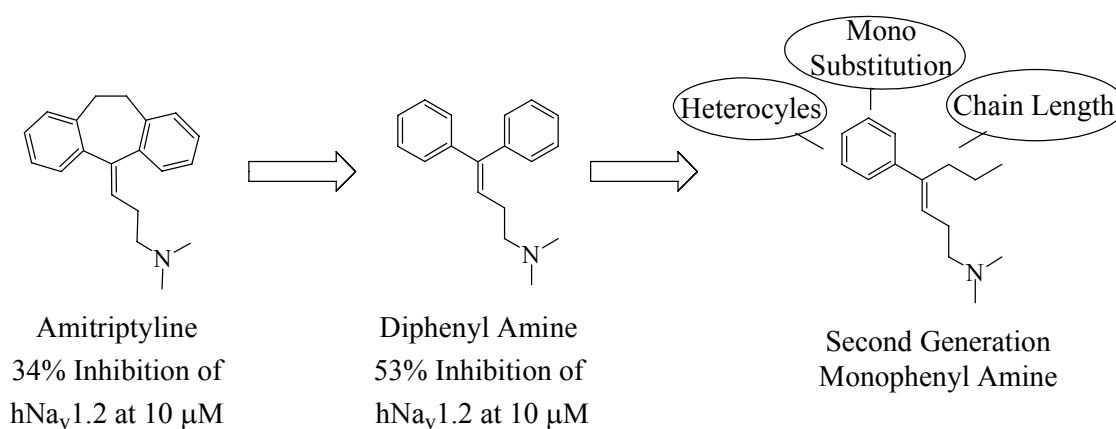


3.2 Design

Our initial SAR proved that elimination of the tricyclic motif resulted in a class of more potent diphenyl inhibitors, through evaluation for current block in hNa_v1.2. Inhibition was increased by almost 50% by the diphenyl analogue (**2.6**) and o-Me substituted derivative (**2.21**). Additionally, all analogues altering the dimethylamine functionality proved to be detrimental to inhibitory effects. Based on these findings, we have chosen not to modify the dimethylamine portion, including the amine group and its

associated chain. Furthermore, the trisubstituted olefin has been deemed essential in inhibition through evaluation of tertiary alcohols (**2.2**), (**2.3**) and (**2.5**). Incorporation of these findings, along with previous CoMFA, investigations has led to the proposal of developing a monophenyl amine class of inhibitors with varying aliphatic chain lengths. Upon determination of this appropriate chain length, heterocyclic isosteres and monosubstitutions of the phenyl ring will also be conducted (Figure 3-2).

Figure 3-2 Design Strategies



3.3 Synthesis and [³H]-BTX Data

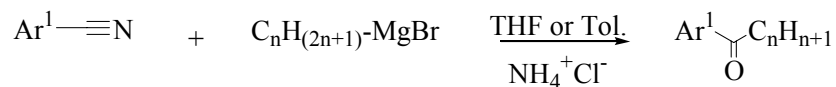
3.3.1 General Synthetic Methods

Analogues were synthesized by initial formation of their corresponding ketone by either Grignard addition or Friedel-Craft acylation reactions, under typical conditions (Scheme 3-1). Ketones were synthesized in relatively high yields ranging from 50%-100%. Subsequent Wittig addition to each ketone derivative was achieved by the addition of 3-dimethylaminopropyl triphenylphosphonium bromide along with a solution of KHMDS in toluene. Product materials incorporating chain length modification (**3.1**)-(**3.6**), heterocycle isosteres (**3.7**)-(**3.10**) and optimization of monophenyl lead (**3.11**)-(**3.22**) were obtained in yields ranging from 18%-93%.

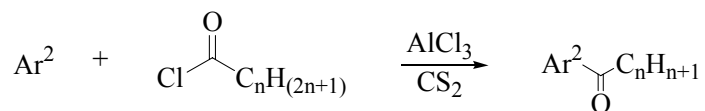
Scheme 3-1 General Synthetic Pathways

A. Preparation of Ketones:

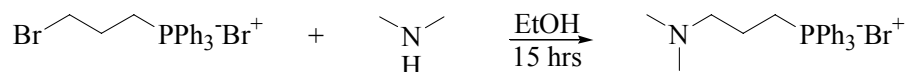
1) Grignard Addition



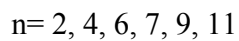
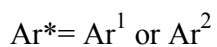
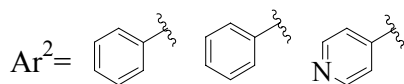
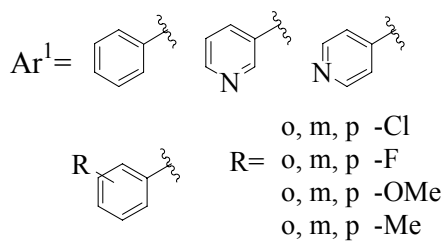
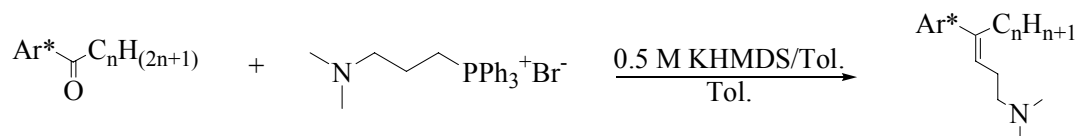
2) Friedel-Craft Acylation



B. Preparation of Phosphonium Salt:



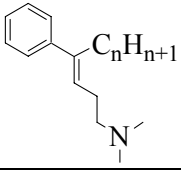
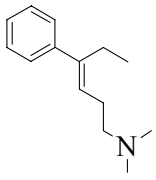
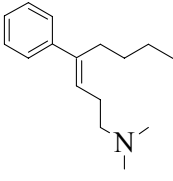
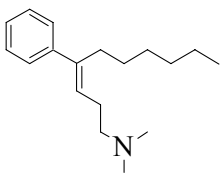
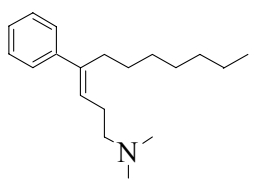
C. Wittig Addition:

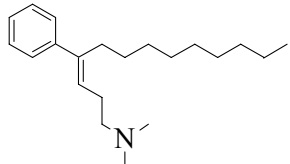
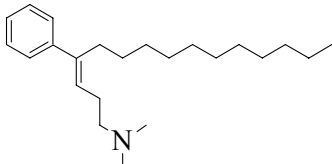


3.3.2 Chain Length Modification

Chain length modifications were carried out with varying lengths of $n=2, 4, 6, 7, 9$, and 11 (Table 3-1). From our initial $[^3\text{H}]$ -BTX screening,² analogue (**3.4**), in which $n=7$, provided the optimal length for sodium channel binding. Shorter and longer chain lengths resulted in diminished activity from that of (**3.4**), with 83.65% at $10\text{ }\mu\text{M}$.

Table 3-1 Chain Length Optimization

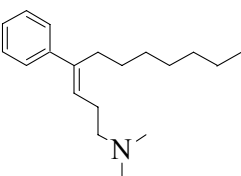
			
Chain Length	ID	Percent Yield	Percent Inhibition of $[^3\text{H}]$ -BTX at $10\text{ }\mu\text{M}$
	3.1	93%	68.75%
	3.2	33%	78.39%
	3.3	59%	78.49%
	3.4	30%	83.65%

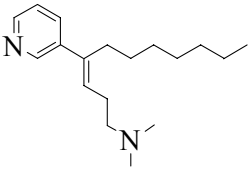
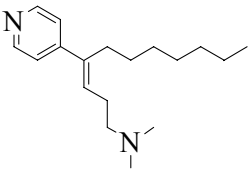
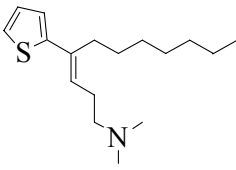
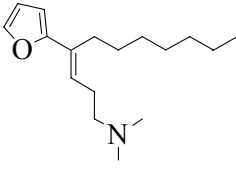
Chain Length	ID	Percent Yield	Percent Inhibition of [^3H]-BTX at 10 μM
	3.5	29%	68.39%
	3.6	44%	60.46%

3.3.3 Heterocycle Isosteres

Upon determination of the optimal chain length, heterocyclic isosteres of the monophenyl ring were constructed (Table 3-2). These analogues included 3-pyridinyl, 4-pyridinyl, 2-thiophenyl, and 2-furanyl and were synthesized in range of 18%- 44% yield. Sodium channel binding assay utilizing [^3H]-BTX demonstrated that pyridinyl analogues (**3.7**) and (**3.8**) had equal activity with 68.46% and 67.58%, respectively at 10 μM . Thiophenyl analogue (**3.9**) provided even less activity with 49.47% inhibition, and furanyl analogue (**3.10**) had no detectable activity in this assay at 10 μM . The more potent heterocyclic analogues (**3.7**) and (**3.8**) still displayed lower activity than our initial monophenyl lead (**3.4**) with 83.65%. Due to these findings, we chose to abandon further heterocyclic isosteres and continue other modifications of analogue (**3.4**) for increased potency.

Table 3-2 Heterocyclic Isosteres of Compound (3.4)



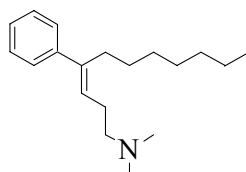
Structure	ID	Percent Yield	Percent Inhibition of [³ H]-BTX at 10 μM
	3.7	44%	68.46%
	3.8	44%	67.58%
	3.9	18%	49.47%
	3.10	22%	-0.84%

3.3.4 Optimization of Monophenyl Lead

Further optimizations of the monophenyl ring were conducted by ortho, meta, and para substitutions by -Cl, -F, -OMe, and -Me groups (Table 3-3). Analogues were synthesized in a range of 18%-85% yield. [³H]-BTX binding assay revealed most derivatives (3.11)-(3.22) of this class provide similar or equal activity to that of

monophenyl lead (**3.4**). Specifically, o-OMe substituted analogue (**3.17**) provided the best sodium channel binding of these derivatives with 86.72% inhibition at 10 μ M.

Table 3-3 Optimization of Compound (**3.4**)



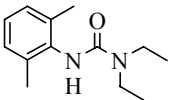
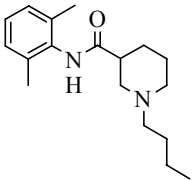
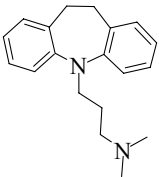
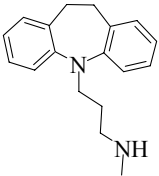
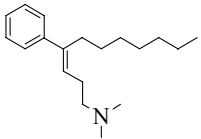
Structure	ID	Percent Yield	Percent Inhibition of [³ H]-BTX at 10 μ M
o-Cl	3.11	18%	72.33%
m-Cl	3.12	73%	64.19%
p-Cl	3.13	85%	75.30%
o-F	3.14	42%	73.92%
m-F	3.15	49%	80.45%
p-F	3.16	46%	78.27%
o-OMe	3.17	38%	86.72%
m-OMe	3.18	71%	83.21%
p-OMe	3.19	64%	84.32%
o-Me	3.20	43%	68.48%
m-Me	3.21	35%	77.36%
p-Me	3.22	66%	81.05%

3.4 Results

3.4.1 IC₅₀ of Lead Monophenyl Analogue

The IC₅₀ of lead monophenyl analogue (**3.4**) was obtained for inhibition of [³H]-BTX binding. This evaluation was carried out so direct comparison to other potent sodium channel blockers in this assay could be determined (Table 3-4).³ Analogue (**3.4**) was found to have an IC₅₀ of 0.87 μM for [³H]-BTX displacement, which is improved potency in comparison to other compounds of the TCA drug class.

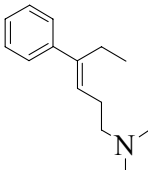
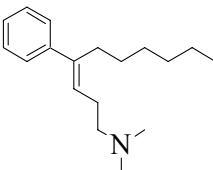
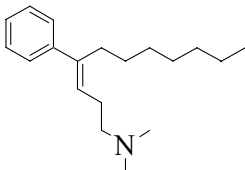
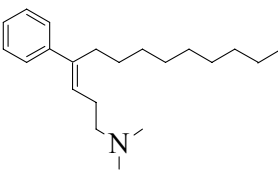
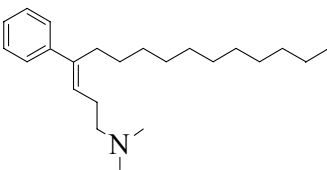
Table 3-4 IC₅₀ of [³H]-BTX Displacement

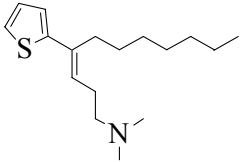
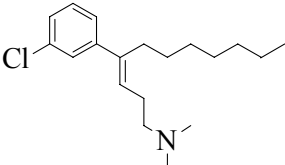
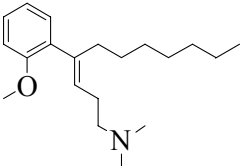
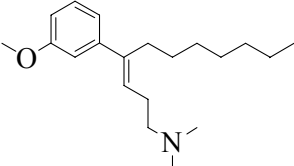
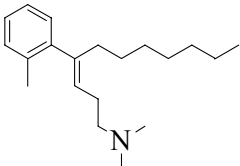
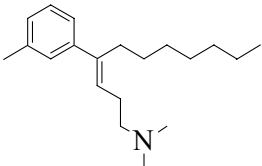
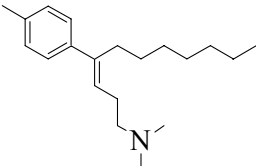
Structure	Drug	IC ₅₀ (μM)
lidocaine		240.0
bupivacaine		5.4
imipramine (TCA)		3.6
desipramine (TCA)		2.4
monophenyl analogue (3.4)		0.87

3.4.2 Functional Block

Analogues providing substantial activity in the [^3H]-BTX assay were further evaluated for inhibitory tonic effects in hNa_v1.2 (Table 3-5). These analogues provided inhibition of sodium channel current in a range of $8.61\% \pm 1.57$ to $100.0\% \pm 0.00$ at 10 μM . Specifically, analogues (3.4), (3.5), (3.6), (3.9), (3.12), and (3.21) provided greater than 90% block of current.

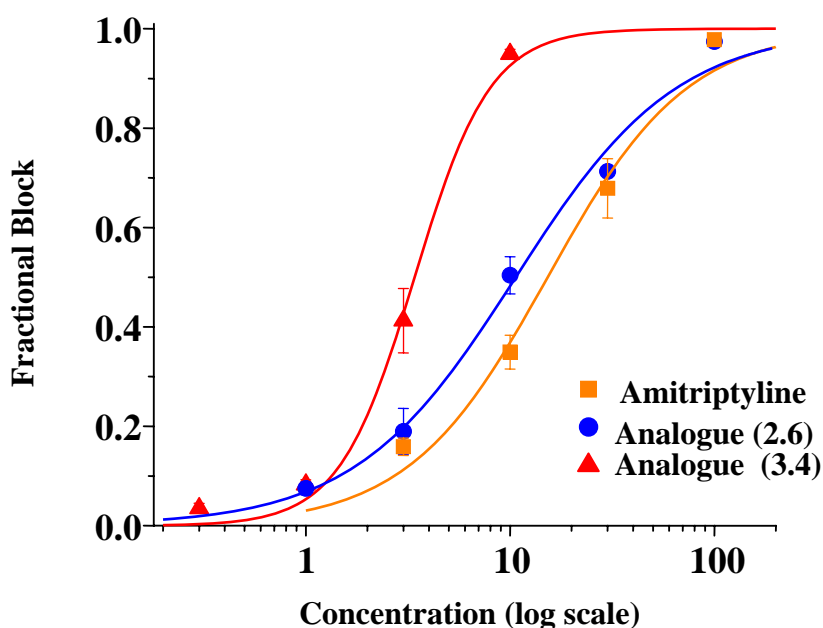
Table 3-5 Percent Block of hNa_v1.2 Current at 10 μM

Compound	ID	Percent Block of hNa _v 1.2 Current at 10 μM
	3.1	10.27 ± 2.79 (n=3)
	3.3	52.6 ± 9.3 (n=4)
	3.4	94.4 ± 1.0 (n=8)
	3.5	95.46 ± 0.81 (n=4)
	3.6	100.00 ± 0.00 (n=5)

Compound	ID	Percent Block of hNa _v 1.2 at 10 μ M
	3.9	95.6 \pm 2.0 (n=3)
	3.12	97.4 \pm 0.5 (n=4)
	3.17	58.93 \pm 3.82 (n=4)
	3.18	84.04 \pm 1.57 (n=3)
	3.20	8.61 \pm 1.57 (n=4)
	3.21	90.42 \pm 2.99 (n=4)
	3.22	86.03 \pm 2.11 (n=5)

Progression of our analogue design from tricyclic, to diphenyl and finally monophenyl derivatives has resulted in an increase of functional block of hNa_v1.2. This relationship can best be seen through a dose response curve of amitriptyline, analogue (2.6) and monophenyl amine (3.4) (Figure 3-3). From these findings, the IC₅₀ of each analogue has been determined, with amitriptyline at 14.6 μ M, diphenyl analogue (2.6) at 10.7 μ M, and monophenyl analogue (3.4) at 3.7 μ M.

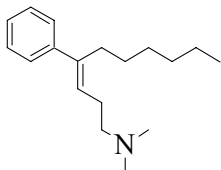
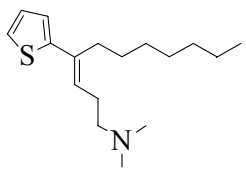
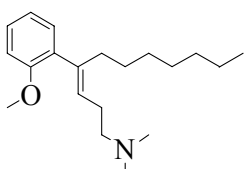
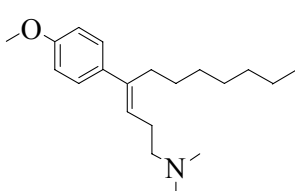
Figure 3-3 Dose Response Curve for Functional Block of hNa_v1.2



3.4.3 FRET Based Assay

Four representative analogues of the monophenyl class were evaluated for inhibitory effects in Na_v1.7 and Na_v1.8 through a modified FRET assay (Table 3-6).⁴ All analogues provided substantial activity with 86%-106% inhibition at 10 μ M, for both isoforms. Methoxy substituted analogues (3.17) and (3.19) proved to be better inhibitors of the analogues tested, with activities of 61%-96% even at lower concentrations of 3 μ M.

Table 3-6 Inhibition Based on FRET Modified Assay

Compound	ID	Na _v 1.7				Na _v 1.8			
		0.3 μM	1 μM	3 μM	10 μM	0.3 μM	1 μM	3 μM	10 μM
	3.3	-7	3	33	93	2	9	45	92
	3.9	-1	8	35	96	1	30	70	96
	3.17	3	23	96	106	-1	28	84	100
	3.19	0	6	72	99	0	11	61	95

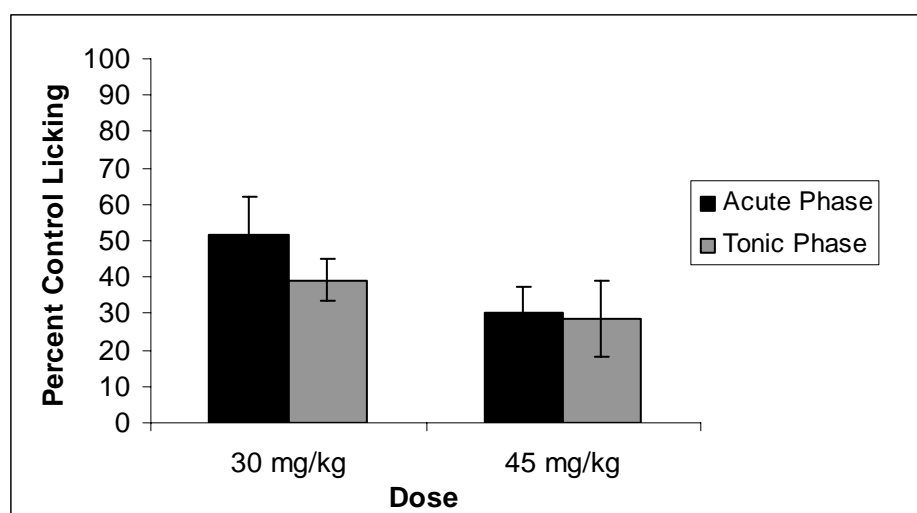
3.4.4 Animal Model of Inflammatory Pain

Animal models of neuropathic pain syndromes, which view the underlying mechanisms of hyperalgesia and allodynia associated with nerve injury or nerve inflammation, are commonly used.⁵ Long duration stimuli tests quantitatively measure resulting behavior upon administration of an irritant, such as formalin. A biphasic response is observed to such stimuli, with an initial acute phase of 3-5 min, followed by 10-15 min of no perceived nociception, and a secondary tonic phase that provides noticeable

inflammatory effects for 20-40 min.⁶ The initial acute phase is thought to be a result of direct chemical stimulation of nociception and the latter a consequence of central processing of this initial response.

Formalin tests were conducted on monophenyl analogue (**3.4**) and results were determined as percent control licking time for both the acute/early and tonic/late phases of response. The irritant was injected into the planter surface of the hind paw and observations were recorded. Analogue (**3.4**) was tested at two doses of 30 mg/kg and 45 mg/kg (Chart 3-1). At 30 mg/kg (**3.4**) did not significantly reduce the acute phase with $51.52\% \pm 10.8$ activity, but did show reduction of the licking time in the inflammatory portion with $39.17\% \pm 5.91$ response. At 45 mg/kg both phases were greatly reduced, with the acute phase and the tonic phase providing $30.28\% \pm 7.14$ and $28.34\% \pm 10.45$ reduction, respectively. No toxicity was observed at either dose and tests were conducted in four trials.

Chart 3-1 Effects of (**3.4**) in Animal Models of Inflammatory Pain



3.4.5 Norepinephrine Transport

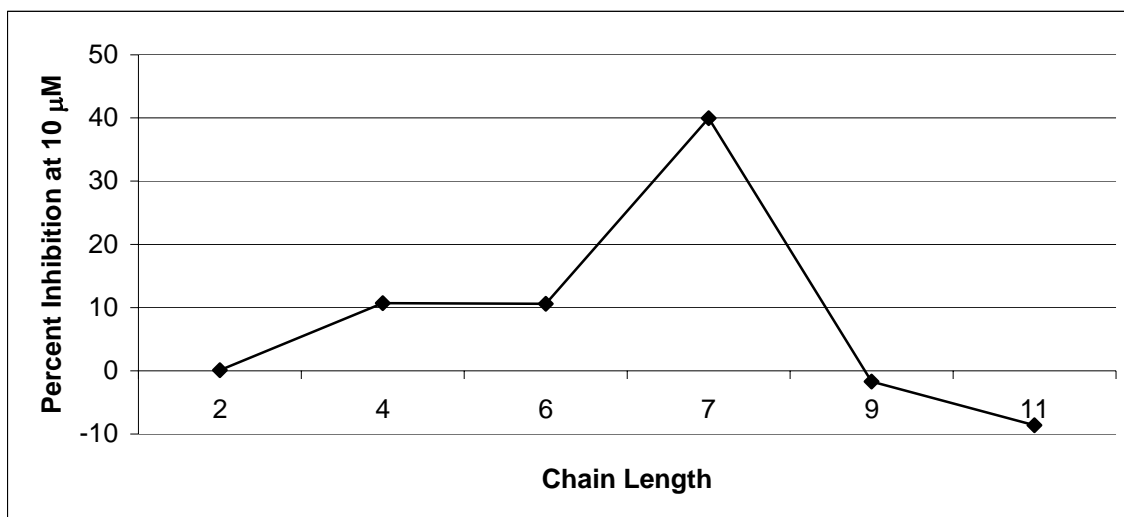
Depressive disorders are known to be associated with deficiency of neurotransmitters, such as norepinephrine. Antidepressants can function by altering levels of norepinephrine through three basic mechanisms, which are increase in release, prevention of inactivation and prevention of reuptake.⁷ Tricyclic antidepressants (TCAs) are known to specifically function by blocking reuptake at nerve terminals. We were highly interested in analyzing our novel monophenyl amine analogues for antidepressant activity, since our original design was derived from a TCA scaffold. Dual activity could potentially increased therapeutic use, as many patients suffering from chronic pain syndromes also have associated depressive disorders.

Norepinephrine activity was readily determined through the use of a [³H]-norepinephrine binding displacement assay. Initial screening began with our standard, amitriptyline, and first generation diphenyl lead analogue (**2.6**) (Table 3-7). From these findings, amitriptyline provided 98.24% inhibition at 10 μ M, and analogue (**2.6**) had reduced activity at 76.96% at the same concentration. Chain length modified analogues (**3.1**)-(**3.6**) were then evaluated and revealed that analogue (**3.4**), where n=7, provided the greatest activity, with 44.56% inhibition at 10 μ M (Chart 3-2).

Table 3-7 [³H]-Norepinephrine Binding Displacement

Compound	Percent Inhibition of [³ H]-Norepinephrine at 10 μ M
amitriptyline	98.24%
analogue (2.6)	76.96%
analogue (3.4)	44.56%

Chart 3-2 Norepinephrine Activity and Chain Length



3.5 Discussion and Conclusion

3.5.1 Discussion

Design and synthesis of a monophenyl amine structural class was successfully pursued, with the construction of numerous analogues that included modified chain lengths (3.1)-(3.6), heterocyclic isosteres (3.7)-(3.10) and monosubstitutions of the phenyl ring. Previous CoMFA investigations of the hydantoin binding site in neuronal VGSCs revealed incorporation of an aliphatic chain significantly lowered [3 H]-BTX IC_{50} values. We were therefore interested in developing monophenyl analogues with various chain lengths, in order to determine the accuracy of our analogues in this predictive model and to optimize potency. We found that analogue (3.4), where $n=7$, provided the optimal chain length and demonstrated 83.65% inhibition of [3 H]-BTX at 10 μ M. Furthermore, analogue (3.4) was found to have a [3 H]-BTX IC_{50} values of 0.87 μ M, which was five times greater than the previously reported hydantoin analogues of the CoMFA model.

Upon determination of appropriate chain length, heterocyclic analogues of **(3.4)** were developed by 3-pyridinyl, 4-pyridinyl, 2-thiophenyl, and 2-furanyl derivatives. The more potent analogues of this class were pyridine analogues **(3.7)** and **(3.8)** which displayed 68.46% and 67.58% inhibition of [^3H]-BTX, respectively. These binding affinities were still much lower than **(3.4)**, and further heterocyclic isosteres were not pursued. Monosubstitutions of the phenyl ring were then constructed by ortho, meta and para substitutions by -Cl, -F, -OMe, and -Me groups. These twelve analogues **(3.11)**-**(3.22)** provided a range of 64.19%-86.72% inhibition of [^3H]-BTX at 10 μM . The methoxy derivatives had the best overall activity with 86.72%, 83.21% and 84.32% for ortho, meta and para positions, respectively.

Evaluation for functional block by electrophysiological methods was then conducted on hNa_v1.2 at 10 μM , for analogues showing significant inhibition of [^3H]-BTX. Upon screening of analogues **(3.1)** and **(3.3)**-**(3.6)**, it was determined that increasing chain length greatly enhanced functional block. A dramatic increase in activity was noticed as progression of chain lengths went from n=2, n=5 and n=7. However, the activity of analogue **(3.4)**, n=7, with $94.4\% \pm 2.79$ current block was not significantly altered by increasing chain length to n=9 with $95.46\% \pm 0.81$, or further to n=11 with 100.00 ± 0.0 activity.

We again find instances of poor correlation between [^3H]-BTX and functional block effects. Heterocyclic isostere **(3.9)**, incorporating a thiophene ring, provided 49.47% displacement of [^3H]-BTX, but evaluation for functional block displayed $95.6\% \pm 2.0$. Conversely, o-Me analogue **(3.20)** had 68.48% activity for sodium channel binding and only $8.61\% \pm 1.57$ block of channel current. Although the binding and

functional assays show poor correlation, we must rely on [^3H]-BTX binding displacement as an initial screening tool as electrophysiological methods are much more laborious.

The potency of this monophenyl amine class was further verified through animal models of inflammatory pain. Formalin tests were conducted on monophenyl analogue (**3.4**) at doses of 30 mg/kg and 45 mg/kg, with greatest effects seen at 45 mg/kg with no observable toxicity. This evaluation further establishes the therapeutic relevancy of this class as potential treatment of chronic pain syndromes, such as inflammation.

From our investigations, two potent classes of sodium channel blockers, diphenyl and monophenyl, have been derived from a TCA scaffold. TCAs are known to affect depressive disorders through block of norepinephrine reuptake, therefore analysis of these two classes was conducted for norepinephrine activity. It was found that modification of the tricyclic motif to a diphenyl class results in loss of activity, which was even further lowered by alteration to monophenyl derivatives.

3.5.2 Conclusion

A novel monophenyl amine class has been constructed with numerous analogues providing significant block of $\text{hNa}_v1.2$ at 10 μM . Specifically, analogue (**3.4**) was found to have $94.4\% \pm 1.0$ block of current, which is a three-fold increase in current block in comparison to amitriptyline. Animal models of inflammatory pain further corroborated the potency and therapeutic potential of (**3.4**). However, norepinephrine activity was found to be diminished through modification of the tricyclic motif.

3.6 Experimental Section

3.6.1 Chemistry

All syntheses requiring anhydrous conditions were kept under inert gas, N₂, and conducted in flame-dried glassware. Solvents were obtained from activated alumina stills or were of commercial grade quality. THF obtained directly from the alumina still was further dried by distillation over CaH₂. Commercial grade toluene was also dried by stirring in MgSO₄ for 15-20 minutes prior to use. N-Butyllithium concentrations were determined by NMR methods. Reactions resulting in a mixture of alkene stereoisomers were used without further separation. ¹H and ¹³C NMRs were conducted on a Varian 300 MHz NMR in CDCl₃ at ambient temperature. High resolution mass spectral (HRMS) data was determined at the University of Illinois Urbana-Champaign School of Chemical Sciences.

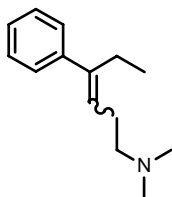
General Procedure A: The nitrile (1.0 equiv) in CH₂Cl₂ was kept under N₂ and held at 0°C, by use of an ice-bath. The Grignard solution (1.5-2.0 equiv) was added dropwise to the flask, and the reaction was allowed to stir overnight with gradual warming to room temp. The mixture was quenched by addition of a sat. NH₄Cl solution. The crude product was extracted with water (2 x 30 mL), CH₂Cl₂ (1x 30 mL), brine (1 x 20 mL), and dried over MgSO₄. The material was then filtered and evaporated to provide the crude product. Flash column chromatography was carried out using a Hex:EtOAc system from (100:0)-(5:1).

General Procedure B: To a flame-dried flask equipped with condenser and stir bar, anhydrous aluminum chloride (1.1-3.0 equiv) was carefully added to the acid chloride (1 equiv) in CS₂ (or benzene), and the reaction mixture was allowed to stir under nitrogen. After several minutes, the aromatic system (1.1-2.0 equiv) was added slowly to the stirring solution and the evolution of gas became visible at this time. The yellow mixture was then stirred at room temp for 2 hrs and then gentle heating was applied for an additional 20 min. After cooling, the reaction was quenched with 20 mL water while at 0°C, and then 30 mL of conc. HCl was added immediately following. Extraction with M CH₂Cl₂ (3x50 mL) was conducted, the organic layers were dried over MgSO₄, and the solution was then evaporated to provide the crude material. Flash column chromatography was carried out using a Hex:EtOAc system from (100:0)-(5:1).

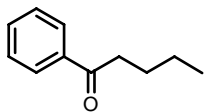
Preparation of (3-Dimethylaminopropyl) triphenylphosphonium bromide: (3-Bromopropyl) triphenylphosphonium bromide (1.0 equiv) was added to a flame dried flask under N₂. The salt was then stirred in absolute EtOH at 0°C and a dimethylamine solution in THF (1.5 equiv) was added dropwise. The solution was stirred with warming to room temp for over 15 hrs. The solvent was then evaporated and the salt used directly without further purification.

General Procedure C: (3-Dimethylaminopropyl) triphenylphosphonium bromide (1.5-2.0 equiv) obtained from the procedure above was placed in a flame dried flask containing dry toluene and kept under N₂. The mixture was cooled to 0°C and a solution of 0.5 M KHMDS in toluene (1.5-2.0 equiv) was added dropwise. Stirring was continued

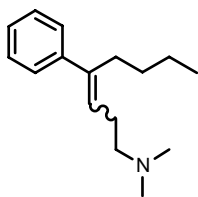
for several minutes, after which the ketone (1.0 equiv) was added slowly. The reaction was allowed to continue stirring overnight with warming to room temp and was later quenched by addition of a sat. NH_4Cl solution. The crude material was then extracted into CH_2Cl_2 (3 x 50 mL), washed with brine (1 x 20 mL), dried over MgSO_4 , filtered, and evaporated to provide the crude product. Flash column chromatography was carried out using a CH_2Cl_2 : MeOH system from (100:0)-(9:1).



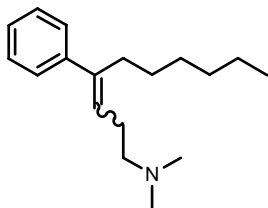
Dimethyl-(4-phenyl-hex-3-enyl)-amine. **(3.1)** Procedure C was carried out using (3-dimethylaminopropyl) triphenylphosphonium bromide (1.6 g, 3.73 mmol), 2.5 M $n\text{BuLi}/\text{Hex}$ (1.5 mL, 3.73 mmol), propiophenone (0.25g, 1.86 mmol), and THF (5 mL). The product was obtained in 0.70 g as a white solid, 93% yield. TLC: CH_2Cl_2 : MeOH (10:1), $R_f=0.6$. ^1H NMR (CDCl_3 , 300 MHz) δ 7.32-7.18 (m, 4H), 7.18-7.08 (appt d, 1H, $J=8.4$), 5.58-5.54 (t, 0.42H, $J=6.8$), 5.41-5.36 (t, 0.58H, $J=7.2$), 2.52-2.44 (m, 4H), 2.38 (s, 3H), 2.27 (s, 3H), 2.21-2.14 (appt q, 2H, $J=7.6$), 0.98-0.90 (m, 3H); ^{13}C NMR (CDCl_3) δ 146.01, 143.97, 142.52, 140.91, 128.28, 128.18, 126.86, 126.39, 123.63, 120.91, 59.02, 58.77, 44.73, 44.15, 32.26, 26.03, 25.68, 23.21, 13.67, 12.97. ESIMS: 204 ($\text{M}+\text{H}$). HRMS calc for $\text{C}_{14}\text{H}_{21}\text{N}$: 204.1747. Found: 204.1752. Found mp=104-110°C.



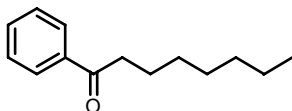
1-Phenyl-pentan-1-one. (**Ketone for 3.2**) Procedure A was carried out using benzonitrile (1.0 g, 7.62 mmol), CH_2Cl_2 (10 mL), and 2 M butylmagnesium chloride/THF (5.7 mL, 11.40 mmol). The product was obtained in 1.3 g as a pale yellow liquid, 83% yield. TLC: Hex: EtOAc (15:1), $R_f=0.44$. ^1H NMR (CDCl_3 , 300 MHz) δ 7.83-7.80 (m, 2H), 7.39-7.25 (m, 3H), 2.81-2.76 (t, 2H, $J=7.4$), 1.60-1.53 (qui, 2H, $J=7.5$), 1.30-1.21 (sxt, 2H, $J=5.7$), 0.84-0.79 (t, 3H, $J=7.4$); ^{13}C NMR (CDCl_3) δ 199.00, 136.14, 131.88, 127.53, 127.02, 37.21, 25.46, 21.51, 12.99.



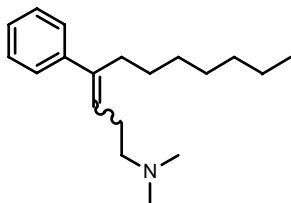
Dimethyl-(4-phenyl-oct-3-enyl)-amine. (**3.2**) Procedure C was carried out using (3-dimethylaminopropyl) triphenylphosphonium bromide (2.0 g, 4.67 mmol), 2.5 M nBuLi/Hex (1.8 mL, 4.66 mmol), 1-phenyl-pentan-1-one (0.5 g, 3.10 mmol), and THF (10 mL). The product was obtained in 0.24 g as a yellow oil, 33% yield. TLC: CH_2Cl_2 : MeOH (10:1), $R_f=0.48$. ^1H NMR (CDCl_3 , 300 MHz) δ 7.31-7.08 (m, 5H), 5.60-5.55 (m, 0.28H), 5.41-5.37 (t, 0.72H, $J=6.0$), 2.51-2.35 (m, 4H), 2.32 (br s, 4H), 2.20 (br s, 5H), 2.15-2.12 (m, 2H),), 0.98-0.88 (m, 3H); ^{13}C NMR (CDCl_3) δ 144.55, 142.87, 142.42, 140.86, 127.94, 127.83, 126.38, 126.31, 126.24, 124.40, 121.94, 59.14, 44.90, 44.55, 31.92, 26.32, 22.82, 13.36, 12.75. ESIMS: 232 (M+H). HRMS calc for $\text{C}_{16}\text{H}_{26}\text{N}$: 232.2065. Found: 232.2061.



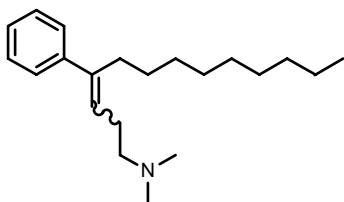
Dimethyl-(4-phenyl-dec-3-enyl)-amine. **(3.3)** Procedure C was carried out using (3-dimethylaminopropyl) triphenylphosphonium bromide (1.7 g, 3.97 mmol), 2.5 M nBuLi/Hex (1.62 mL, 3.90 mmol), hexyl phenyl ketone (0.5 g, 2.63 mmol), and THF (10 mL). The product was obtained in 0.40 g as a pale orange oil, 59% yield. TLC: CH₂Cl₂: MeOH (10:1), R_f=0.57. ¹H NMR (CDCl₃, 300 MHz) δ 7.32-7.23 (m, 4H), 7.13-7.11 (m, 1H), 5.62-5.58 (m, 0.24H), 5.44-5.39 (m, 0.76H), 2.50-2.42 (m, 3H), 2.35 (s, 2H), 2.33-2.30 (m, 1H), 2.25 (s, 4H), 2.19-2.16 (m, 1H), 1.26-1.25 (br s, 9H), 0.87-0.83 (m, 3H); ¹³C NMR (CDCl₃) δ 144.49, 144.46, 141.88, 129.02, 128.97, 127.46, 125.99, 123.78, 60.09, 45.97, 45.48, 40.18, 32.49, 30.77, 30.11, 29.67, 29.50, 28.82, 27.21, 23.45, 14.91. ESIMS: 260 (M+H).



1-Phenyl-octan-1-one. (**Ketone for 3.4**) Procedure B was carried out using octanoyl chloride (1.0 g, 6.14 mmol), CS₂ (5 mL), AlCl₃ (0.5 g, 2.63 mmol), and benzene (0.8 mL, 9.2 mmol). The product was obtained in 0.90 g as a yellow liquid, 72% yield. TLC: Hex: EtOAc (7:1), R_f=0.75. ¹H NMR (CDCl₃, 300 MHz) δ 7.96-7.93 (d, 2H, *J*=8.1), 7.46-7.43 (m, 3H), 2.97-2.92 (t, 2H, *J*=7.4), 1.74-1.70 (t, 2H, *J*=6.0), 1.33-1.28 (m, 8H), 0.89-0.86 (m, 3H); ¹³C NMR (CDCl₃) δ 200.46, 132.75, 128.44, 127.96, 38.52, 31.63, 29.25, 29.07, 24.30, 22.55, 14.00. ESIMS: 205 (M+H).

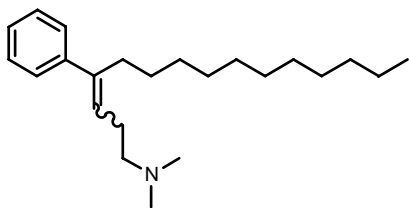


Dimethyl-(4-phenyl-undec-3-enyl)-amine. **(3.4)** Procedure C was carried out using (3-dimethylaminopropyl) triphenylphosphonium bromide (1.8 g, 4.17 mmol), 2.5 M nBuLi/Hex (1.6 mL, 4.17 mmol), 1-phenyl-octan-1-one (0.5 g, 2.45 mmol), and THF (10 mL). The product was obtained in 0.67 g as a yellow oil, 30% yield. TLC: CH₂Cl₂: MeOH (10:1), R_f=0.57. ¹H NMR (CDCl₃, 300 MHz) δ 7.34-7.23 (m, 3H), 7.12-7.10 (d, 2H, *J*=8.1), 5.43-5.38 (t, 1H, *J*=7.5), 2.47-2.42 (t, 2H, *J*=7.8), 2.37-2.31 (m, 2H), 2.27 (s, 6H), 2.23-2.15 (m, 2H), 1.21 (br s, 10H), 0.86-0.81 (t, 3H, *J*=7.5); ¹³C NMR (CDCl₃) δ 143.28, 140.46, 127.67, 127.61, 126.11, 122.21, 58.63, 44.02, 38.84, 31.33, 28.62, 27.52, 25.72, 22.14, 13.60. ESIMS: 274 (M+H). HRMS calc for C₁₉H₃₂N: 274.2535. Found: 274.2523.

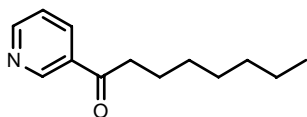


Dimethyl-(4-phenyl-tridec-3-enyl)-amine. **(3.5)** Procedure C was carried out using (3-dimethylaminopropyl) triphenylphosphonium bromide (0.9 g, 2.06 mmol), 0.6 M NaHMDS/Tol (3.3 mL, 2.06 mmol), decanophenone (0.4 g, 1.72 mmol), and THF (5 mL). The product was obtained in 0.15 g as a yellow oil, 29.4% yield. TLC: CH₂Cl₂: MeOH (10:1), R_f=0.39. ¹H NMR (CDCl₃, 300 MHz) δ 7.28-7.21 (m, 2H), 7.21-7.17 (t, 1H, *J*=6.3), 7.09-7.05 (m, 1H), 5.40-5.35 (t, 1H, *J*=6.8), 2.49-2.42 (m, 2H), 2.27 (br s, 8H), 2.21-2.13 (m, 2H), 1.19 (br s, 13H), 0.85-0.79 (m, 3H); ¹³C NMR (CDCl₃) δ

144.15, 141.07, 128.33, 126.83, 122.66, 59.21, 44.59, 39.52, 32.06, 29.74, 29.61, 29.48, 29.34, 28.17, 26.92, 22.86, 14.32. ESIMS: 302 (M+H). HRMS calc for C₂₁H₃₆N: 302.2848. Found: 302.2846.

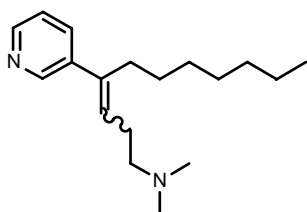


Dimethyl-(4-phenyl-pentadec-3-enyl)-amine. **(3.6)** Procedure C was carried out using (3-dimethylaminopropyl) triphenylphosphonium bromide (0.8 g, 1.85 mmol), 0.6 M NaHMDS/Tol (3.0 mL, 1.85 mmol), dodecanophenone (0.4 g, 1.54 mmol), and THF (5 mL). The product was obtained in 0.22 g as a pale yellow oil, 44% yield. TLC: CH₂Cl₂: MeOH (10:1), R_f=0.39. ¹H NMR (CDCl₃, 300 MHz) δ 7.38-7.27 (m, 4H), 7.18-7.16 (m, 1H), 5.67-5.65 (m, 0.14H), 5.48-5.45 (t, 0.86H, *J*=8.4), 2.56-2.40 (br m, 4H), 2.38 (s, 1H), 2.26 (s, 5H), 2.22-2.17 (m, 2H), 1.30 (br s, 18H), 0.94-0.91 (t, 3H, *J*=9.0); ¹³C NMR (CDCl₃) δ 143.40, 141.93, 141.34, 128.44, 128.25, 126.70, 126.54, 125.68, 123.65, 59.73, 45.51, 45.14, 39.55, 32.13, 29.84, 29.65, 29.56, 29.39, 28.27, 26.96, 22.91, 14.35. ESIMS: 330 (M+H). HRMS calc for C₂₃H₄₀N: 330.3161. Found: 330.3169.

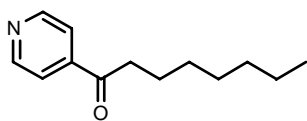


1-Pyridin-3-yl-octan-1-one. (*Ketone for 3.7*) Procedure A was carried out using 3-cyanopyridine (0.75 g, 7.21 mmol), CH₂Cl₂ (5 mL), and 1 M heptylmagnesium bromide/Et₂O (10.8 mL, 10.8 mmol). The product was obtained in 1.0 g as a pale orange solid, 71% yield. TLC: Hex: EtOAc (5:1), R_f=0.40. ¹H NMR (CDCl₃, 300 MHz) δ 8.87 (s, 1H), 8.46-8.43 (m, 1H), 7.94-7.90 (m, 1H), 7.17-7.09 (m, 1H), 2.72-2.67 (m, 2H),

1.44-1.41 (t, 2H, $J=6.6$), 1.04-0.98 (br s, 8H), 0.57-0.56 (t, 3H, $J=5.1$); ^{13}C NMR (CDCl_3) δ 198.67, 153.03, 149.39, 134.98, 131.96, 123.33, 38.60, 31.49, 29.02, 23.77, 22.41, 13.85. ESIMS: 206 ($\text{M}+\text{H}$). HRMS calc for $\text{C}_{13}\text{H}_{20}\text{NO}$: 206.1545. Found: 206.1547.

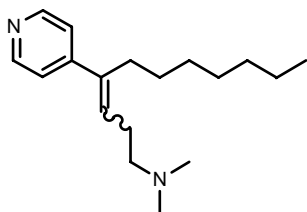


Dimethyl-(4-pyridin-3-yl-undec-3-enyl)-amine. (**3.7**) Procedure C was carried out using (3-dimethylaminopropyl) triphenylphosphonium bromide (1.56 g, 3.64 mmol), 0.5 M KHMDs/Tol (7.2 mL, 3.60 mmol), 1-pyridin-3-yl-octan-1-one (0.5 g, 2.44 mmol), and Tol (5 mL). The product was obtained in 0.48 g as a pale orange oil, 44% yield. TLC: CH_2Cl_2 : MeOH (11:1), $R_f=0.34$. ^1H NMR (CDCl_3 , 300 MHz) δ 8.45-8.33 (br m, 2H), 7.33-7.31 (d, 1H, $J=7.5$), 7.12 (br s, 1H), 5.43-5.38 (t, 1H, $J=7.2$), 2.29-2.18 (m, 4H), 2.11 (br s, 6H), 1.07 (br s, 10H), 0.72-0.68 (t, 3H, $J=6.5$); ^{13}C NMR (CDCl_3) δ 149.11, 147.81, 139.55, 136.40, 135.53, 125.23, 123.05, 58.97, 44.61, 38.90, 31.61, 28.88, 27.77, 26.50, 22.46, 13.93. ESIMS: 275 ($\text{M}+\text{H}$). HRMS calc for $\text{C}_{18}\text{H}_{31}\text{N}_2$: 275.2487. Found: 275.2489.

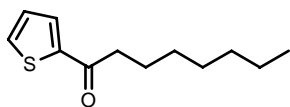


1-Pyridin-4-yl-octan-1-one. (**Ketone for 3.8**) Procedure A was carried out using 4-cyanopyridine (0.75 g, 7.21 mmol), CH_2Cl_2 (5 mL), and 1 M heptylmagnesium bromide/ Et_2O (10.8 mL, 10.8 mmol). The product was obtained in 1.0 g as a pale yellow solid, 71% yield. TLC: Hex: EtOAc (5:1), $R_f=0.50$. ^1H NMR (CDCl_3 , 300 MHz) δ

8.75-8.73 (m, 2H), 7.68-7.66 (m, 2H), 2.94-2.87 (m, 2H), 1.70-1.65 (m, 2H), 1.28 (br s, 8H), 0.83-0.80 (m, 3H); ^{13}C NMR (CDCl_3) δ 199.17, 150.63, 120.81, 38.56, 31.49, 28.96, 25.76, 23.61, 22.42, 13.84.

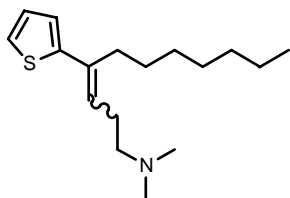


Dimethyl-(4-pyridin-4-yl-undec-3-enyl)-amine. **(3.8)** Procedure C was carried out using (3-dimethylaminopropyl) triphenylphosphonium bromide (1.56 g, 3.64 mmol), 0.5 M KHMDS/Tol (7.2 mL, 3.60 mmol), 1-pyridin-4-yl-octan-1-one (0.5 g, 2.44 mmol), and Tol (5 mL). The product was obtained in 0.29 g as an orange oil, 44% yield. TLC: CH_2Cl_2 : MeOH (11:1), R_f =0.45. ^1H NMR (CDCl_3 , 300 MHz) δ 8.46-8.44 (d, 2H, J =5.4), 6.97-6.95 (d, 2H, J =5.1), 5.44-5.39 (t, 3H, J =7.1), 2.22-2.15 (m, 4H), 2.04 (s, 6H), 2.00-1.96 (m, 2H), 1.13 (br s, 10H), 0.77-0.72 (t, 3H, J =6.8); ^{13}C NMR (CDCl_3) δ 149.77, 149.51, 140.15, 126.32, 123.64, 59.72, 45.45, 38.61, 31.91, 29.17, 28.13, 27.44, 22.75, 14.22. ESIMS: 275 ($\text{M}+\text{H}$). HRMS calc for $\text{C}_{18}\text{H}_{31}\text{N}_2$: 275.2487. Found: 275.2476.

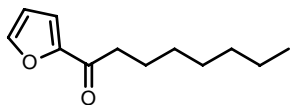


1-Thiophen-2-yl-octan-1-one. (**Ketone for 3.9**) Procedure B was carried out using octanoyl chloride (2.4 g, 14.81 mmol), benzene (30 mL), AlCl_3 (1.97 g, 14.81 mmol), and thiophene (1.0 g, 11.85 mmol). The product was obtained in 2.60 g as an orange liquid, 100% yield. TLC: Hex: EtOAc (15:1), R_f =0.57. ^1H NMR (CDCl_3 , 300 MHz) δ 7.52-7.51 (d, 1H, J =3.6), 7.42-7.40 (d, 1H, J =4.8), 6.90-6.89 (m, 1H), 2.71-2.66 (t, 2H,

$J=7.4$), 1.54-1.49 (m, 2H), 1.12-1.09 (m, 8H), 0.70-0.68 (m, 3H); ^{13}C NMR (CDCl_3) δ 192.79, 144.40, 133.05, 131.52, 127.91, 39.07, 31.59, 29.15, 29.04, 24.55, 22.51, 13.93.

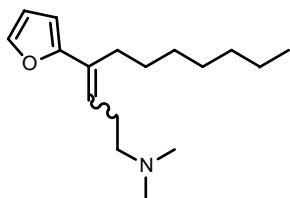


Dimethyl-(4-thiophen-2-yl-undec-3-enyl)-amine. **(3.9)** Procedure C was carried out using (3-dimethylaminopropyl) triphenylphosphonium bromide (1.53 g, 3.57 mmol), 2.5 M $n\text{BuLi}/\text{Hex}$ (1.44 mL, 3.60 mmol), 1-thiophen-2-yl-octan-1-one (0.5 g, 2.44 mmol), and Tol (5 mL). The product was obtained in 0.11 g as a pale yellow oil, 18% yield. TLC: CH_2Cl_2 : MeOH (10:1), $R_f=0.39$. ^1H NMR (CDCl_3 , 300 MHz) δ 7.23-7.22 (d, 1H, $J=5.1$), 7.00-6.97 (t, 1H, $J=8.4$), 6.90-6.89 (d, 1H, $J=3.6$), 5.49 (m, 1H), 2.43-2.42 (m, 2H), 2.39-2.34 (m, 4H), 2.27 (s, 6H), 1.41-1.37 (t, 2H, $J=6.6$), 1.24 (br s, 8H), 0.88-0.83 (appt t, 3H, $J=6.6$); ^{13}C NMR (CDCl_3) δ 142.20, 134.91, 126.53, 125.81, 125.32, 124.10, 59.22, 44.87, 39.83, 31.69, 29.02, 28.95, 28.58, 27.17, 22.51, 13.96. ESIMS: 280 (M+H). HRMS calc for $\text{C}_{17}\text{H}_{30}\text{NS}$: 280.2099. Found: 280.2107.

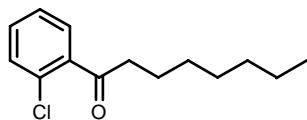


1-Furan-2-yl-octan-1-one. **(Ketone for 3.10)** Procedure A was carried out using 2-furanonitrile (0.60 g, 6.44 mmol), CH_2Cl_2 (5 mL), and 1 M heptylmagnesium bromide/ Et_2O (9.6 mL, 9.6 mmol). The product was obtained in 0.9 g as an orange liquid, 74% yield. TLC: Hex: EtOAc (9:1), $R_f=0.71$. ^1H NMR (CDCl_3 , 300 MHz) δ 7.52 (s, 1H), 7.13-7.12 (d, 1H, $J=3.6$), 6.48-6.46 (m, 1H), 2.76-2.73 (t, 2H, $J=7.8$), 1.69-

1.62 (m, 2H), 1.28-1.23 (br s, 8H), 0.83-0.81 (m, 3H); ^{13}C NMR (CDCl_3) δ 188.48, 152.25, 145.44, 115.90, 111.39, 37.67, 31.03, 28.60, 28.45, 23.53, 21.93, 13.29.

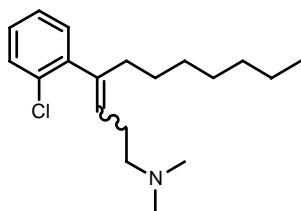


(4-Furan-2-yl-undec-3-enyl)-dimethyl-amine. (**3.10**) Procedure C was carried out using (3-dimethylaminopropyl) triphenylphosphonium bromide (1.32 g, 3.08 mmol), 0.5 M KHMDS/Tol (6.0 mL, 3.08 mmol), 1-furan-2-yl-octan-1-one (0.4 g, 2.44 mmol), and Tol (5 mL). The product was obtained in 0.12 g as an orange oil, 22% yield. TLC: CH_2Cl_2 : MeOH (11:1), R_f =0.31. ^1H NMR (CDCl_3 , 300 MHz) δ 7.38 (s, 1H), 6.39-6.37 (m, 1H), 6.27-6.26 (appt d, 1H, J =3.3), 5.42-5.38 (t, 1H, J =6.8), 2.60-2.53 (q, 2H, J =7.3), 2.42-2.40 (m, 4H), 2.35 (s, 6H), 1.45-1.40 (t, 2H, J =6.8), 1.25 (br s, 8H), 0.88-0.84 (m, 3H); ^{13}C NMR (CDCl_3) δ 154.42, 141.23, 130.56, 125.82, 110.83, 108.25, 59.82, 45.53, 36.17, 32.03, 29.65, 29.54, 29.32, 27.78, 22.84, 14.30. ESIMS: 264 ($\text{M}+\text{H}$). HRMS calc for $\text{C}_{17}\text{H}_{30}\text{NO}$: 264.2327. Found: 264.2316.

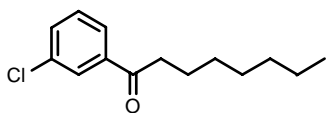


1-(2-Chloro-phenyl)-octan-1-one. (**Ketone for 3.11**) Procedure A was carried out using 2-chlorobenzonitrile (0.75 g, 5.50 mmol), CH_2Cl_2 (10 mL), and 1 M heptylmagnesium bromide/ Et_2O (8.2 mL, 8.2 mmol). The product was obtained in 1.1 g as a yellow liquid, 85% yield. TLC: Hex: EtOAc (15:1), R_f =0.55. ^1H NMR (CDCl_3 , 300 MHz) δ 7.38-7.24 (m, 4H), 2.88-2.83 (appt t, 2H, J =7.4), 1.69-1.62 (m, 2H), 1.26-1.22 (br s, 8H), 0.84-0.82 (m, 3H); ^{13}C NMR (CDCl_3) δ 203.52, 139.66, 132.73, 131.33, 130.29, 128.60,

126.77, 42.85, 38.46, 31.61, 29.06, 24.07, 22.55, 13.99. ESIMS: 239.1 (M+H). HRMS calc for $C_{14}H_{20}OCl$: 239.1203. Found: 239.1212.

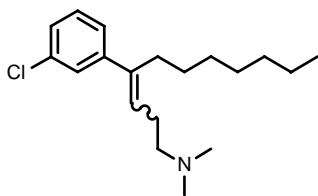


[4-(2-Chloro-phenyl)-undec-3-enyl]-dimethyl-amine. (**3.11**) Procedure C was carried out using (3-dimethylaminopropyl) triphenylphosphonium bromide (0.8 g, 1.89 mmol), 0.5 M KHMDS/Tol (3.8 mL, 1.90 mmol), 1-(2-chloro-phenyl)-octan-1-one (0.3 g, 1.26 mmol), and Tol (5 mL). The product was obtained in 0.07 g as a yellow oil, 18% yield. TLC: CH_2Cl_2 : MeOH (9:1), R_f =0.36. 1H NMR ($CDCl_3$, 300 MHz) δ 7.40-7.37 (m, 1H), 7.29-7.20 (m, 2H), 7.09-7.06 (m, 1H), 5.53-5.49 (t, 1 H, J =7.2), 2.55-2.50 (appt t, 2H, J =7.2), 2.32 (s, 8H), 2.10-2.02 (m, 2H), 1.24 (br s, 10H), 0.89-0.84 (appt t, 3H, J =6.6); ^{13}C NMR ($CDCl_3$) δ 141.53, 139.63, 132.55, 130.40, 129.48, 128.16, 126.58, 123.94, 58.36, 44.29, 38.20, 31.80, 29.28, 29.12, 27.63, 26.18, 22.61, 14.07. ESIMS: 308 (M+H), 310 (M+3H). HRMS calc for $C_{19}H_{31}NCl$: 308.2145. Found: 308.2145.

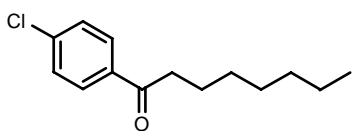


1-(3-Chloro-phenyl)-octan-1-one. (**Ketone for 3.12**) Procedure A was carried out using 3-chlorobenzonitrile (6.0 g, 44.0 mmol), CH_2Cl_2 (20 mL), and 1 M heptylmagnesium bromide/ Et_2O (40 mL, 40.0 mmol). The product was obtained in 5.4 g as a yellow oil, 52% yield. TLC: Hex: EtOAc (15:1), R_f =0.55. 1H NMR ($CDCl_3$, 300 MHz) δ 7.92-7.91 (d, 1H, J =1.8), 7.84-7.81 (m, 1H), 7.53-7.50 (m, 1H), 7.42-7.37 (appt t, 1H, J =5.0), 2.96-2.91 (appt t, 2H, J =7.4), 1.75-1.68 (m, 2H), 1.34-1.28 (br s, 8H), 0.88-0.86 (m, 3H);

^{13}C NMR (CDCl_3) δ 199.41, 138.82, 135.10, 133.01, 130.12, 128.40, 126.35, 38.93, 31.92, 29.47, 29.35, 24.40, 22.85, 14.32.

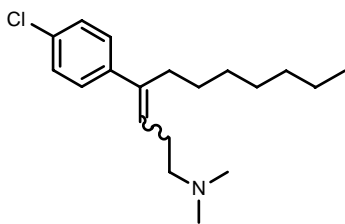


[4-(3-Chloro-phenyl)-undec-3-enyl]-dimethyl-amine. (**3.12**) Procedure C was carried out using (3-dimethylaminopropyl) triphenylphosphonium bromide (0.87 g, 2.0 mmol), 0.5 M KHMDS/Tol (4.0 mL, 2.0 mmol), 1-(3-chloro-phenyl)-octan-1-one (0.32 g, 1.35 mmol), and Tol (5 mL). The product was obtained in 0.30 g as a pale yellow oil, 73% yield. TLC: CH_2Cl_2 : MeOH (9:1), R_f =0.30. ^1H NMR (CDCl_3 , 300 MHz) δ 7.23-7.21 (m, 2H), 7.02-7.00 (m, 2H), 5.57 (s, 0.1H), 5.43-5.38 (t, 0.9H, J =7.2), 2.26-2.24 (m, 2H), 2.22-2.19 (m, 2H), 2.09 (s, 6H), 2.05-2.02 (m, 2H), 1.18 (br s, 10H), 0.82-0.78 (t, 3H, J =6.6); ^{13}C NMR (CDCl_3) δ 141.05, 139.40, 131.73, 129.41, 128.29, 128.13, 127.95, 124.73, 59.46, 45.15, 45.02, 38.93, 31.54, 28.82, 27.79, 27.03, 22.36, 13.82. ESIMS: 308 (M+H). HRMS calc for $\text{C}_{19}\text{H}_{31}\text{NCl}$: 308.2145. Found: 308.2124.

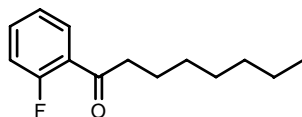


1-(4-Chloro-phenyl)-octan-1-one. (**Ketone for 3.13**) Procedure A was carried out using 4-chlorobenzonitrile (1.0 g, 7.27 mmol), CH_2Cl_2 (5 mL), and 1 M heptylmagnesium bromide/ Et_2O (10.9 mL, 10.9 mmol). The product was obtained in 1.5 g as a yellow solid, 87% yield. TLC: Hex: EtOAc (15:1), R_f =0.51. ^1H NMR (CDCl_3 , 300 MHz) δ 7.91-7.88 (d, 2H, J =8.7), 7.44-7.41 (d, 2H, J =8.4), 2.95-2.90 (appt t, 2H, J =7.4), 1.72-1.69 (m, 2H), 1.33-1.28 (br s, 8H), 0.88-0.85 (m, 3H); ^{13}C NMR (CDCl_3) δ 199.52,

139.46, 135.56, 129.68, 129.06, 128.76, 128.41, 38.83, 31.93, 29.52, 29.37, 24.51, 22.86, 14.33.

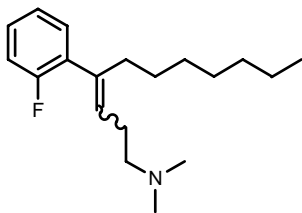


[4-(4-Chloro-phenyl)-undec-3-enyl]-dimethyl-amine. (**3.13**) Procedure C was carried out using (3-dimethylaminopropyl) triphenylphosphonium bromide (1.35 g, 3.15 mmol), 0.5 M KHMDS/Tol (6.4 mL, 3.20 mmol), 1-(4-chloro-phenyl)-octan-1-one (0.5 g, 2.11 mmol), and Tol (10 mL). The product was obtained in 0.55 g as a yellow oil, 85% yield. TLC: CH₂Cl₂: MeOH (10:1), R_f=0.48. ¹H NMR (CDCl₃, 300 MHz) δ 7.29-7.22 (m, 2H), 7.05-7.02 (d, 2H, *J*=8.1), 5.55-5.52 (m, 0.8H), 5.41-5.37 (t, 0.92H, *J*=6.9), 2.54-2.49 (appt t, 2H, *J*=7.5), 2.42 (s, 2H), 2.33 (s, 6H), 2.19-2.16 (m, 2H), 1.19 (br s, 10H), 0.85-0.81 (appt t, 3H, *J*=6.7); ¹³C NMR (CDCl₃) δ 143.16, 139.35, 129.75, 128.58, 123.10, 58.96, 44.50, 39.39, 31.98, 29.26, 28.11, 26.18, 22.81, 14.28. ESIMS: 308 (M+H). HRMS calc for C₁₉H₃₁NCl: 308.2145. Found: 308.2136.

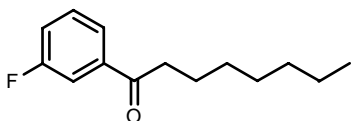


1-(2-Fluoro-phenyl)-octan-1-one. (**Ketone for 3.14**) Procedure A was carried out using 2-fluorobenzonitrile (0.5 g, 3.75 mmol), CH₂Cl₂ (5 mL), and 1 M heptylmagnesium bromide/Et₂O (5.6 mL, 5.6 mmol). The product was obtained in 0.7 g as a yellow liquid, 78% yield. TLC: Hex: EtOAc (15:1), R_f=0.31. ¹H NMR (CDCl₃, 300 MHz) δ 7.87-7.82 (m, 1H), 7.53-7.48 (m, 1H), 7.26-7.09 (m, 2H), 2.99-2.93 (m, 1H), 1.73-1.68 (m, 2H), 1.59 (s, 1H), 1.32-1.25 (br s, 8H), 0.90-0.85 (appt t, 3H, *J*=6.8); ¹³C NMR (CDCl₃)

δ 199.27, 134.70, 131.08, 126.35, 124.81, 117.20, 116.88, 44.03, 32.18, 29.61, 29.35, 24.47, 23.09, 14.5.

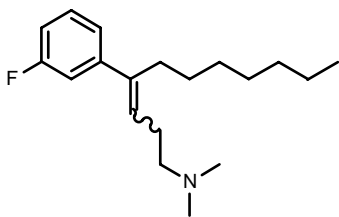


[4-(2-Fluorophenyl)-undec-3-enyl]-dimethyl-amine. (**3.14**) Procedure C was carried out using (3-dimethylaminopropyl) triphenylphosphonium bromide (1.73 g, 4.04 mmol), 0.5 M KHMDS/Tol (8.0 mL, 4.0 mmol), 1-(2-fluoro-phenyl)-octan-1-one (0.6 g, 2.70 mmol), and Tol (5 mL). The product was obtained in 0.33 g as a yellow oil, 42% yield. TLC: CH₂Cl₂: MeOH (10:1), R_f =0.46. ¹H NMR (CDCl₃, 300 MHz) δ 7.26-7.19 (m, 1H), 7.10-7.00 (m, 3H), 5.55-5.51 (t, 1H, J =7.2), 2.42-2.36 (appt t, 2H, J =7.8), 2.30 (s, 2H), 2.23 (s, 6H), 2.10-2.03 (m, 2H), 1.21 (br s, 10H), 0.86-0.82 (t, 3H, J =6.6); ¹³C NMR (CDCl₃) δ 160.44, 158.49, 137.13, 130.53, 128.40, 125.61, 123.77, 115.52, 115.34, 58.85, 44.72, 38.56, 31.75, 29.05, 27.89, 26.89, 22.57, 14.03. ESIMS: 292 (M+H). HRMS calc for C₁₉H₃₁NF: 292.2441. Found: 292.2448.

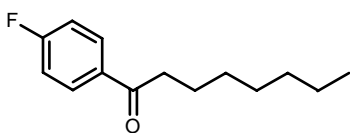


1-(3-Fluoro-phenyl)-octan-1-one. (**Ketone for 3.15**) Procedure A was carried out using 3-fluorobenzonitrile (0.5 g, 4.13 mmol), CH₂Cl₂ (5 mL), and 1 M heptylmagnesium bromide/Et₂O (6.2 mL, 6.2 mmol). The product was obtained in 1.05 g as a yellow liquid, 100% yield. TLC: Hex: EtOAc (15:1), R_f =0.35. ¹H NMR (CDCl₃, 300 MHz) δ 7.94-7.89 (m, 1H), 7.68-7.54 (m, 1H), 7.37-7.32 (m, 1H), 7.07-7.01 (m, 1H), 2.89-2.84 (m, 2H), 1.66-1.64 (m, 2H), 1.27-1.20 (br s, 8H), 0.82-0.80 (m, 3H); ¹³C NMR (CDCl₃) δ

198.67, 167.15, 130.55, 130.43, 128.57, 115.53, 115.27, 38.36, 31.56, 29.17, 29.0, 24.19, 22.47, 13.89.

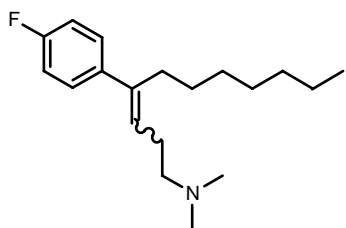


[4-(3-Fluoro-phenyl)-undec-3-enyl]-dimethyl-amine. **(3.15)** Procedure C was carried out using (3-dimethylaminopropyl) triphenylphosphonium bromide (1.70 g, 3.97 mmol), 0.5 M KHMDS/Tol (8.2 mL, 4.1 mmol), 1-(3-fluoro-phenyl)-octan-1-one (0.6 g, 2.70 mmol), and Tol (10 mL). The product was obtained in 0.38 g as a yellow oil, 49% yield. TLC: CH₂Cl₂: MeOH (10:1), R_f=0.54. ¹H NMR (CDCl₃, 300 MHz) δ 7.29-7.22 (m, 1H), 6.93-6.81 (m, 3H), 5.65 (s, 0.1H), 5.46-5.41 (t, 0.9H, *J*=7.1), 2.29-2.25 (m, 4H), 2.15 (s, 6H), 2.11-2.06 (m, 2H), 1.22 (br s, 10H), 0.87-0.83 (t, 3H, *J*=6.6); ¹³C NMR (CDCl₃) δ 163.56, 161.60, 143.50, 141.45, 129.37, 124.81, 123.99, 115.03, 113.16, 59.61, 45.18, 39.10, 31.77, 29.04, 28.00, 27.14, 22.59, 14.03. ESIMS: 292 (M+H). HRMS calc for C₁₉H₃₁NF: 292.2441. Found: 292.2435.

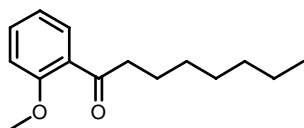


1-(4-Fluoro-phenyl)-octan-1-one. **(Ketone for 3.16)** Procedure A was carried out using 4-fluorobenzonitrile (0.5 g, 4.13 mmol), CH₂Cl₂ (5 mL), and 1 M heptylmagnesium bromide/Et₂O (6.2 mL, 6.2 mmol). The product was obtained in 1.08 g as a yellow oil, 100% yield. TLC: Hex: EtOAc (15:1), R_f=0.41. ¹H NMR (CDCl₃, 300 MHz) δ 7.96-7.91 (m, 2H), 7.09-7.03 (t, 2H, *J*=8.7), 2.90-2.85 (t, 2H, *J*=7.5), 1.70-1.65 (m, 2H), 1.29-

1.21 (br s, 8H), 0.86-0.81 (appt t, 3H, $J=6.3$); ^{13}C NMR (CDCl_3) δ 199.03, 167.47, 133.64, 130.88, 130.76, 115.88, 115.59, 38.69, 31.91, 29.50, 29.35, 24.52, 22.82, 14.24.

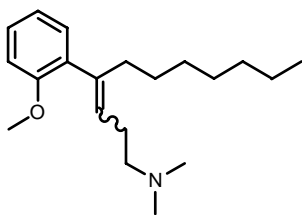


[4-(4-Fluoro-phenyl)-undec-3-enyl]-dimethyl-amine. (**3.16**) Procedure C was carried out using (3-dimethylaminopropyl) triphenylphosphonium bromide (1.44 g, 3.40 mmol), 0.5 M KHMDS/Tol (6.8 mL, 3.4 mmol), 1-(4-fluoro-phenyl)-octan-1-one (0.5 g, 2.30 mmol), and Tol (5 mL). The product was obtained in 0.30 g as a yellow oil, 46% yield. TLC: CH_2Cl_2 : MeOH (10:1), $R_f=0.39$. ^1H NMR (CDCl_3 , 300 MHz) δ 7.28-7.23 (m, 1H), 7.10-6.936 (m, 3H), 5.54-5.50 (t, 0.27H, $J=6.8$), 5.42-5.37 (t, 0.73H, $J=5.0$), 2.49-2.43 (m, 3H), 2.41 (s, 1H), 2.35 (s, 5H), 2.19-2.16 (m, 2H), 1.25-1.21 (br s, 10H), 0.86-0.82 (t, 3H, $J=6.8$); ^{13}C NMR (CDCl_3) δ 142.88, 129.98, 129.88, 128.08, 127.98, 123.44, 115.36, 115.08, 59.31, 45.21, 44.81, 39.58, 32.01, 29.29, 28.16, 26.56, 22.84, 14.30. ESIMS: 292 (M+H). HRMS calc for $\text{C}_{19}\text{H}_{31}\text{NF}$: 292.2441. Found: 292.2443.

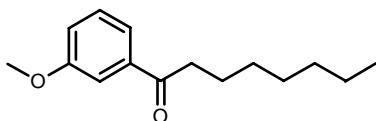


1-(2-Methoxy-phenyl)-octan-1-one. (**Ketone for 3.17**) Procedure A was carried out using 2-methoxybenzonitrile (0.5 g, 3.76 mmol), CH_2Cl_2 (5 mL), and 1 M heptylmagnesium bromide/ Et_2O (5.6 mL, 5.6 mmol). The product was obtained in 0.83 g as a clear oil, 94% yield. TLC: Hex: EtOAc (15:1), $R_f=0.46$. ^1H NMR (CDCl_3 , 300 MHz) δ 7.62-7.59 (dd, 1H, $J=9.6$), 7.40-7.34 (m, 1H), 6.95-6.88 (m, 2H), 3.82 (s, 3H), 2.94-2.89 (t, 2H, $J=7.5$), 1.66-1.61 (m, 2H), 1.29-1.24 (br s, 8H), 0.86-0.82 (appt t, 3H, $J=6.8$); ^{13}C

NMR (CDCl₃) δ 203.35, 158.52, 133.29, 130.26, 128.91, 120.74, 111.67, 55.60, 43.99, 31.95, 29.58, 29.41, 24.64, 22.85, 14.30.

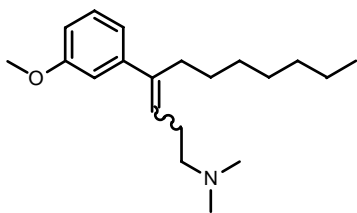


[4-(2-Methoxy-phenyl)-undec-3-enyl]-dimethyl-amine. **(3.17)** Procedure C was carried out using (3-dimethylaminopropyl) triphenylphosphonium bromide (0.96 g, 2.24 mmol), 0.5 M KHMDS/Tol (4.4 mL, 2.2 mmol), 1-(2-methoxy-phenyl)-octan-1-one (0.35 g, 1.45 mmol), and Tol (10 mL). The product was obtained in 0.17 g as a yellow oil, 38% yield. TLC: CH₂Cl₂: MeOH (10:1), R_f =0.48. ¹H NMR (CDCl₃, 300 MHz) δ 7.27-7.21 (m, 1H), 6.96-6.87 (m, 3H), 5.46-5.42 (m, 1H), 3.78 (s, 3H), 2.59-2.54 (m, 2H), 2.34 (s, 6H), 2.28-2.27 (m, 2H), 2.15-2.09 (m, 2H), 1.24-1.21 (br m, 10H), 0.87-0.83 (m, 3H); ¹³C NMR (CDCl₃) δ 156.31, 141.68, 130.03, 129.41, 128.20, 122.52, 120.37, 110.77, 58.31, 55.36, 43.87, 38.28, 31.83, 29.21, 29.14, 27.89, 25.66, 22.63, 14.09. ESIMS: 304 (M+H). HRMS calc for C₂₀H₃₄NO: 304.2640. Found: 304.2642.

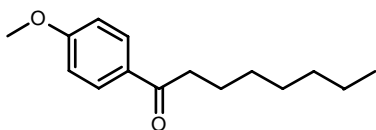


1-(3-Methoxy-phenyl)-octan-1-one. **(Ketone for 3.18)** Procedure A was carried out using 3-methoxybenzonitrile (0.5 g, 3.76 mmol), CH₂Cl₂ (5 mL), and 1 M heptylmagnesium bromide/Et₂O (5.6 mL, 5.6 mmol). The product was obtained in 0.68 g as a yellow oil, 76% yield. TLC: Hex: EtOAc (15:1), R_f =0.47. ¹H NMR (CDCl₃, 300 MHz) δ 7.37-7.33 (m, 2H), 7.18-7.13 (t, 1H, J =7.5), 6.92-6.89 (m, 1H), 3.64 (s, 3H), 2.77-2.72 (t, 2H, J =7.4), 1.58-1.54 (m, 2H), 1.17-1.11 (br s, 8H), 0.77-0.72 (appt t, 3H, J =6.6); ¹³C NMR

(CDCl₃) δ 199.72, 159.89, 138.52, 129.51, 120.63, 119.05, 112.43, 55.19, 38.66, 31.89, 29.46, 29.37, 24.44, 22.78, 14.17.

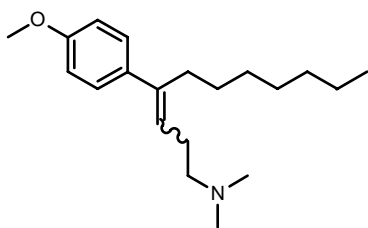


[4-(3-Methoxy-phenyl)-undec-3-enyl]-dimethyl-amine. **(3.18)** Procedure C was carried out using (3-dimethylaminopropyl) triphenylphosphonium bromide (1.04 g, 2.43 mmol), 0.5 M KHMDS/Tol (4.8 mL, 2.4 mmol), 1-(3-methoxy-phenyl)-octan-1-one (0.38 g, 1.62 mmol), and Tol (10 mL). The product was obtained in 0.35 g as a pale yellow oil, 71% yield. TLC: CH₂Cl₂: MeOH (10:1), R_f =0.57. ¹H NMR (CDCl₃, 300 MHz) δ 7.27-7.18 (m, 1H), 6.77-6.66 (m, 3H), 5.45-5.38 (m, 1H), 3.81 (s, 1H), 3.78 (s, 2H), 2.30-2.25 (m, 4H), 2.18 (s, 6H), 2.17-2.09 (m, 2H), 2.15-2.09 (m, 2H), 1.23 (br s, 10H), 0.87-0.82 (m, 3H); ¹³C NMR (CDCl₃) δ 159.29, 142.79, 142.53, 128.95, 124.12, 120.82, 114.08, 111.63, 59.83, 55.01, 45.26, 39.31, 31.83, 29.12, 28.11, 27.22, 22.63, 14.07. ESIMS: 304 (M+H). HRMS calc for C₂₀H₃₄NO: 304.2640. Found: 304.2638.

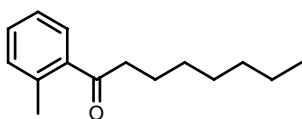


1-(4-Methoxy-phenyl)-octan-1-one. **(Ketone for 3.19)** Procedure A was carried out using 4-methoxybenzonitrile (0.8 g, 6.0 mmol), CH₂Cl₂ (5 mL), and 1 M heptylmagnesium bromide/Et₂O (9.0 mL, 9.0 mmol). The product was obtained in 0.7 g as a clear oil, 50% yield. TLC: Hex: EtOAc (15:1), R_f =0.48. ¹H NMR (CDCl₃, 300 MHz) δ 7.92 (d, 2H), 6.83 (d, 2H), 3.84 (s, 3H), 2.88 (t, 2H), 1.72 (m, 2H), 1.24 (m, 8H), 0.81 (t, 3H); ¹³C

NMR (CDCl₃) δ 199.72, 163.79, 130.80, 130.73, 114.15, 55.92, 38.81, 32.21, 31.39, 29.66, 23.11, 14.57.

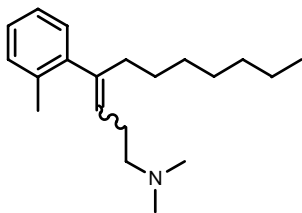


[4-(4-Methoxy-phenyl)-undec-3-enyl]-dimethyl-amine. **(3.19)** Procedure C was carried out using (3-dimethylaminopropyl) triphenylphosphonium bromide (1.10 g, 2.57 mmol), 0.5 M KHMDS/Tol (5.2 mL, 2.6 mmol), 1-(4-methoxy-phenyl)-octan-1-one (0.30 g, 1.28 mmol), and Tol (5 mL). The product was obtained in 0.25 g as a pale yellow oil, 64% yield. TLC: CH₂Cl₂: MeOH (10:1), R_f =0.43. ¹H NMR (CDCl₃, 300 MHz) δ 7.04-7.01 (appt d, 2H, J =8.4), 6.88-6.84 (appt d, 2H, J =6.0), 5.48-5.45 (m, 0.06H), 5.36-5.32 (t, 0.94H, J =6.9), 3.80 (s, 3H), 2.63-2.58 (m, 2H), 2.48 (s, 1H), 2.41 (s, 5H), 2.28-2.26 (m, 4H), 1.20 (br s, 10H), 0.85-0.81 (m, 3H); ¹³C NMR (CDCl₃) δ 158.55, 144.42, 133.00, 129.40, 127.54, 121.51, 113.80, 58.81, 55.43, 44.16, 39.62, 32.03, 29.31, 28.20, 25.72, 22.85, 14.32. ESIMS: 304 (M+H). HRMS calc for C₂₀H₃₄NO: 304.2640. Found: 304.2632.

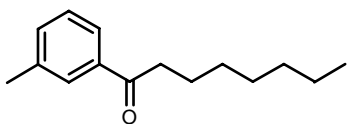


1-*o*-Tolyl-octan-1-one. (**Ketone for 3.20**) Procedure A was carried out using 2-tolylbenzonitrile (2.0 g, 17.01 mmol), CH₂Cl₂ (5 mL), and 1 M heptylmagnesium bromide/Et₂O (25.0 mL, 25.0 mmol). The product was obtained in 2.0 g as a clear oil, 54% yield. TLC: Hex: EtOAc (15:1), R_f =0.55. ¹H NMR (CDCl₃, 300 MHz) δ 7.67-7.51 (m, 1H), 7.42-7.08 (m, 3H), 2.88 (t, 2H), 2.48 (s, 3H), 1.83-1.54 (m, 2H), 1.47-1.08

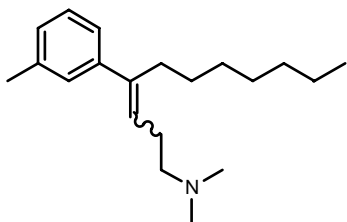
(m, 8H), 0.88 (t, 3H); ^{13}C NMR (CDCl_3) δ 205.53, 138.93, 138.28, 132.26, 131.48, 128.75, 126.11, 42.22, 32.23, 29.82, 29.66, 24.96, 23.13, 21.67, 14.58.



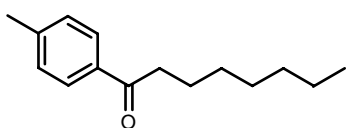
Dimethyl-(4-*o*-tolyl-undec-3-enyl)-amine. **(3.20)** Procedure C was carried out using (3-dimethylaminopropyl) triphenylphosphonium bromide (0.9 g, 1.95 mmol), 0.5 M KHMDS/Tol (3.9 mL, 1.95 mmol), 1-*m*-tolyl-octan-1-one (0.30 g, 1.28 mmol), and Tol (5 mL). The product was obtained in 0.17 g as a yellow oil, 43% yield. TLC: CH_2Cl_2 : MeOH (10:1), R_f =0.47. ^1H NMR (CDCl_3 , 300 MHz) δ 7.61-7.55 (m, 4H), 5.29-5.27 (m, 0.52H), 2.65-2.60 (m, 2H), 2.51-2.48 (m, 2H), 2.37 (s, 6H), 2.13 (s, 3H), 1.99-1.89 (m, 4H), 1.37-1.32 (br s, 8H), 0.98-0.95 (m, 3H); ESIMS: 288 ($\text{M}+\text{H}$). HRMS calc for $\text{C}_{20}\text{H}_{34}\text{N}$: 288.2691. Found: 288.2689.



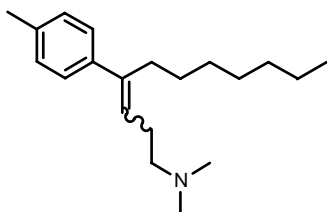
1-*m*-Tolyl-octan-1-one. **(Ketone for 3.21)** Procedure A was carried out using 3-tolylbenzonitrile (0.97 g, 8.25 mmol), CH_2Cl_2 (5 mL), and 1 M heptylmagnesium bromide/ Et_2O (12.4 mL, 12.4 mmol). The product was obtained in 1.40 g as a clear oil, 78% yield. TLC: Hex: EtOAc (15:1), R_f =0.48. ^1H NMR (CDCl_3 , 300 MHz) δ 7.60-7.53 (m, 1H), 7.45-7.10 (m, 3H), 2.88 (t, 2H), 2.50 (s, 3H), 1.83-1.54 (m, 2H), 1.47-1.10 (m, 8H), 0.86 (t, 3H); ^{13}C NMR (CDCl_3) δ 205.60, 139.00, 138.28, 132.26, 131.48, 128.75, 126.11, 42.22, 32.23, 29.82, 29.66, 24.96, 23.13, 21.66, 14.60.



Dimethyl-(4-*m*-tolyl-undec-3-enyl)-amine. **(3.21)** Procedure C was carried out using (3-dimethylaminopropyl) triphenylphosphonium bromide (0.9 g, 1.95 mmol), 0.5 M KHMDS/Tol (3.9 mL, 1.95 mmol), 1-*m*-tolyl-octan-1-one (0.30 g, 1.28 mmol), and Tol (5 mL). The product was obtained in 0.14 g as a pale yellow oil, 35% yield. TLC: CH₂Cl₂: MeOH (10:1), *R_f*=0.51. ¹H NMR (CDCl₃, 300 MHz) δ 7.18-6.89 (m, 4H), 5.37-5.36 (m, 0.52H), 5.36-5.35 (m, 0.48H), 2.50-2.47 (m, 2H), 2.39-2.38 (m, 2H), 2.30 (s, 6H), 2.19 (s, 3H), 2.07-2.06 (m, 2H), 1.20 (s, 10H), 0.85-0.81 (m, 3H); ¹³C NMR (CDCl₃) δ 144.98, 139.27, 136.23, 134.16, 134.13, 129.43, 120.82, 59.66, 45.08, 44.97, 40.03, 34.61, 32.61, 32.54, 29.92, 29.89, 23.39, 14.89. ESIMS: 288 (M+H).



1-*p*-Tolyl-octan-1-one. **(Ketone for 3.22)** Procedure A was carried out using 4-tolylbenzonitrile (2.0 g, 17.10 mmol), CH₂Cl₂ (5 mL), and 1 M heptylmagnesium bromide/Et₂O (25.0 mL, 25.0 mmol). The product was obtained in 2.60 g as a clear oil, 70% yield. TLC: Hex: EtOAc (15:1), *R_f*=0.52. ¹H NMR (CDCl₃, 300 MHz) δ 7.92 (d, 2H), 6.83 (d, 2H), 3.90 (s, 3H), 2.89 (t, 2H), 1.72 (m, 2H), 1.24 (m, 8H), 0.88 (t, 3H); ¹³C NMR (CDCl₃) δ 205.72, 139.79, 138.80, 130.73, 124.15, 55.92, 38.81, 32.21, 31.39, 29.66, 25.15, 23.11, 14.57.



Dimethyl-(4-*p*-tolyl-undec-3-enyl)-amine. **(3.22)** Procedure C was carried out using (3-dimethylaminopropyl) triphenylphosphonium bromide (1.10 g, 2.57 mmol), 0.5 M KHMDS/Tol (5.2 mL, 2.6 mmol), 1-*p*-Tolyl-octan-1-one (0.30 g, 1.28 mmol), and Tol (5 mL). The product was obtained in 0.25 g as a pale yellow oil, 64% yield. TLC: CH₂Cl₂: MeOH (10:1), *R*_f=0.55. ¹H NMR (CDCl₃, 300 MHz) δ 7.13-7.10 (d, 2H, *J*=7.5), 6.97-6.95 (d, 2H, *J*=8.1), 5.33-5.29 (t, 1H, *J*=7.2), 2.80-2.75 (m, 2H), 2.47 (s, 4H), 2.32 (s, 2H), 2.28-2.27 (m, 4H), 1.96 (s, 3H), 1.19 (s, 10H), 0.85-0.81 (appt t, 3H, *J*=6.8); ¹³C NMR (CDCl₃) δ 145.86, 137.93, 137.03, 129.51, 128.43, 120.84, 57.61, 42.95, 39.89, 32.34, 29.64, 28.41, 24.69, 23.18, 23.00, 21.71, 14.63. ESIMS: 288 (M+H). HRMS calc for C₂₀H₃₄N: 288.2691. Found: 288.2703.

3.6.2 Biology

[³H]-BTX experiment. In the sodium channel evaluation, the IC₅₀, which represents the micromolar concentration of compound required to displace 50% of specifically bound [³H]-BTX, was determined using rat cerebral cortex synaptoneurosomes. In brief, rat forebrain membranes were incubated with [³H]-Batrachotoxin (30-60 Ci/mmol). Reactions are carried out in 50 mM HEPES (pH 7.4) containing 130 mM choline chloride at 37°C for 60 minutes. The reaction was terminated by rapid vacuum filtration of the reaction contents onto glass fiber filters. Radioactivity trapped onto the filters was determined and compared to control values in order to ascertain any interactions of the

test compound with the sodium channel site 2 binding site. Aconitine [1 μ M] was used as a positive control.

Cell Culture and Electrophysiology. Human embryonic kidney (HEK 293) cells stably expressing Na_v1.2 were grown in DMEM/F12 media (Invitrogen Corp, CA, USA) supplemented with 10% fetal bovine serum, penicillin (100 U/ml), streptomycin (100 μ g/ml) and geneticin (G418) (500 μ g/ml; Sigma, MO, USA). Cells were grown in a humidified atmosphere of 5% CO₂ and 95% air at 37°C.

Sodium currents were recorded using the whole-cell configuration of the patch clamp technique with an Axopatch 200B amplifier (Axon Instruments, Foster City, CA). All voltage protocols were applied using pCLAMP 8 software (Axon, USA) and a Digidata 1322 (Axon, USA). Currents were amplified and low pass filtered (2 kHz) and sampled at 33 kHz. Cells were plated on glass coverslips and superfused with the following solution: 130 mM NaCl, 4 mM KCl, 1 mM CaCl, 5 mM MgCl₂, 5 mM HEPES, and 5 mM glucose (pH adjusted to 7.4 with NaOH). Compounds were prepared as 100 mM stock solutions in dimethylsulfoxide (DMSO) and diluted to desired concentration in perfusion solution. The maximum DMSO concentration of 0.3% had no effect on current amplitude. Borosilicate glass pipettes were pulled using a Brown-Flaming puller (model P87, Sutter Instruments Co, Novato, CA) and heat polished to produce electrode resistances of 0.8-2.6 M Ω when filled with the following electrode solution: 130 mM CsCl, 1 mM MgCl₂, 5 mM MgATP, 10 mM HEPES, and 10 mM BAPTA (pH adjusted to 7.4 with NaOH). Experiments were performed at room temperature (20-22°C).

Data Analysis. All data analysis was performed using Clampfit 8 software (Axon Instruments, CA, USA), Excel (Microsoft), and Origin 6.0 (Microcal Software, MA, USA). Statistical analyses were performed using a *t* test for normally distributed data, or the Wilcoxon signed rank test for non-normalized data (Sigma Stat, Jandel). Averaged data were presented as means \pm standard error of the mean (S.E.M.). Significance values of $p < 0.05$ were considered.

3.7 References

- 1) Brown, M.L.; Zha, C.C.; Van Dyke, C.C.; Brown, G.B.; Brouillette, W.J. “Comparative molecular field analysis of hydantoin binding to the neuronal voltage-dependent sodium channel,” *J. Med. Chem.* **1998**, *42*, 1537-1545.
- 2) Worley, P.F.; Baraban, J.M. “Site of anticonvulsant action on sodium channels: autoradiographic and electrophysiological studies in rat brain,” *Proc. Natl. Acad. Sci.* **1987**, *84*, 3051-3055.
- 3) McNeal, E.; Lewandowski, G.A.; Daly, J.W.; Creveling, C.R. [³H] Batrachotoxinin A 20 α -benzoate binding to voltage-sensitive sodium channels: a rapid and quantitative assay for local anesthetic activity in a variety of drugs,” *J. Med. Chem.* **1985**, *28*, 381-388.
- 4) Liu, C.J.; Priest, B.T.; Bugianesi, R.M.; Dulski, P.M.; Felix, J.P.; Dick, I.E.; Brochu, R.M.; Knaus, H.G.; Middleton, R.E.; Kaczorowski, G.J.; Slaughter, R.S.; Garcia, M.L.; Kohler, M.G. “A high-capacity membrane potential FRET-based assay for Na_v1.8 channels,” *Assay Drug Dev. Tech.* **2006**, *4*, 37-48.
- 5) Moalem, G.; Tracey, D.J. “Immune and inflammatory mechanism in neuropathic pain,” *Brain Res. Rev.* **2006**, *51*, 240-264.
- 6) Wheeler-Aceto, H.; Cowan, A. “Standardization of the rat paw formalin test for the evaluation of analgesics,” *Psychopharmacol.* **1991**, *104*, 35-44.
- 7) Blakely, R.D.; De Felice, L.J.; Hartzell, H.C. “Molecular physiology of norepinephrine and serotonin transporters,” *J. Exp. Biol.* **1994**, *196*, 263-281.

Chapter 4

Introduction to Calcium Channels

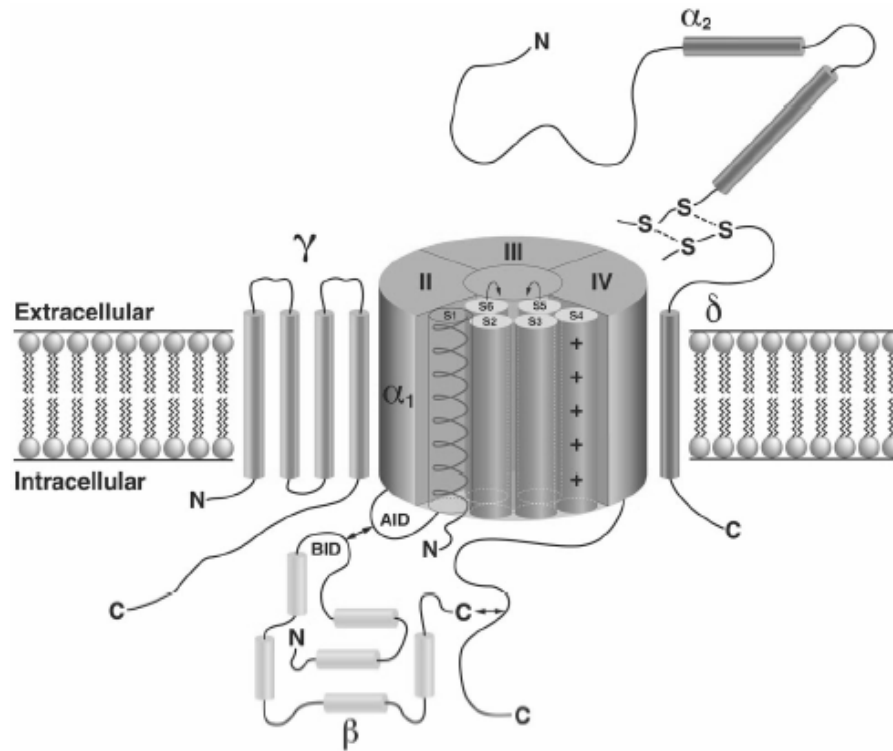
The voltage gated calcium channel (VGCC) is similar in structure and function to the voltage gated sodium channel (VGSC) and both belong to the superfamily of transmembrane ion channel proteins. The VGCC is responsible for mediating calcium influx in to numerous biological processes, such as muscle contraction and neurotransmission. These processes occur through the propagation of action potential by the VGCCs, which occurs in a membrane potential dependent manner. Localization of calcium channel subtypes L, P/Q, N, R, and T are regulated within living systems for specific function. However, all calcium channel isoforms are essential to the cellular signaling processes required for life.

4.1 The Voltage Gated Calcium Channel (VGCC)

4.1.1 Structure

Structurally the voltage gated calcium channel consists of five possible subunits which are α_1 , α_2 , δ , β , and γ . Current models of VGCCs in skeletal muscle depict the transmembrane α_1 subunit of 190 kDa to be associated with a disulfide-linked $\alpha_2\delta$ dimer of 170 kDa, an intracellular β subunit of 55 kDa, and a transmembrane γ subunit of 33 kDa (Figure 4-1).¹ However it is believed that all other VGCCs, such as those found in neurons, endocrine cells and smooth and cardiac muscle, lack inclusion of this γ subunit. Basic channel function can be obtained from the α_1 subunit alone, and coexpression with $\alpha_2\delta$ and β subunits help to confer proper kinetics and voltage dependence of calcium current.²

Figure 4-1 Structural Overview of the VGCC



The α_1 subunit forms the pore region and is comprised of four homologous domains (I-IV) each containing six transmembrane segments (S1-S6), much like the α subunit of VGSCs.³ Both channels contain a conserved series of positively charged amino acid residues in the S4 segment, which functions as the channel's voltage sensor.⁴ Regulation of channel function by toxin and drug binding is known to occur in the α_1 and α subunits of VGCCs and VGSCs, respectively. The S6 segment has been found to permeate the central lining of both channel pores, and membrane associated loops between S5 and S6 segments of each domain serve to form the pore lining, in both cases. Interestingly, alteration of just three amino acid residues in these pore forming loops, specifically in domains I, III, and IV, result in conversion of a sodium channel for calcium ion selectivity.⁵

4.1.2 Subtypes

Differences derived from α_1 subunits have resulted in the classification of several distinct channel subtypes (Table 4-1).⁶ Distribution of these subtypes is regulated to particular localities of the body, such as smooth muscle, heart and brain, for specific functioning. Four L-type channels, $\text{Ca}_v1.1$ - $\text{Ca}_v1.4$, have been identified, as well as three T-type channels, $\text{Ca}_v3.1$ - $\text{Ca}_v3.3$. These variations within subtypes are primarily caused by differing β subunits, in association with the same α_1 unit. Additionally, three other subtypes $\text{Ca}_v2.1$ - $\text{Ca}_v2.3$ have been found and correspond to P/Q, N, and R channels.

Table 4-1 Subtypes of the VGCCs

Channel	Current	Tissue Localization	Antagonist
$\text{Ca}_v1.1$	L	skeletal muscle	phenylalkylamines, dihydropyridines, benzothiazepines
$\text{Ca}_v1.2$	L	heart, smooth muscle, brain	
$\text{Ca}_v1.3$	L	brain, kidney, ovary	
$\text{Ca}_v1.4$	L	retina	
$\text{Ca}_v2.1$	P/Q	brain, pituitary	ω -agatoxine IVA
$\text{Ca}_v2.2$	N	brain, nervous system	ω -conotoxine GVIA
$\text{Ca}_v2.3$	R	brain, retina, heart	Ni^{2+}
$\text{Ca}_v3.1$	T	brain, nervous system	mibefradil, Ni^{2+}
$\text{Ca}_v3.2$	T	brain, kidney, heart	
$\text{Ca}_v3.3$	T	brain	

VGCCs are known to elicit five types of current, which are L, P/Q, N, R, and T types. Biochemical studies have identified two distinct P- and Q- currents, but coexpression of the two has led to one type known as P/Q.⁷ L-type currents are the main currents responsible for muscle contraction and hormone secretion.⁸ These currents are high voltage activated (HVA) requiring strong depolarization of 30 mV for activation and are typically long lasting. L-type channels are affected by three drug classes, known as phenylalkylamines, dihydropyridines and benzothiazepines. P/Q-, N- and R-type currents are also HVA, but are unaffected by the L-type channel antagonists mentioned. These currents are typically elicited in neurons and are blocked only by polypeptide snail and spider toxins.⁹ T-type currents are low voltage activated (LVA) requiring weak depolarization of 10 mV for activation and are brief in duration. However, these currents are resistant to effects by both L-type blocking drugs, as well as P/Q-, N- and R-type inhibiting toxins.

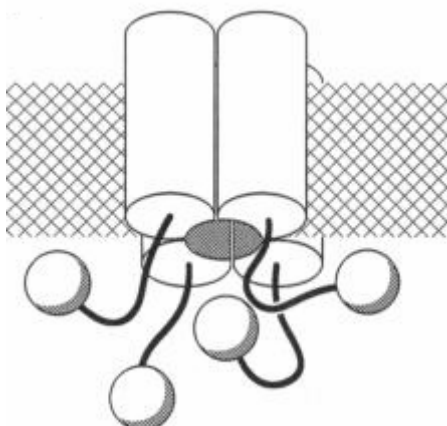
4.1.3 Function

Much like the VGSCs, VGCCs induce physiological processes by the propagation of action potentials, through a membrane potential dependent process. This process has been extensively discussed in relation to VGSCs (see Chapter 1), with three main states of the channel being involved. Initially the channel is in a resting state, depolarization occurs, repolarization then causes an inactivated state, and restoration of potential results in a closed state.

The channel is able to close through a process called gating, in which a portion of the protein is responsible for physically acting as a gate in order to block the channel. All voltage gated ion channels gate through a similar mechanism which has been described

by a ball and chain model (Figure 4-2).¹⁰ In this model, there are four ball and chain modules which can bind to the pore region and block conductance. However, inhibition is caused by the binding of a single module, which serves to prevent association of the voltage sensors.

Figure 4-2 Ball and Chain Model of Inactivation

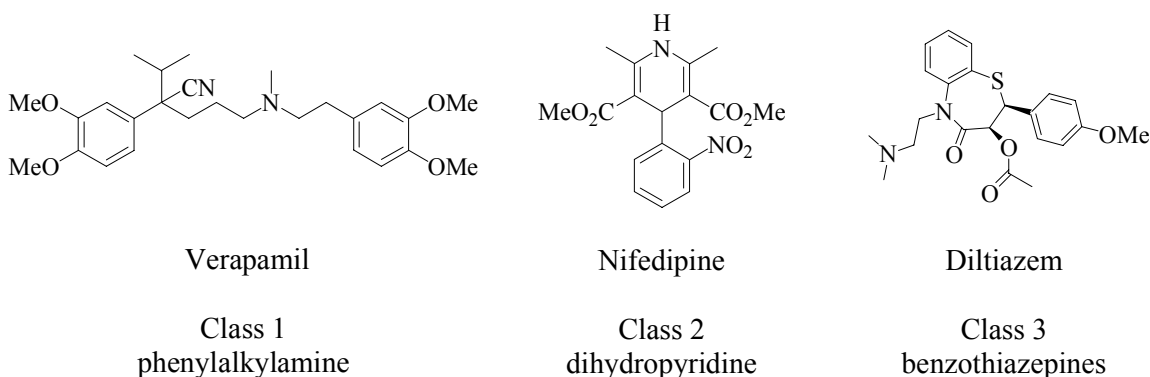


VGCC's have a large channel lumen of approximately 6 Å, but preferentially accommodate calcium ion flux over other monovalent cations. Permeability can occur through either of two mechanisms, which are selective rejection or selective affinity.¹¹ Selective rejection involves rejection of sodium ions in the presence of calcium due to high affinity calcium binding sites. In this model, calcium ions are first bound to the channel and released from discrete sites which have enhanced affinity for calcium, thereby disallowing sodium ions from displacing the already bound cations. Selective affinity involves the binding of calcium into particular localities within the lumen, where electrostatic repulsion then acts to push the calcium ions through the channel. It has been observed that when no external concentration of calcium is found, that sodium ions are also capable of permeating the channel pore. Due to these observations, the latter mechanism is better accepted as the method of calcium binding and translocation.¹²

4.1.4 Antagonists and Binding Sites

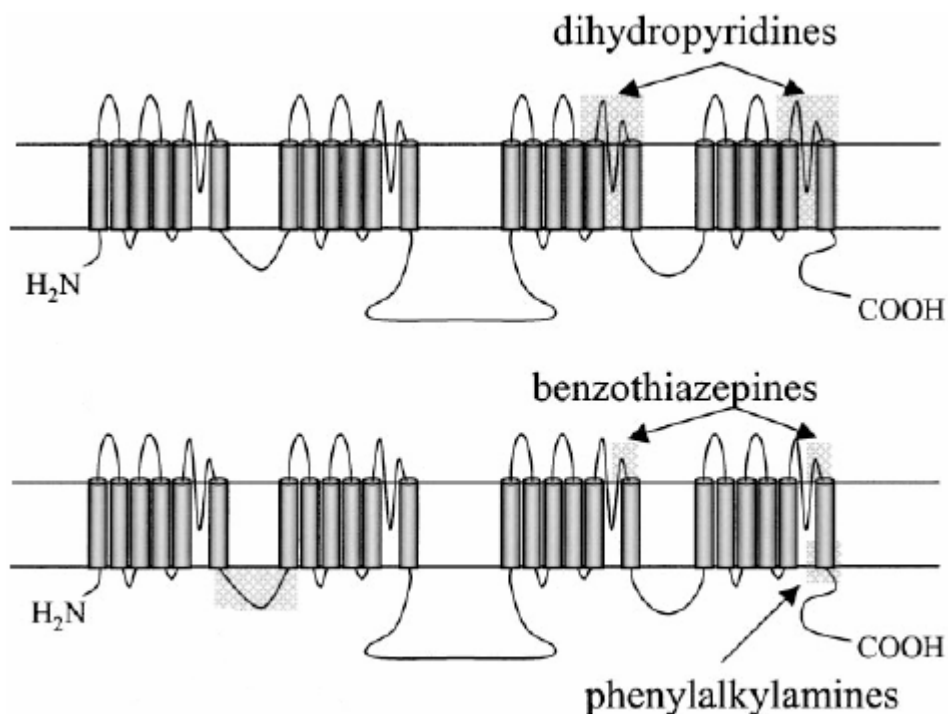
Calcium channel antagonists can be classified into three major categories, which include inorganic ions, large peptide toxins and small organic molecules. Inorganic ions serve as potent blockers of VGCC through physical occlusion of the channel pore, but have little therapeutic utility due to their high degree of toxicity. Large peptide toxins have been found in predatory animals, such as conotoxins from marine snails and agatoxins from funnel web spiders. These toxins serve as selective inhibitors of VGCCs and have been utilized in the characterization of distinct calcium channel subtypes. Recently, a synthetic version of ω -conotoxin, ziconotide, has been marketed as a therapeutic treatment for chronic pain syndromes due to its ability to selectively block N-type channels.¹³ Small organic molecules can affect channel function by either modulation of gating or physical occlusion of the pore. Structurally these molecules can be classified into three types which are phenylalkylamine, dihydropyridine and benzothiazepines, with representative analogues being verapamil, nifedipine and diltiazem, respectively (Figure 4-3).

Figure 4-3 Three Drug Classes of VGCCs



VGCCs are thought to have at least seven distinct binding sites within the channel protein, which account for both toxin and drug sites of interaction (Figure 4-4).¹⁴ Unfortunately many of these sites are still currently unresolved, but the binding sites of most VGCC antagonists have been well characterized. Phenylalkylamines cause physical occlusion of the channel pore from the cytoplasmic side by binding to S6 segment of the DIV domain. Dihydropyridines, which have been the most extensively studied class of VGCC antagonists, are known to bind to the S5 and S6 segments of DIII and DIV domains. These drugs are capable of discriminating between isoforms of L-type channels and alter channel function by shifting voltage dependence. Benzothiazepines have been found to bind to extracellular portions of the S5 and S6 segments of DIII and DIV domains, which greatly overlap the phenylalkylamine site.

Figure 4-4 Binding Sites of VGCC Antagonists



4.2 References

- 1) Randall, A.; Benham, C.D. "Recent advances in the molecular understanding of voltage-gated Ca^{2+} channels," *Mol. Cell. Neurosci.* **1999**, *14*, 255-272.
- 2) Dolphin, A.C. " β subunits of voltage-gated calcium channels," *J. Bioenerg. Biomembr.* **2003**, *35*, 599-620.
- 3) Jones, S.W. "Calcium channels: unanswered questions," *J. Bioenerg. Biomembr.* **2003**, *35*, 461-475.
- 4) Yamaguchi, H.; Muth, J.N.; Varadi, M.; Schwartz, A.; Varadi, G. "Critical role of conserved proline residues in the transmembrane segment 4 voltage sensor function and in the gating of L-type calcium channels," *Proc. Natl. Acad. Sci.* **1999**, *96*, 1357-1362.
- 5) Varadi, G.; Strobeck, M.; Koch, S.; Caglioti, L.; Zucchi, C.; Palyi, G. "Molecular elements of ion permeation and selectivity within calcium channels," *Crit. Rev. Biochem. Mol. Bio.* **1999**, *34*, 181-214.
- 6) Ertel, E.A.; Campbell, K.P.; Harpold, M.M.; Hofmann, F.; Mori, Y.; Perez-Reyes, E.; Schwartz, A.; Snutch, T.P.; Tanabe, T.; Birnbaumer, L.; Tsien, R.W.; Catterall, W.A. "Nomenclature of voltage-gated calcium channels," *Neuron.* **2000**, *25*, 533-535.
- 7) Catterall, W.A. "Structure and function of neuronal Ca^{2+} channels and their role in neurotransmitter release," *Cell Calcium.* **1998**, *24*, 307-323.

- 8) Catterall, W.A.; Perez-Reyes, E.; Snutch, T.P.; Striessnig, J. "International union of pharmacology. XLVIII. Nomenclature and structure-function relationships of voltage-gated calcium channels, *Pharmacol. Rev.* **2005**, *57*, 411-415.
- 9) Miljanich, G.P.; Ramachandran, J. "Antagonists of neuronal calcium channels: structure, function, and therapeutic implications," *Annu. Rev. Pharmacol. Toxicol.* **1995**, *35*, 707-734.
- 10) Timpe, L.C.; Peller, L. "A random flight chain model for the tether of the shaker K^+ channel inactivation domain," *Biophys. J.* **1995**, *69*, 2415-2418.
- 11) Nayler, W.G. Ion-conducting channels: calcium. *Calcium Antagonists*; Academic Press, Inc: San Diego, CA, 1998; p 23-44.
- 12) Jones, S. "Overview of voltage-dependent calcium channels," *J. Bioenerg. Biomembr.* **1998**, *30*, 299-312.
- 13) Miljanich, G.P. "Ziconotide: neuronal calcium channel blockers for treating severe chronic pain," *Current Med. Chem.* **2004**, *11*, 3029-3040.
- 14) Doering, C.J.; Zamponi, G.W. "Molecular pharmacology of high voltage-activated calcium channels," *J. Bioenerg. Biomembr.* **2003**, *35*, 491-505.

Chapter 5

Dual Calcium/ Sodium Channel Blocker Derived from a Verapamil Scaffold

Previous investigations utilizing comparative molecular field analysis (CoMFA) have led to the discovery of potential new targets as sodium channel inhibitors. These targets were designed from a verapamil scaffold and contained either a hydantoin or α -hydroxy amide insertion. Subsequent synthesis of these compounds and analysis by [^3H]-BTX displacement has validated their affinity for sodium channel binding. Our lead compound, containing an α -hydroxy amide motif and verapamil, a potent L-type calcium channel inhibitor, were then evaluated by patch clamp electrophysiology for effects on P/Q-, N-, and L-type calcium channels. The results of our study reveal that modification to the verapamil core scaffold has resulted in a dual inhibitor of both sodium and calcium channels.

5.1 Calcium Antagonists and Therapeutic Use

5.1.1 Verapamil

Verapamil, commercially known as Isoptin[™] and Calan[™], has been utilized as a highly successful therapeutic agent towards the clinical treatment of angina,¹ arrhythmia,^{2,3} and hypertension.⁴ Initially discovered two decades ago as a coronary dilator, verapamil's negative inotropic effects were revealed soon afterward. The drug's main method of action being selective prevention of transmembrane calcium influx in cardiac cells, through the slow L-type channels while retaining normal ionic flow through the fast T-type channels.^{5,6} This lack of calcium influx serves as an uncoupler of cardiac excitation-contraction coupling, thereby causing a state of vasodilation and increased relaxation of the cardiac muscle.

Structurally verapamil belongs to the class of phenylalkylamine derivatives of calcium antagonists and is administered as the racemate, although the S(-) enantiomer has shown superior activity in blocking VGCCs than the R(+) enantiomer. Despite its high potency and wide usage, verapamil suffers from extensive first pass metabolism and has a lowered level of bioavailability.^{7,8} Therefore, development of new verapamil analogues has been extensively sought for increased metabolic efficiency, greater levels of potency, and to elucidate the drug-receptor interactions.

Verapamil is often considered the prototype “calcium antagonist” from which several other generations of bioactive drugs have evolved, with interest primarily being focused on effects of regulating cardiac function. However, recent studies utilizing competitive inhibition of [³H]-BTX have indicated verapamil’s high potency toward sodium channel binding.⁹ This new discovery has initiated the development of verapamil analogues with potent local anesthetics activity and improved pharmacokinetic profile.

5.1.2 Clinical Relevance of Dual Inhibitors

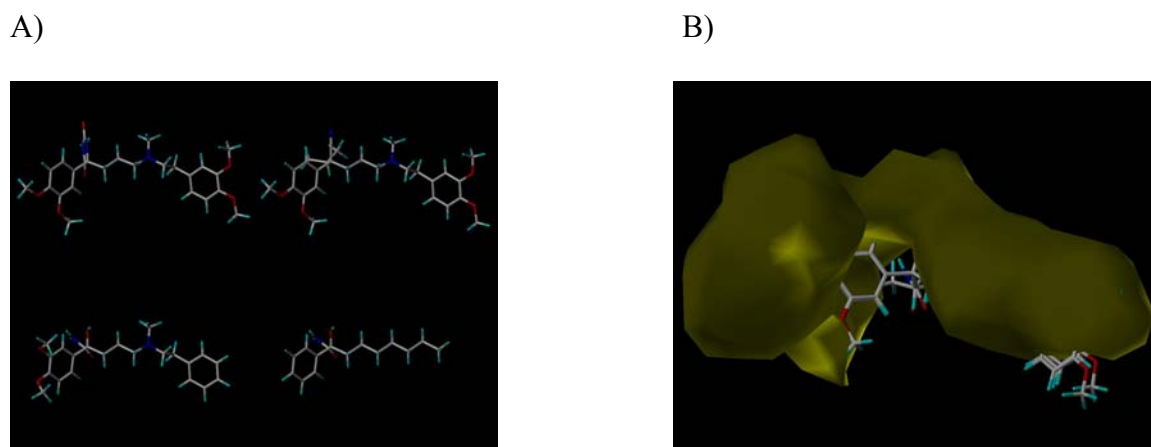
We were also intrigued by the possibility of producing a highly active, dual Na⁺ and Ca²⁺ channel inhibitor and the clinical applications of such a compound. It has been observed that when Ca²⁺ influx is inhibited by the presence of a Ca²⁺ channel blocker, a transitory increase in Ca²⁺ influx still exists.¹⁰ It has been further postulated that this Ca²⁺ influx is a result of promiscuous conductance of Ca²⁺ through Na⁺ channels, which can thereby signal release of more Ca²⁺ from intracellular calcium stores in the sarcoplasmic reticulum (SR).¹¹ This increase of calcium concentration is due to depletion of ATP, as a consequence of aberrant energy-dependent ion homeostasis during ischemic conditions.¹² This phenomenon is known as calcium overload and is the major cause of nerve cell

death associated with cerebral injury, such as stroke and trauma.¹³ Additionally, it should be noted that aberrant intercellular Na^+ concentrations can serve as another pathway for excessive Ca^{2+} accumulation, also leading to cell death. Prolonged opening of VGSC can result in Na^+ overload and may also increase the depletion of ATP. Therefore a dual $\text{Ca}^{2+}/\text{Na}^+$ inhibitor could serve as a potent agent preventing cellular overloading of calcium during pathological or ischemic conditions.¹⁴

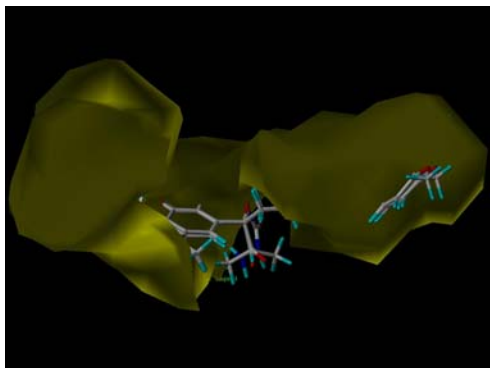
5.2 Design and Synthesis

Two novel compounds were predicted to have potent activity against NVGSC, based on a prior CoMFA model conducted within our laboratory (Figure 5-1). The CoMFA fields for the model developed from test set compounds are shown (A). The electrostatic contours which increase binding results from placing more positive (+) charge near blue and negative (-) charge near red are also provided. Steric contours that increased binding results by placing more bulk near green and less bulk near yellow are depicted, (B) and (C). Finally, overlap of analogues (**5.5**), (**5.6**) and verapamil are shown with a potent sodium channel blocker, in yellow.¹⁵

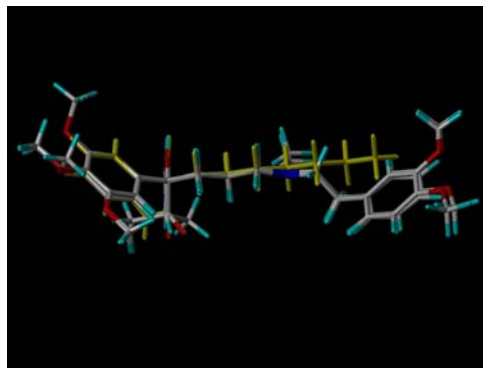
Figure 5-1 Electrostatic and Steric CoMFA Fields



C)

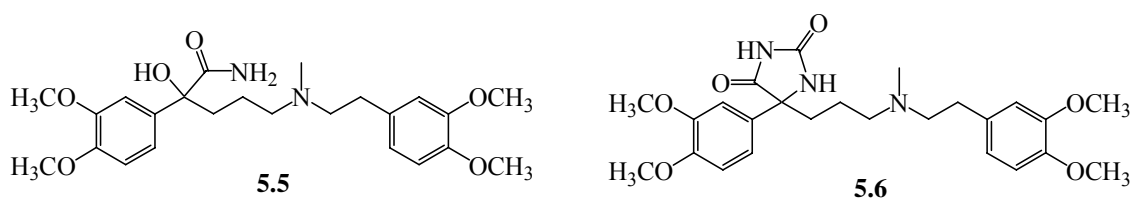


D)



Based on this design, the novel analogues were then constructed by incorporation of α -hydroxy amide and hydantoin motifs into a verapamil scaffold (Figure 5-2). Synthesis of these analogues and analysis by [^3H]-BTX displacement validated their affinity for sodium channel binding. Additionally analysis within calcium channel subtypes has shown that our lead compound (**5.5**), containing an α -hydroxy amide motif, was a potent calcium channel blocker with equal affinity to that of verapamil.

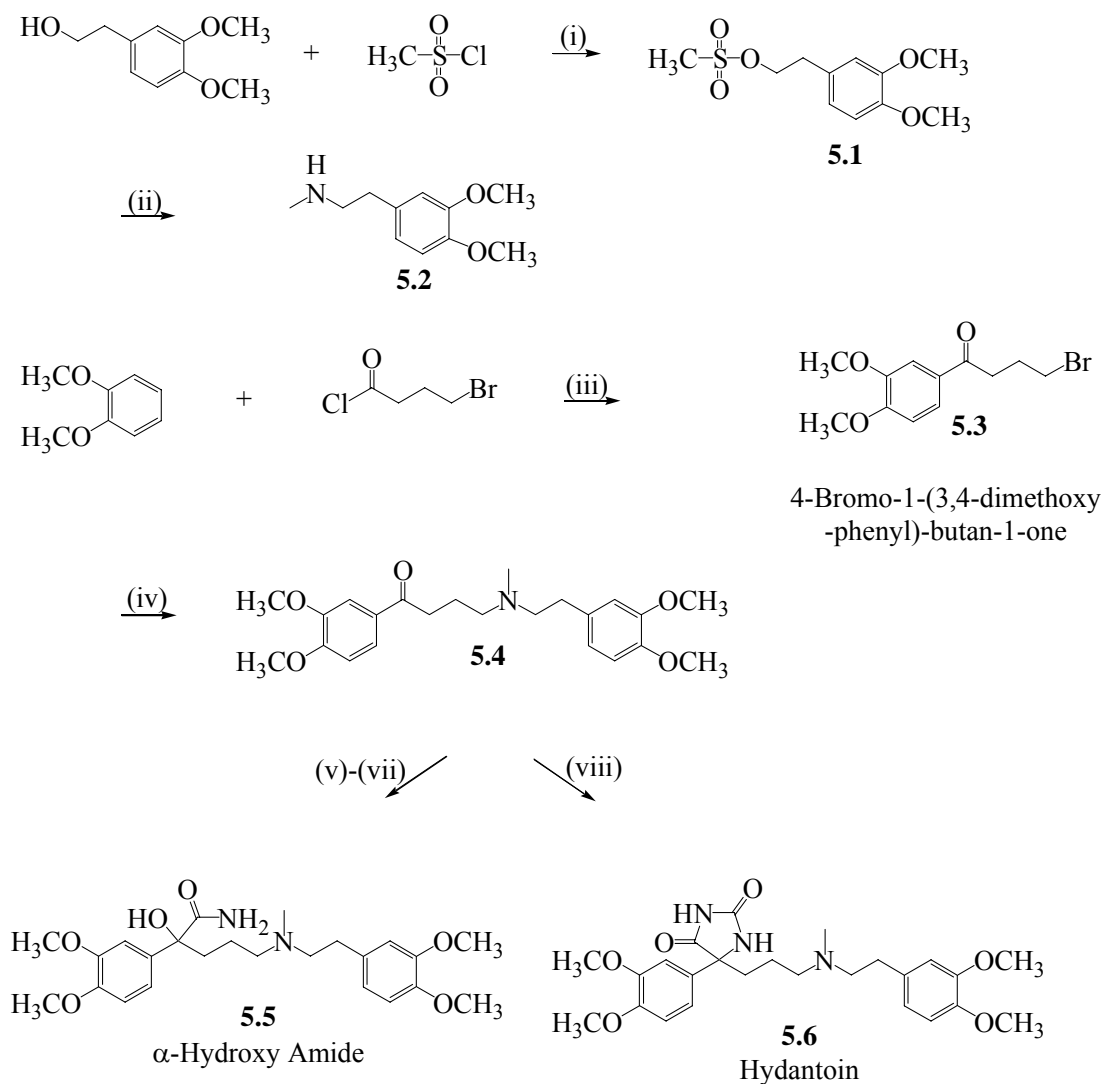
Figure 5-2 Potential Sodium Channel Blockers Based on a Previous CoMFA Model



Synthetic routes towards these derivatives began with mesylation of 3,4-dimethoxyphenethyl alcohol in order to generate compound (**5.1**) (Scheme 5-1). Subsequent addition of methylamine to (**5.1**) generated compound (**5.2**), which was later coupled to 4-bromo-1-(3,4-dimethoxy)-phenyl-butanone (**5.3**), in order to produce ketone (**5.4**). Synthesis of analog (**5.5**) was initiated by formation of the TMS protected cyanohydrin, which has trapped as the silyl ether in order to prevent collapse of the

intermediate back to the starting ketone. Afterward addition of concentrated HCl, followed by HCl gas, cleaved the TMS group and converted the nitrile into an α -hydroxy amide group. Intermediate (**5.4**) was again employed in the construction of compound (**5.6**) by use of Bucherer-Bergs conditions to give the analogous hydantoin.

Scheme 5-1 α -Hydroxy Amide and Hydantoin Analogues of Verapamil



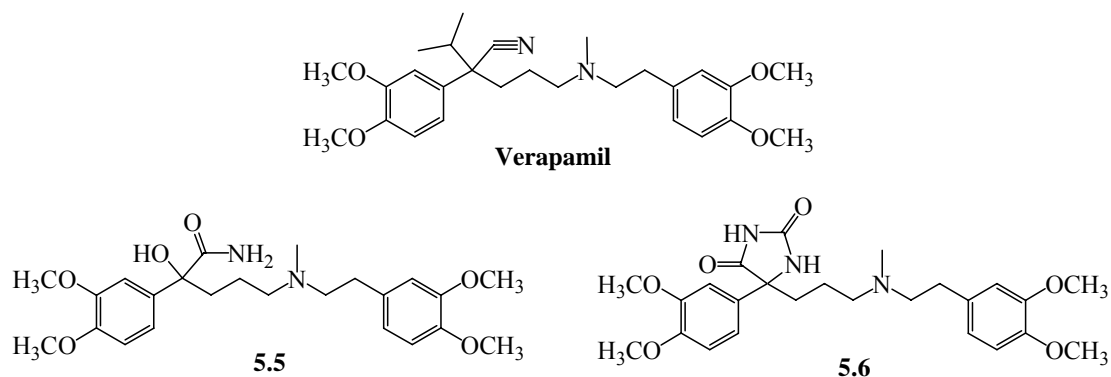
^aConditions: (i) $\text{CH}_2\text{Cl}_2/\text{pyr}$, 0°C -RT; 100% (ii) MeNH_2 , MeOH ; 73% (iii) AlCl_3 , CS_2 ; 87% (iv) **5.2**, K_2CO_3 , DMF , RT; 44% (v) TMSCN , KCN , 18-C-6; (vi) 1,4-Dioxane, HCl cct, 0°C ; (vii) HCl gas, 0°C -RT; 31%, 3 steps (viii) KCN , $(\text{NH}_4)_2\text{CO}_3$, 50% EtOH ; 93%

5.3 Results

5.3.1 Binding Assay

Compounds were evaluated at 40 μM , the IC_{50} for phenytoin, for the ability to displace [^3H]-BTX binding to the NVGSC in prepared rat synaptosomes, with all evaluations carried out in duplicate. The α -hydroxy amide analogue (**5.5**) provided 93% inhibition, in comparison to the hydantoin analogue (**5.6**) which gave 85% inhibition (Table 5-1). Due to the similarity of the α -hydroxy amide analog (**5.5**) to verapamil, we chose to further look at its effects within P/Q-, N-, and L-type Ca^{2+} channels.

Table 5-1 Predicted and Actual NVGSC Activity of Verapamil Analogues



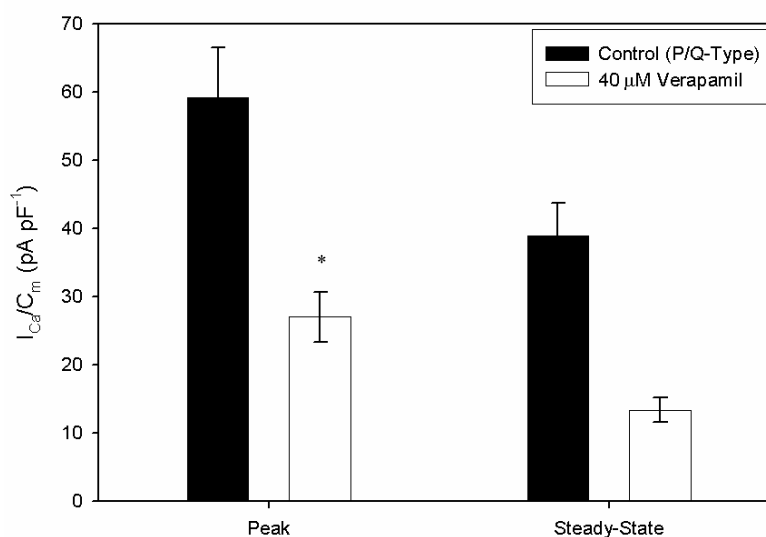
Compound	Percent Inhibition of [^3H]-BTX at 40 μM	-log IC_{50}	
		Obsd	Pred
Verapamil	90.65 %	-0.52*	-1.14
5.5	92.91%	nd	-0.96
5.6	84.47%	nd	-1.06

* See reference 6

5.3.2 Electrophysiological Methods

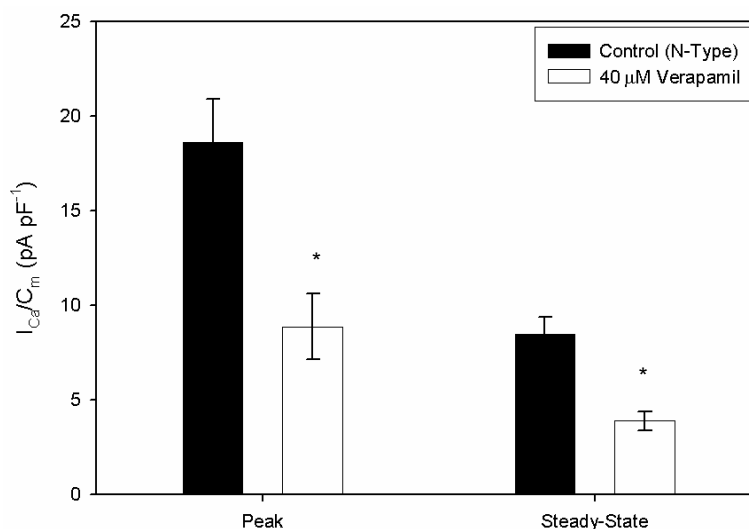
P/Q-type VGCCs in HEK293 cells were exposed to 40 μ M verapamil and were compared to a control of P/Q-type VGCCs in HEK293 cells without any drug treatment. Ten minutes after application of verapamil, at 40 μ M, peak $I_{Ca(P/Q)}$ was reduced from 59.2 ± 7.3 ($n = 30$ control cells) to 27.0 ± 3.6 ($n = 34$ treated cells), indicating a 54.4% reduction in current (Chart 5-1). Steady-state $I_{Ca(P/Q)}$ diminished from 38.9 ± 4.8 (control) to 13.4 ± 1.8 (treated), marking a 65.6% reduction in current. Peak and steady-state measurements were obtained from the same signal acquired at a holding potential of +20 mV.

Chart 5-1 Effects of Verapamil on P/Q-Type VGCCs



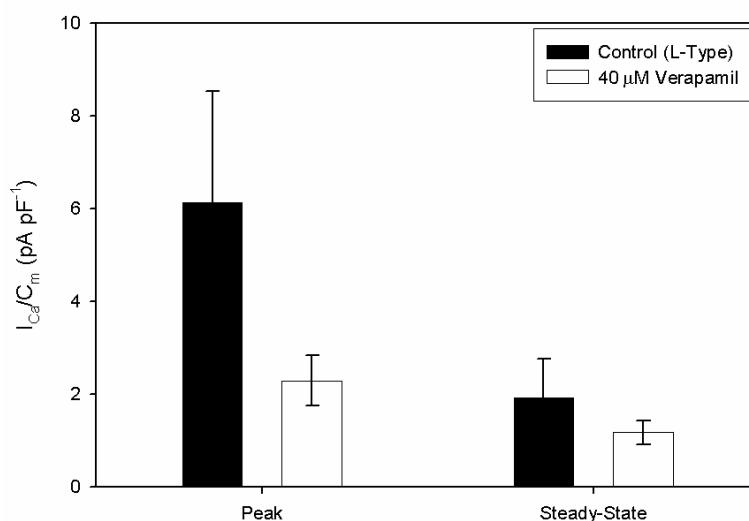
In HEK293 cells expressing N-type VGCCs, 40 μ M of verapamil reduced peak $I_{Ca(N)}$ from 18.6 ± 2.3 ($n = 24$ control cells) to 8.9 ± 1.7 ($n = 22$ treated) and steady-state $I_{Ca(N)}$ from 8.5 ± 0.9 to 3.9 ± 0.5 (Chart 5-2). The percent reductions were 52.2% and 54.1% for peak and steady-state $I_{Ca(N)}$, respectively. Peak occurrences for N-type VGCCs occurred at a V_H of +30 mV.

Chart 5-2 Effects of Verapamil on N-Type VGCCs



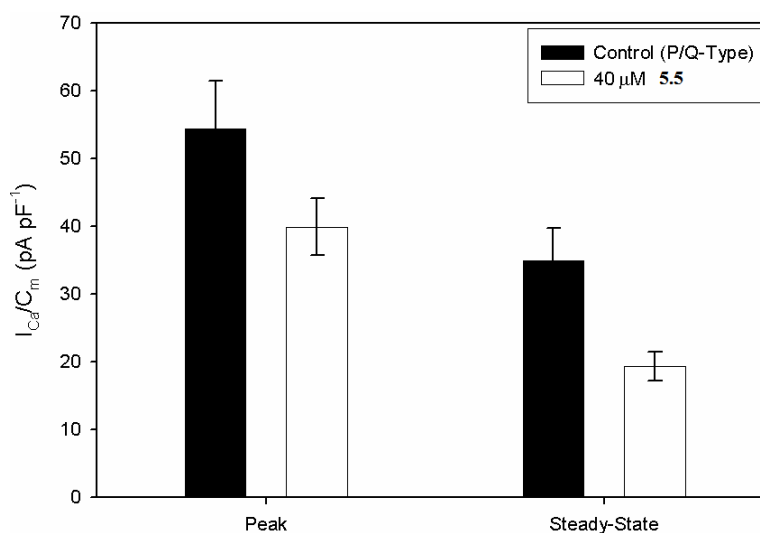
L-type VGCCs generally exhibited smaller current densities than either P/Q- or N-type VGCCs. At 40 μ M verapamil, peak $I_{Ca(L)}$ changed from 6.1 ± 2.4 ($n = 7$ control cells) to 2.3 ± 0.5 ($n = 7$ treated cells), and steady-state $I_{Ca(L)}$ changed from 1.9 ± 0.9 to 1.2 ± 0.3 (Chart 5-3). The percent reductions for L-type VGCCs were 62.2% and 36.8% for peak and steady-state $I_{Ca(L)}$, respectively. Though these reductions were clearly observable, the quantitative inhibitions were not statistically significant.

Chart 5-3 Effects of Verapamil on L-type VGCCs



Compound (**5.5**) was evaluated in a similar manner to verapamil. Ten minutes after application of the compound, $I_{Ca(P/Q)}$ decreased from 54.4 ± 7.1 ($n = 23$ control cells) to 39.9 ± 4.2 ($n = 26$ treated cells), indicating a 26.7% reduction in P/Q current (Chart 5-4). Steady-state $I_{Ca(P/Q)}$ was reduced from 35.0 ± 4.7 to 19.3 ± 2.1 , marking a 44.9% reduction in current. Peak and steady-state measurements were obtained from the same signal acquired at a V_H of +20 mV. In comparison with verapamil data, compound (**5.5**) was only 49.1% as effective in reducing peak $I_{Ca(P/Q)}$ and 68.4% as effective in reducing steady-state $I_{Ca(P/Q)}$.

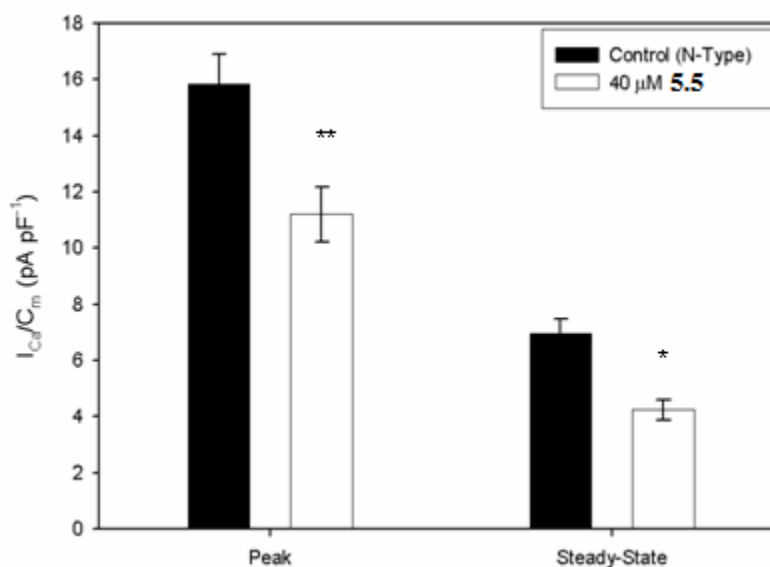
Chart 5-4 Effects of (**5.5**) of P/Q Type VGCCs



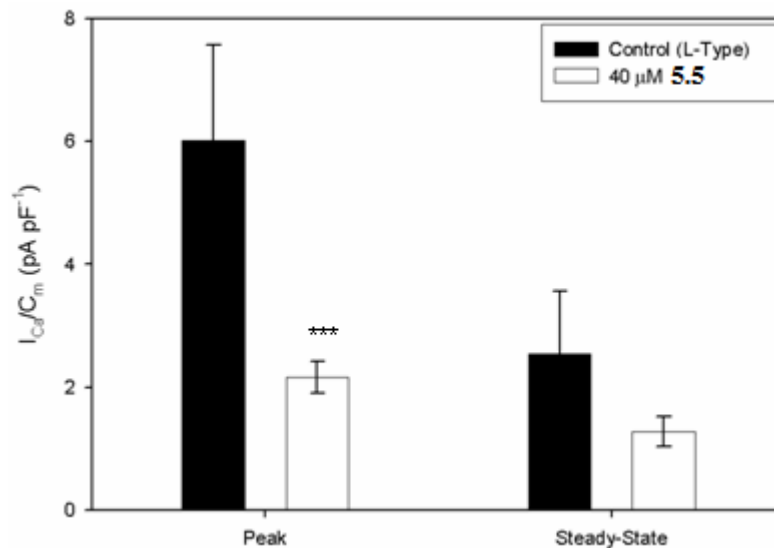
In HEK293 cells expressing N-type VGCCs, compound (**5.5**) at 40 μ M reduced peak $I_{Ca(N)}$ from 15.8 ± 1.1 ($n = 34$ control cells) to 11.2 ± 1.0 ($n = 30$ treated) and steady-state $I_{Ca(N)}$ from 6.9 ± 0.5 to 4.2 ± 0.4 (Chart 5-5). The percent reductions were 29.1% and 39.1% for peak and steady-state $I_{Ca(N)}$, respectively. Compared to verapamil reductions, compound (**5.5**) was 55.7% as effective in inhibiting peak $I_{Ca(N)}$ and 72.3% as effective in inhibiting steady-state $I_{Ca(N)}$. Peak occurrences for N-type VGCCs typically

occurred at a V_H of +20 mV, and maximum steady-state $I_{Ca(N)}$ occurred at +20 mV, as well.

Chart 5-5 Effects of (**5.5**) on N-Type VGCCs



HEK293 cells expressing L-type VGCCs also demonstrated a strong reduction in $I_{Ca(L)}$. At 40 μ M compound (**5.5**), reduced peak $I_{Ca(L)}$ from 6.0 ± 1.6 ($n = 10$ control cells) to 2.2 ± 0.3 ($n = 10$ treated cells), and steady-state $I_{Ca(L)}$ from 2.5 ± 1.0 to 1.3 ± 0.2 (Chart 5-6). The percent reductions for L-type VGCCs were 63.3% for peak current, which was similar to the effectiveness of verapamil, and 48.0% for steady state $I_{Ca(L)}$, which was an increase of 30.4% in effectiveness when compared to verapamil. Though these numbers suggest that compound (**5.5**) may be at least as strong an inhibitor of L-type VGCCs as verapamil. Most importantly compound (**5.5**) has shown to be a more selective inhibitor of L-type calcium channels over other subtypes than its predecessor verapamil. In summary, at a concentration of 40 μ M, verapamil reduced peak I_{Ca} by 54.4%, 52.2%, and 62.2% in P/Q-, N-, and L-type VGCCs, respectively, while (**5.5**) reduced peak I_{Ca} in the same channels by 26.7%, 29.1%, and 63.3%, respectively.

Chart 5-6 Effects of (**5.5**) of L-Type VGCCs

5.4 Discussion

A previous CoMFA model obtained from our laboratory has led to the discovery of two new compounds, which contain a verapamil scaffold. Synthesis of these compounds were carried out in a straightforward manner to provide both analogues in satisfactory yields. Subsequent analysis in a [³H]-BTX assay has shown the α -hydroxy amide analogue (**5.5**) to have an inhibition of 93% at 40 μ M in sodium channels. However, hydantoin analogue (**5.6**) provided only 85% inhibition at 40 μ M in sodium channels.

Thus far analogue (**5.5**) seemed to be our more potent lead, and we therefore chose to conduct an extensive electrophysiological characterization of it within several subtypes of Ca²⁺ channel. We based this analysis upon (**5.5**) having a structural similarity to that of verapamil, a known potent L-type calcium channel inhibitor. Initially studies with our standard, verapamil, show a reduction of activity within P/Q-, N-, and L-type calcium channels at 40 μ M concentration. These reductions occurred at 52.1%, 50.2%,

and 62.7%, respectively, suggesting that verapamil acts as a non-specific Ca^{2+} channel antagonist. We can therefore propose that the clinical efficacy of verapamil may be due to the combined inhibitory effects on all three channel subtypes. In comparison, (**5.5**) reduced activity in P/Q-, N-, and L-type Ca^{2+} channels by 25.7%, 29.5%, and 63.5% at 40 μM . This indicates that (**5.5**) is a non-specific inhibitor, but has enhanced selectivity for L-type calcium channels over other isoforms, in comparison to verapamil.

Our data strongly suggests that verapamil's efficacy is not from action at one site alone, but rather from a combination of effects at numerous sites. Verapamil may be acting at multiple voltage gated channels, such as both calcium and sodium.^{16,17} This could possibly be due to the similar homology between sodium and calcium channels.

Our overall intention in design and synthesis of these compounds was to obtain potent sodium channel blockers that could potentially be used as therapeutics in the treatment of ailments such as pain, seizures, and arrhythmias. Finding the dual activity of our potent lead compound (**5.5**) in Ca^{2+} channels has further expanded its clinical implications. We are highly excited about the possible application of (**5.5**) in Ca^{2+} channel overloading and thereby serving as a neuroprotective agent. Additionally the selective nature of this analogue for L-type Ca^{2+} channels could have diverse application and may serve as a less toxic therapeutic.

5.5 Conclusion

Previous CoMFA models led the development of a new structural class of compounds predicted to have potent NVSC activity. Upon completion of the synthesis and subsequent evaluation in a [^3H]-BTX displacement assay has proven our initial CoMFA to be true and accurate. Further analysis within P/Q-, N-, and L-type Ca^{2+}

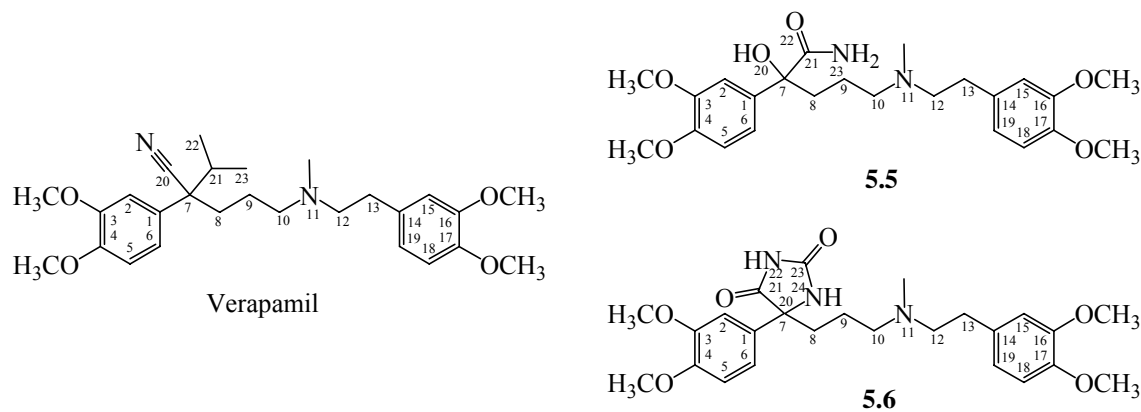
channel has shown that our novel compound (**5.5**) has enhanced affinity for L-type Ca^{2+} channels, which may have interesting physiological implications. We hope to further analyze (**5.5**) in order to determine any possible CNS activity and cardiac effects.

5.6 Experimental Section

5.6.1 Molecular Modeling

Conformational Analysis. The x-ray coordinates for verapamil and analogues were utilized in this study.¹⁸ The conformation of the test set compounds (**5.5**)-(**5.6**) (Figure 5-3) were constructed from the verapamil crystal structure using the Build/Edit mode in SYBYL 7.0. These modified structures were energy-minimized with the Tripos force field,¹⁹ without solvent, using default bond distances and angles and neglecting electrostatics. The minimization was completed by aggregating using the SYBYL/AGGREGATE module for only the x-ray structure atoms and allowing the modified portion to minimize. For internal consistency, we used only the *R*-configuration for all chiral compounds. To determine the low-energy conformation for (**5.5**)-(**5.6**), we utilized GRIDSEARCH on rotatable bonds over 360° in 1° increments. The atomic charges for all analogues were calculated using AM1 (MOPAC).

Figure 5-3 Test Set Analogues Used in CoMFA Model



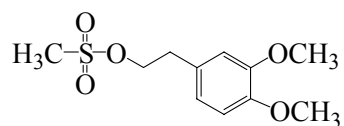
Molecular Alignment. Analogues (5.5)-(5.6) of the test set were fit to overlap C1 and C4 carbons of phenyl ring 1, as well as C14 and C17 carbons of phenyl ring 2. Analogue (5.5) was further aligned by fitting C20 carbon of the nitrile to the OH and C21 carbon of the isopropyl, to the carbonyl carbon of the amide moiety. Analogue (5.6) was also further aligned by overlap of C20 carbon of the nitrile, to the C20 carbonyl of the hydantoin group.

CoMFA Calculations. CoMFA, using default parameter except where noted, was calculated in the QSAR options of SYBYL 6.8 on a Silicon Graphics Octane II R12000 dual processor computer. The CoMFA grid spacing was 2.0 Å in the x , y , and z directions, and the grid region was automatically generated by the CoMFA routine to encompass all molecules with an extension of 4.0 Å in each direction. An sp^3 carbon and charge of +1.0 were used as probes to generate the interaction energies at each lattice point. The default value of 30 kcal/mol was used as the maximum electrostatic and steric energy cutoff.

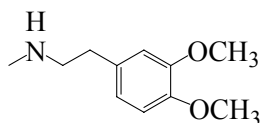
Partial Least Squares (PLS) Regression Analysis. A single conformer for each compound was selected by the smallest cross-validated residual value. Using the cross-validated CoMFA test set conformations for compounds (5.5)-(5.6) were predicted. Single conformers of each training set compound were used in both the non-crossvalidated model and the crossvalidated. We used the final non-crossvalidated CoMFA model to predict the sodium channel binding activities for all the low-energy conformations of the test set compounds (5.5)-(5.6). On the basis of this analysis, the sodium channel binding activities for the low-energy conformers of analogues (5.5)-(5.6), from the test set were predicted.

5.6.2 Chemistry

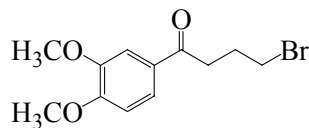
All syntheses requiring anhydrous conditions were kept under inert gas, N₂, and conducted in flame-dried glassware. Solvents were obtained from activated alumina stills or were of commercial grade quality. Melting points were recorded from an Electrothermal Mel-Temp™ melting point apparatus and are uncorrected. IR spectras were obtained from a Nicolet IR/42 spectrometer. ¹H and ¹³C NMRs were conducted on a Varian 300 MHz NMR in CDCl₃ at ambient temperature. High resolution mass spectral (HRMS) data was determined at the University of Illinois Urbana-Champaign School of Chemical Sciences.



Methanesulfonic acid 2-(3,4-dimethoxy-phenyl)-ethyl ester. **(5.1)** 3,4-dimethoxyphenethyl alcohol (10 g, 54.95 mmol) was dissolved in 200 mL CH₂Cl₂: Pyr (9:1) in a flame dried flask kept under nitrogen at 0°C. Methanesulfonyl chloride (4.25 mL, 54.95 mmol) was then added dropwise over a 10 min period, and the yellow solution stirred for 17 h with warming to room temp. At this time 200 mL of water was added, and the solution extracted with CH₂Cl₂ (3 x 200 mL), aqueous sol. CuSO₄ (3 x 50 mL), and water (2 x 50 mL). The organic layers were then combined and dried over Na₂SO₄. The product was obtained in 15.1 g as a yellow oil in 100% yield. TLC: Hex: EtOAc (0:1), R_f=0.8. ¹H NMR (CDCl₃, 300 MHz) δ 6.87-6.66 (m, 3H), 4.37 (t, 2H, *J*=7Hz), 3.85 (s, 3H), 3.83 (s, 3H), 2.97 (t, 2H, *J*=7Hz), 2.85 (s, 3H); ¹³C NMR (CDCl₃, 75.5MHz) δ149.5, 148.6, 129.3, 121.5, 112.7, 111.9, 71.0, 56.4, 37.8, 35.7; IR (neat) 3012, 2959, 2939, 2833, 1609, 1516, 1465, 1351, 1264, 1239, 1173, 1029, 958, 815, 765 cm⁻¹.

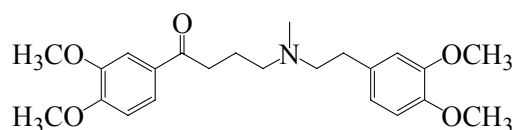


2-(3,4-Dimethoxy-phenyl)-ethylamine. **(5.2)** Methanesulfonic acid 2-(3,4-dimethoxy-phenyl)-ethyl ester (9.9 g, 38 mmol) was dissolved in 100 mL MeOH under N₂, and the methylamine (50 mL, 100 mmol) subsequently added. The stirring solution was then kept at approx. 40°C with heating for a period of 38 h. Upon cooling, the solvent was removed in vacuo and 100 mL of water added. The solution was acidified, to pH=1 with 37% HCl solution, and washed with Et₂O (3 x 100 mL). The aqueous layer was then basified, with NH₄OH to pH=9, and the product extracted with Et₂O (6 x 150 mL). The combined organic layers were washed with water (3 x 100 mL), dried over Na₂SO₄ and evaporated. The product was obtained in 5.4 g as an orange oil in 73% yield. TLC: CH₂Cl₂: EtOH (2:1), R_f=0.14. ¹H NMR (CDCl₃, 300 MHz) δ 6.70-6.48 (m, 3H), 3.77 (s, 3H), 3.75 (s, 3H), 2.72-2.67 (m, 4H), 2.34 (s, 3H), 1.13 (s, 1H); ¹³C NMR (CDCl₃, 75.5 MHz) δ 149.3, 147.9, 133.1, 121.0, 112.4, 111.8, 56.3, 56.2, 53.8, 36.9, 36.3; IR (neat) 3412, 2943, 2835, 2775, 1597, 1520, 1464, 1264, 1236, 1159, 1026, 809, 760.



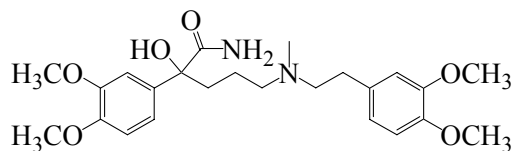
4-Chloro-1-(3,4-dimethoxy-phenyl)-butan-1-one. **(5.3)** Aluminium chloride (7.4 g, 55.5 mmol) was added slowly to a solution of 4-bromobutyryl chloride (5.8 mL, 50.0 mmol) in 55 mL of CS₂. veratrole (7.07 mL, 55.5 mmol) in 55 mL of CS₂ was then added dropwise and the reaction mix was stirred for 30 min, until the gas evolution stopped, and then heated to 40°C for 15 min. After cooling to room temp, the solvent was removed under reduced pressure and 20 mL of water was slowly added, followed by 20 mL of

concentrated HCl. The precipitated product was filtered and triturated in Pet Ether: Hex (1:4). The product was obtained in 10.6 g as a slightly green solid in 87% yield. ^1H NMR (CDCl_3 , 300 MHz) δ 7.63 (dd, 1H, J = 8.4, 1.8 Hz), 7.53 (d, 1H, J = 1.8 Hz), 6.91 (d, 1H, J = 8.4 Hz), 3.94 (s, 3H), 3.93 (s, 3H), 3.56 (t, 2H, J = 6.3 Hz), 3.16 (t, 2H, J = 7.2 Hz), 2.32 (quin, 2H, J = 6.6 Hz); ^{13}C NMR (CDCl_3 , 75.5 MHz) δ 197.9, 153.9, 149.6, 130.5, 123.2, 110.6, 56.6, 56.5, 36.6, 34.2, 27.7; IR (neat) 1583, 1656 cm^{-1} .



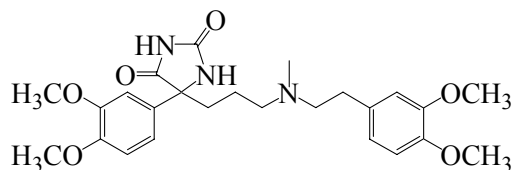
1-(3,4-Dimethoxy-phenyl)-4-([2-(3,4-dimethoxy-phenyl)-ethyl]-methyl-amino} butan-1-one. **(5.4)** Potassium carbonate (5.52 g, 40.0 mmol) and potassium iodine (0.55 g, 3.3 mmol) were flame dried under vacuum. After cooling to room temp, the [2-(3,4-dimethoxy-phenyl)-ethyl]-methyl-amine (3.68 mL, 20.0 mmol) in 5 mL dry DMF was added under a N_2 atmosphere. The reaction mixture was stirred 5 min and then 4-chloro-1-(3,4-dimethoxy-phenyl)-butan-1-one (4.85 g, 20 mmol) in 5 mL of dry DMF was added. After refluxing for 24 h, the reaction mixture was cooled to room temp, quenched by addition of 20 mL of water and extracted with EtOAc (5 x 20 mL). The combined organic extracts were washed with water (8 x 10 mL), dried over Na_2SO_4 , filtered and conc. under reduced pressure. The crude oil was purified by flash chromatography with EtOAc: MeOH (1:0)-(3:2) as the eluent. The product was obtained in 3.54 g as a slightly green oil in 44% yield. ^1H NMR (CDCl_3 , 300 MHz) δ 7.58 (dd, 1H, J = 8.4 Hz), 7.53 (d, 2H, J = 1.5 Hz), 6.89 (d, 1H, J = 8.1 Hz), 6.78-6.71 (m, 3H), 3.94 (s, 3H), 3.93 (s, 3H), 3.86 (s, 3H), 3.83 (s, 3H), 2.97 (t, 2H, J = 6.9 Hz), 2.72-2.60 (m, 4H), 2.52 (t, 2H, J = 7.2 Hz), 2.32 (s, 3H), 1.95 (quin, 2H, J = 6.9 Hz); ^{13}C NMR (CDCl_3 , 75.5 MHz) δ 198.5,

152.9, 148.7, 148.5, 147.0, 132.9, 130.0, 122.4, 120.3, 111.8, 111.0, 109.8, 109.7, 59.2, 56.5, 55.8, 55.7, 55.6, 55.5, 41.8, 35.4, 33.0, 21.8; IR (neat) 1265, 1519, 1677, 2953 cm^{-1} ; APCIMS: m/z 402 (MH^+); HRMS calcd for $\text{C}_{23}\text{H}_{32}\text{N}_2\text{O}_5$: 402.2280; Found: 402.2281.



2-(3,4-Dimethoxy-phenyl)-5-([2-(3,4-dimethoxy-phenyl)-ethyl]-methyl-amino)-2-hydroxy-pentanoic Acid Amide. **(5.5)** 1-(3,4-Dimethoxy-phenyl)-4-([2-(3,4-dimethoxy-phenyl)-ethyl]-methyl-amino) butan-1-one (1.4 g, 3.48 mmol), potassium cyanide (35 mg, 0.53 mmol), 18-crown-6 (35 mg, 0.13 mmol) and trimethylsilyl cyanide (1.02 mL, 7.67 mmol) were dissolved in 20 mL of dry CH_2Cl_2 under a N_2 atmosphere and stirred at room temp. for 24 h. After evaporation under reduced pressure, the residue was dissolved in 15 mL of 1,4-dioxane, cooled to 0°C and 15 mL of refrigerated conc. HCl were added dropwise over a 30 min period. HCl gas was slowly bubbled through the solution for 1 h at 0°C . The solution was allowed to sit without stirring for 2 days, then extracted with CH_2Cl_2 (5 x 20 mL). The combined organic extracts were washed with brine (2 x 5 mL), dried over Na_2SO_4 , filtered and concentrated under reduced pressure. Purification by flash chromatography with a gradient of $\text{EtOAc}:\text{MeOH}$ (100:0)-(4:1) was conducted. The product was obtained in 0.48 g as a brown solid in 31% yield. ^1H NMR (CDCl_3 , 300 MHz) δ 6.90 (bs, 1H), 6.87 (d, 1H, $J = 8.4$ Hz) 6.74-6.63 (m, 4H), 6.49 (bs, 1H), 5.88 (t, 1H, $J = 7.5$ Hz), 3.79 (s, 3H), 3.77 (s, 6H), 3.75 (s, 3H), 3.22-2.58 (m, 13H); ^{13}C NMR (CDCl_3 , 75.5 MHz) δ 170.5, 149.0, 147.9, 140.5, 129.2, 128.3, 125.7, 120.6, 119.6, 111.9, 111.3, 110.9, 109.8, 69.9, 57.3, 56.7, 55.8, 55.7, 54.8, 40.0, 29.8, 24.5; IR (neat) 1669, 2615, 2845, 2961, 3405 cm^{-1} ; ESIMS: m/z 472.3 (MH^+); HRMS calcd for

$C_{24}H_{34}N_2O_6$: 446.2417; Found [(m/z)-H₂O]= 429.3. mp: 41-42°C.



5-(3,4-Dimethoxy-phenyl)-5-(3-{[2-(3,4-dimethoxy-phenyl)-ethyl]-methyl-amino}-propyl)-imidazolidine-2,4-dione. (**5.6**) To a stirred solution of 1-(3,4-dimethoxy-phenyl)-4-{[2-(3,4-dimethoxy-phenyl)-ethyl]-methyl-amino} butan-1-one (1.05 g, 2.61 mmol) in 10 mL of aq. EtOH (50%) were added potassium cyanide (0.51 g, 7.84 mmol) and ammonium carbonate (151 g, 15.70 mmol). The reaction mixture was heated to 65°C for 11 days. After cooling to room temp, careful acidification of the reaction mixture was conducted by the addition of conc. HCl until pH=2. The product was obtained in 1.15 g as a gray solid in 93% yield. ¹H NMR (CDCl₃, 300 MHz) δ 7.63 (d, 1H, *J* = 7.2 Hz), 7.15 (bs, 1H), 6.92 (d, 1H, *J* = 8.4Hz), 6.80 (m, 3H), 3.95 (2s, 6H), 3.88 (s, 3H), 3.86 (s, 3H), 3.28-2.75 (m, 11H), 2.18 (m, 2H); ¹³C NMR (CDCl₃, 75.5 MHz) δ 196.6, 153.4, 148.9, 148.7, 147.9, 129.1, 128.0, 122.7, 120.5, 111.8, 111.2, 109.8, 109.6, 57.9, 56.9, 55.8, 55.6, 55.0, 39.9, 34.4, 29.6, 17.9; IR (neat) 1670, 1733, 2837, 2965, 3411 cm⁻¹ ESIMS: m/z 472.3 (MH⁺); HRMS calcd for C₂₅H₃₄N₃O₆: 472.2448; Found: 472.2453. mp: 60-62°C.

5.6.3 Biology

Cell Culture. HEK293 cells individually expressing P/Q, N, L-type calcium channels were obtained as a gift from Dr. Kenneth A. Stauderman at the Salk Institute Biotechnology/Industrial Associates, Incorporated, were employed in this study under whole-cell patch-clamp conditions. Cultures were maintained in RPMI 1640 with 10%

heat-inactivated fetal bovine serum supplemented with 1% penicillin/streptomycin. Flasks containing cells were incubated at 37°C in 5% CO₂ and air. The cells were subcultured every 3 to 4 days by mechanical disassociation. Prior to each patch-clamp experiment, cells were immobilized on glass coverslips coated with poly-L-lysine.

Solutions. The internal solution (inside the patch pipette) contained (in mM): 1 CaCl₂, 2 MgCl₂, 120 CsCl, 11 EGTA (NaOH), 20 TEA-Cl, and 10 HEPES (NaOH). The external solution contained (in mM): 130 NaCl, 5 KCl, 10 CaCl₂, 5 Glucose, and 10 HEPES (NaOH). Additionally, 20 BaCl₂ was added to the external solution used in measuring L-type VGCC currents. All solutions were stored at 4°C and warmed to room temperature before experiments. Both internal and external solutions were adjusted to a pH of 7.2 with NaOH and were filtered through a 0.2-μm Millipore filter before use.

Application of drug compounds. For experiments involving (**5.5**), we first dissolved the compound in dimethyl sulfoxide (DMSO) to form a 10 mM stock solution. Similarly, we dissolved verapamil in dH₂O to make a 10 mM stock solution. Preliminary experiments demonstrated no effect of DMSO or dH₂O on VGCC currents in the concentrations used throughout this study. For experimentation, we prepared test concentrations by diluting the appropriate stock solution into 2 mL of external solution, yielding a final concentration of 1% DMSO or dH₂O or DMSO, for (**5.5**) or verapamil, respectively. In all experiments, we used a concentration of 40 μM as a point for comparison between the two compounds.

Whole-cell patch-clamp recording. This study employed the standard patch-clamp technique to record VGCC currents. Patch pipettes were fashioned from Kimax capillary tubes (1.5-1.8 mm inner-outer diameter) and then heat polished at the tips with an L/M-

CPZ-101 pipette forge. Pipettes typically had resistances of 1-2 M Ω , corresponding to an inner-lumen tip diameter of about 1-2 μ m. After whole-cell patch-clamp configuration was achieved, VGCC currents were elicited by a voltage pulse sequence using a List EPC-7 patch-clamp amplifier. Prior to the pulse sequence, a +20 mV test potential at a rate of 10 Hz induced a repeated transient current, the step response of the series combination of R_s and C_m with a relaxation time of $R_s C_m$. Using the patch-clamp amplifier, the cancellation of the transient current yielded values for R_s and C_m .

Voltage-clamp data acquisition and analysis. VGCC currents were elicited by a voltage pulse sequence initiated 30-60 seconds after establishing the whole-cell recording configuration at room temperature. Depolarizing step potentials of 350 ms in duration then evoked currents from a holding potential of -80 mV. The depolarizing steps ranged from -60 to +90 mV in 10 mV intervals. The sampling rate of these currents was 10 kHz.

Statistics. Data are presented as mean \pm S.E.M. in units of picoamps (pA) or picoamps per picofarads (pA/pF), with regard to the number of cells tested per group (n). Because a 10-20 mV shift in the voltage-dependence of channel gating can occur during the first 10-15 minutes of recording, statistical comparisons were made between separate control and drug-treated cells. Current magnitudes were normalized using C_m , which typically ranged from 10-30 pF and did not show any correlation with drug treatment. Statistical significance was evaluated using a student's t test.

5.7 References

- 1) De Rosa, M.L.; Giordano, A.; Melfi, M.; Guardia, D.G.; Ciaburri, F.; Rengo, F.
“Antianginal efficacy over 24 hours and exercise hemodynamic effects of once
daily sustained-release 300 mg diltiazem and 240 mg verapamil in stable angina
pectoris,” *Intl. J. Cardiol.* **1998**, *63*, 27-35.
- 2) Novo, S.; Abrignani, M.G.; Novo, G.; Nardi, E.; Dominguez, L.J.; Strano, A.;
Barbagallo, M. “Effects of drug therapy on cardiac arrhythmias and ischemia in
hypertensives with LVH,” *Am. J. Hypertension.* **2001**, *14*, 637-643.
- 3) Hassan, S.A.; Oral, H.; Scharf, C.; Chugh, A.; Pelosi, F.; Knight, B.P.;
Strickberger, S.A. “Rate-dependent effect of verapamil on atrial refractoriness,”
J. Am. Coll. Cardiol. **2003**, *41*, 446-451.
- 4) Messerli, F.H. “Calcium antagonists in hypertension: from hemodynamics to
outcomes,” *Am. J. Hypertension.* **2002**, *15*, 94-97.
- 5) Frishman, W.H.; Michaelson, M.D. “Use of calcium antagonists in patients with
ischemic heart disease and systemic hypertension,” *Am. J. Cardiol.* **1997**, *79*, 33-
38.
- 6) Opie, L.H. “Calcium ions, drug action and the heart-with special reference to
calcium antagonist drugs,” *Pharmac. Ther.* **1984**, *25*, 271-295.
- 7) Choi, J.S.; Burm, J.P. “Pharmacokinetics of verapamil and its major metabolite,
norverapamil from oral administration of verapamil in rabbits with hepatic failure
induced by carbon tetrachloride, *Arch. Pharm. Res.* **2005**, *28*, 483-487.
- 8) Messerli, F. “What, if anything, is controversial about calcium antagonists,” *Am.*
J. Hypertension. **1996**, *9*, 177-181.

- 9) McNeal, E.; Lewandowski, G.A.; Daly, J.W.; Creveling, C.R. “[³H] Batrachotoxinin A 20 α -benzoate binding to voltage-sensitive sodium channels: a rapid and quantitative assay for local anesthetic activity in a variety of drugs,” *J. Med. Chem.* **1985**, 28, 381-388.
- 10) Santana, L.F.; Gomez, A.M.; Lederer, W.J. “Ca²⁺ flux through promiscuous cardiac Na⁺ channels: slip-mode conductance,” *Science*. **1998**, 279, 1027-1032.
- 11) Lipton, P. “Ischemic cell death in brain neurons,” *Physiol. Rev.* **1999**, 79, 1432-1516.
- 12) Annoura, H.; Nakanishi, K.; Uesugi, M.; Fukunaga, A.; Imajo, S.; Miyajima, A.; Tamura-Horikawa, Y.; Tamura, S. “Synthesis and biological evaluation of new 4-arylpiperdines and 4-aryl-4-piperidinols: dual Na⁺ and Ca²⁺ channel blockers with reduced affinity for dopamine D₂ receptors,” *Bioorg. Med. Chem.* **2002**, 10, 371-383.
- 13) Tatsumi, S.; Itoh, Y.; Ukai, Y. “A novel Na⁺/Ca²⁺ channel blocker, NS-7, suppresses hypoxic injury in rat cerebrocortical slices,” *Naunyn-Schmiedeberg's Arch Pharmacol.* **1998**, 358, 191-196.
- 14) Pauwels, P.J.; Leysen, J.E.; Janssen, P. “Minireview: Ca²⁺ and Na⁺ channels involved in neuronal cell death. protection by flunarizine,” *Life Sci.* **1991**, 48, 1881-1893.
- 15) Anderson, J.D.; Hansen, T.P.; Lenkowski, P.W.; Walls, A.M.; Choudhury, I.M.; Schenck, H.A.; Friehling, M.; Holl, G.M.; Patel, M.K.; Sikes, R.A.; Brown, M.L. “Voltage-gated sodium channel blockers as cytostatic inhibitors of the androgen-

- independent prostate cancer cell line PC-3,” *Mol. Cancer Ther.* **2003**, *2*, 1149-1154.
- 16) Shi, E.; Kazui, T.; Jiang, X.; Washiyama, N.; Suzuki, K.; Yamashita, K.; Terada, H. “NS-7, a novel $\text{Na}^+/\text{Ca}^{2+}$ channel blocker, prevents neurological injury after spinal cord ischemia in rabbits,” *J. Thorac. Cardiovasc. Surg.* **2005**, *129*, 364-371.
- 17) Youdim, M.; Buccafusco, J.J. “Multifunctional drugs for various CNS targets in the treatment of neurodegenerative disorders,” *Trends Pharmacol. Sci.* **2005**, *26*, 27-35.
- 18) Camerman, A.; Camerman, N. “The stereochemical basis of anticonvulsant drug action. I. The crystal and molecular structure of diphenylhydantoin, a noncentrosymmetric structure solved by centric symbolic addition,” *Acta Crystallogr.* **1971**, *B27*, 2205-2211.
- 19) Clark, M.D.; Cramer, R.D.; Opdenbosch, N.V. “Validation of the general purpose Tripos 5.2 force field,” *J. Comput. Chem.* **1989**, *10*, 982-1012.

Chapter 6

Agonists of Calcium-ATPase Activity

Cardiac forms of Ca^{2+} -ATPases (SERCA2a) play a major role in the excitation and contraction of cardiac muscle. Due to the mechanisms by which these processes occur, it has been established that agonists of Ca^{2+} -ATPases activity may function in the treatment of cardiomyopathies. Herein, we have been able to design new compounds based on a combined scaffold, of verapamil and either diphenyl or monophenyl amine, and successfully synthesize them in adequate quantities. Biological examination for stimulatory activity has shown analogue (6.5) to have exceptional activity, which is much greater than our standard, the natural product gingerol.

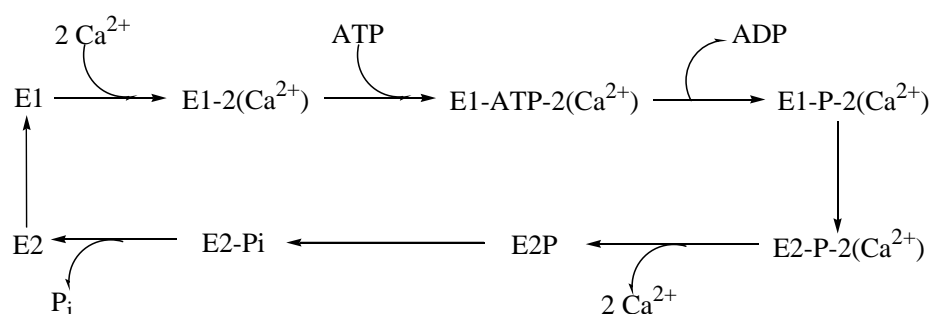
6.1 Ca^{2+} -ATPase Pump

6.1.1 Structure and Function

The sarcoplasmic reticulum (SR) is an intracellular membrane system that extends from the nuclear envelope and is known to contain high levels of Ca^{2+} -ATPase.¹ Three Ca^{2+} -ATPase genes have currently been identified that splice to over seven isoforms, which are found in cardiac and skeletal muscle, epithelial cells and neurons. Cardiac SR Ca^{2+} -ATPases (SERCA2a) play a major role in the excitation-contraction of cardiac muscle, by storage and distribution of calcium in the SR.² Minor fluxes of calcium concentration through L-type VGCCs results in a major release of calcium from internal stores within the SR, in a response known as calcium induced calcium release (CICR).³ The calcium then binds to troponin C which promotes crossbridging between actin and myosin myofibrils, thereby allowing for contraction.⁴ Subsequent removal of calcium from the extracellular lumen by Ca^{2+} -ATPase then results in relaxation.

Calcium-ATPases are P-type pumps which participate in the active transport of calcium ions at the expense of ATP.⁵ During this process, the protein is known to assume one of two possible conformations, the E1 or E2 state (Figure 6-1).⁶ In the E1 state, the protein binds two calcium ions from the cytoplasm with high affinity. Subsequent binding of ATP results in phosphorylation of the protein and conversion to the low affinity E2 state. Calcium is now released into the luminal side and dephosphorylation returns the protein to the initial E1 state.⁷

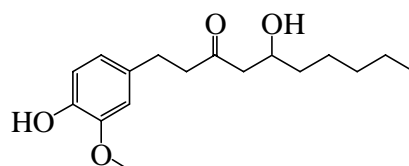
Figure 6-1 Mechanism of Ca^{2+} -ATPase Function



6.1.2 Stimulants of Activity

Gingerol, isolated from the rhizome of ginger, has been found to be effective in the stimulation of Ca^{2+} -ATPase activity of canine cardiac muscle (Figure 6-2).^{8,9} It is known that the amount of Ca^{2+} accumulated by SR Ca^{2+} -ATPases during diastole is proportional the force of the next systole, and that decreased levels of SR Ca-ATPase in the heart contribute to diminished cardiac contractility. Therefore, agonists of Ca^{2+} -ATPases activity, such as gingerol, are highly effective in treating cardiomyopathies.¹⁰

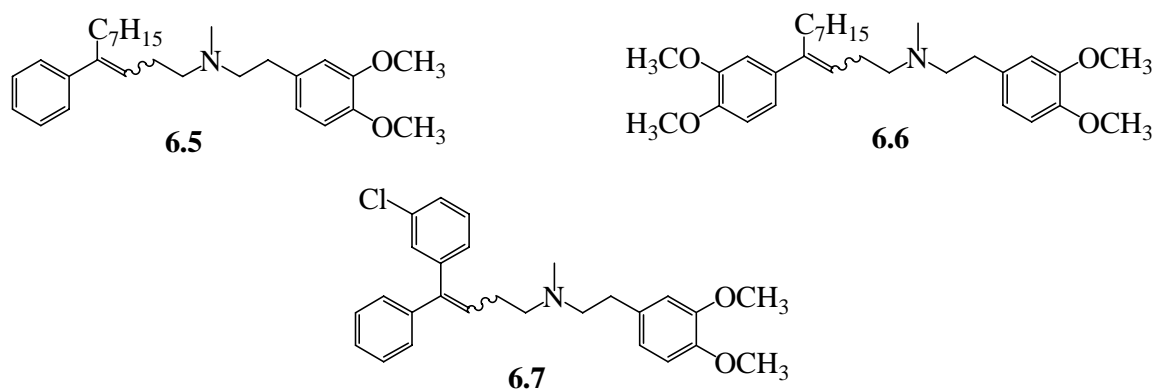
Figure 6-2 Structure of Gingerol



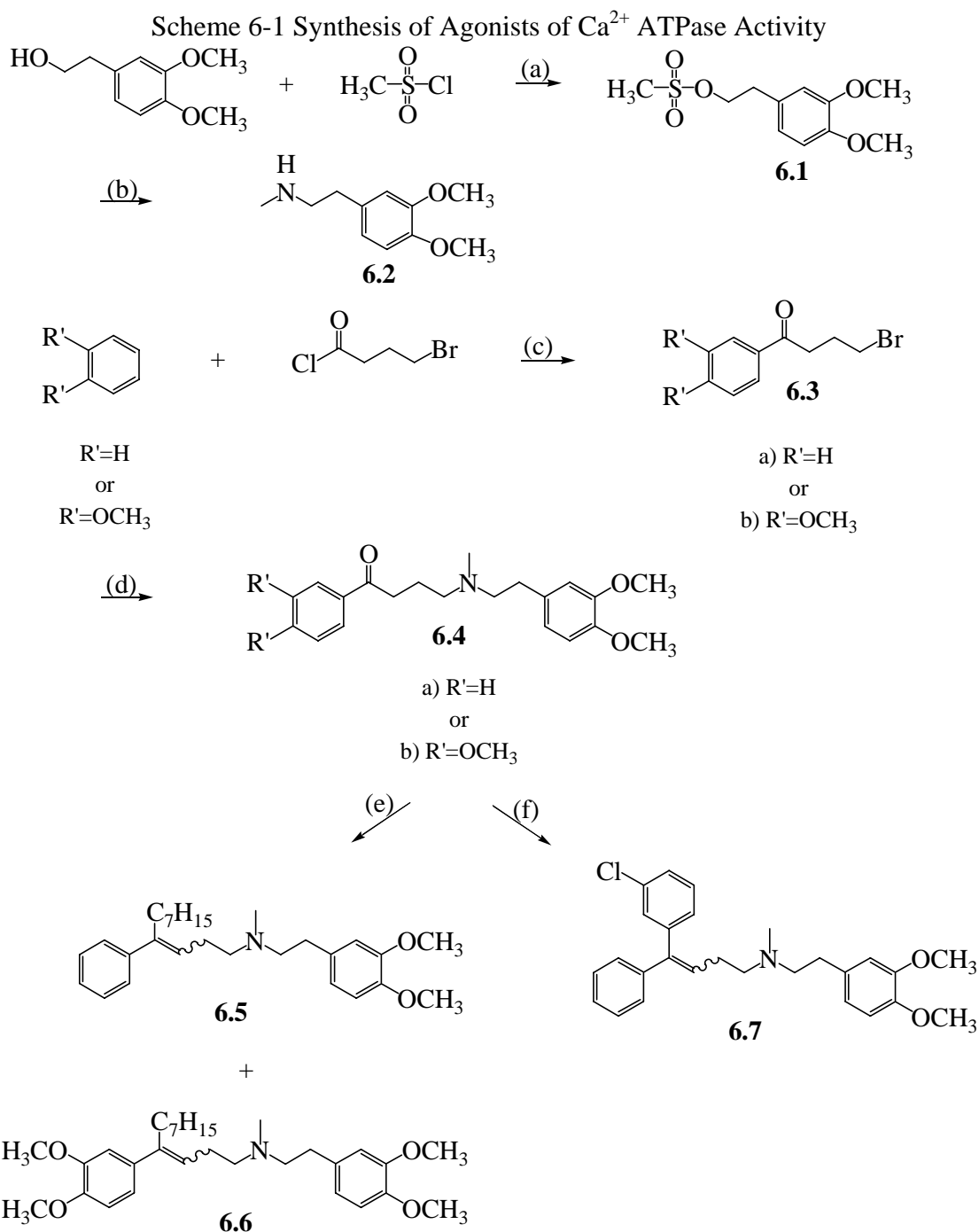
6.2 Design and Synthesis

Our continuing efforts to develop potent ion channel inhibitors led us to analogues based on a combined scaffold, of verapamil and either diphenyl or monophenyl amine series (Figure 6-3). Analogues derived from the monophenyl series contained the optimal seven carbon chain length, found from our previous investigations. Two analogues of this type were constructed and explore the necessity of the dimethoxy group. Additionally, a diphenyl series analogue was created with m-Cl monosubstitution.

Figure 6-3 Agonists of Calcium-ATPase Activity



3,4-Dimethoxyphenethyl alcohol was mesylated to generate compound (6.1). (Scheme 6-1). Subsequent addition of methylamine to (6.1) provided compound (6.2), which was later coupled to either 4-bromo-1-phenyl-butan-1-one (6.3a) or 4-bromo-1-(3,4-dimethoxy)-phenyl-butanone (6.3b). These couplings resulted in the formation of ketones (6.4a) and (6.4b). Synthesis of analogs (6.5) and (6.6) were accomplished by addition of heptylmagnesium bromide to their corresponding ketone, followed by dehydration to provide a mixture of stereoisomers. Analog (6.7) was synthesized by the addition of 3-chlorophenylmagnesium bromide and subsequent dehydration to provide the desired product in adequate yield. All product materials were isolated as a mixture of stereoisomers and were evaluated for biological activity without further separation.

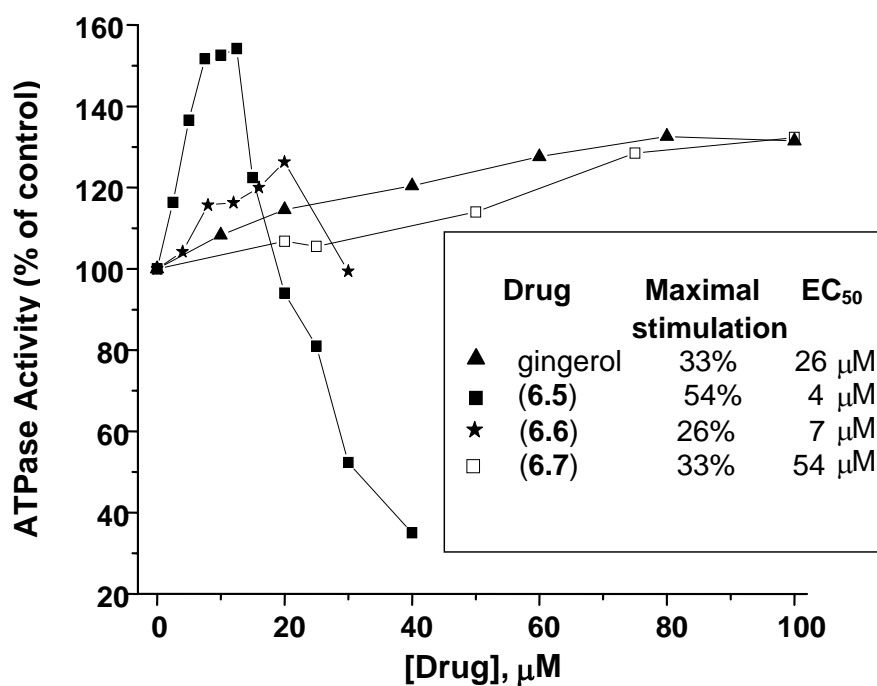


Conditions: (a) $\text{CH}_2\text{Cl}_2/\text{Py}$, 0°C-RT ; 100% (b) MeNH_2 , MeOH ; 73% (c) AlCl_3 , CS_2 ; $\text{R}'=\text{H}$, 95%; $\text{R}'=\text{OCH}_3$, 87% (d) **2**, K_2CO_3 , DMF , RT ; $\text{R}'=\text{H}$, 32%; $\text{R}'=\text{OCH}_3$, 44% (e) i. Heptyl-MgBr, NH_4Cl , ii. 7 M HCl/EtOH , reflux; 2 steps, $\text{R}'=\text{H}$, 37%; $\text{R}'=\text{OCH}_3$, 58% (f) 3-Chlorophenyl-MgBr, NH_4Cl , ii. 7M HCl/EtOH , reflux; 2 steps, $\text{R}'=\text{H}$, 44%.

6.3 Results

Analogue (6.5) was analyzed for stimulatory activity of Ca^{2+} -ATPase in cardiac SR. Our findings reveal that analogue (6.5) was found to have the best activity with 54% maximal stimulation and an EC_{50} of 4 μM (Chart 6-1). When compared to our standard gingerol, with 33% maximal stimulation and an EC_{50} of 26 μM , we find this novel analogue (6.5) provides an exceptional increase in stimulatory activity. Diphenyl analogue (6.7) was found to have lower activity than gingerol, and analogue (6.6) displayed increased activity in comparison to the standard, but was not as significant as analogue (6.5).

Chart 6-1 Ca^{2+} -ATPase Activity in Cardiac Sarcoplasmic Reticulum



6.4 Discussion and Conclusion

6.4.1 Discussion

We have been able to design new compounds based on a combined scaffold, of verapamil and either diphenyl or monophenyl amine and successfully synthesize them in adequate quantities. Analogue design was based on our previous investigations of ion channel blockers, which revealed two potent classes of analogues, the diphenyl and monophenyl amine series. Optimizations of these classes led us towards our current design.

Incorporation of m-Cl substitution of the diphenyl analogue (**6.7**) was conducted, but biological evaluation for stimulatory effects of cardiac Ca^{2+} -ATPase revealed lower activity than gingerol. However, both monophenyl amine analogues (**6.5**) and (**6.6**), containing the optimal chain length of $n=7$, were found to have enhanced stimulatory activity in comparison to the standard. These two analogues differ only by incorporation of two methoxy groups, but substantial differences in their biological activity were found. Specifically, analogue (**6.5**) was found to have 54% maximal stimulation and an EC_{50} of 4 μM , whereas analogue (**6.6**) provided 26% maximal stimulation at an EC_{50} of 7 μM . Therefore, the methoxy groups have been found to lower the overall activity of these derivatives.

Interestingly, we also find a resemblance of our novel analogues to potent agonist, gingerol. These shared structural features may play a significant role in the activity of our compounds and aid in understanding of necessary structural requirements. Analysis of these analogues for myocardial contractility in mouse hearts is currently underway, and preliminary findings show promising results.

6.4.2 Conclusion

From our findings, we have been able to determine that analogues based on a combined scaffold, of verapamil and monophenyl amine, are potent agonists of Ca^{2+} - ATPase activity. Our lead analogue (**6.5**) was found to have 54% stimulation concentration and an EC_{50} of 4 μM , which was much greater than our standard. We propose that this potent activity may be due to the similar structural features of our novel class to the agonist, gingerol.

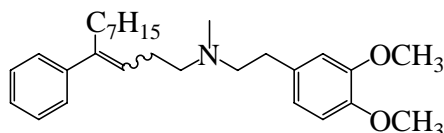
6.5 Experimental Section

6.5.1 Chemistry

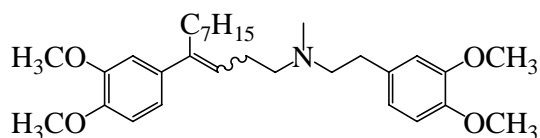
All syntheses requiring anhydrous conditions were kept under inert gas, N_2 , and conducted in flame-dried glassware. Solvents were obtained from activated alumina stills or were of commercial grade quality. ^1H and ^{13}C NMRs were conducted on a Varian 300 MHz NMR in CDCl_3 at ambient temperature. High resolution mass spectral (HRMS) data was determined at the University of Illinois Urbana-Champaign School of Chemical Sciences.

General Procedure A: The ketone (1.0 equiv) in CH_2Cl_2 (or Tol) was kept under N_2 and held at 0°C , by use of an ice-bath. The Grignard solution (1.5-2.0 equiv) was added dropwise to the flask, and the reaction was allowed to stir overnight with gradual warming to room temp. The mixture was quenched by addition of a sat. NH_4Cl solution. The crude product was extracted with water (2 x 30 mL), CH_2Cl_2 (1x 30 mL), brine (1 x 20 mL), and dried over MgSO_4 . The material was then filtered and evaporated to provide the crude product. Subsequent dehydration was conducted by refluxing in an

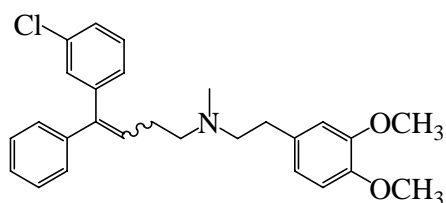
ethanolic solution of 2M HCl (> 25 equiv) for 3-4 hrs. The solution was now evaporated, dissolved in water, and basified to a pH=10 with K₂CO₃. The material was taken up in CH₂Cl₂ and extracted (3 x 50 mL), dried over MgSO₄, filtered and evaporated. Flash column chromatography of the crude material was carried out using a CH₂Cl₂: MeOH system from (100:0)-(10:1).



[2-(3,4-Dimethoxy-phenyl)-ethyl]-methyl-(4-phenyl-undec-3-enyl)-amine. **(6.5)** Procedure A was carried out using 4-{[2-(3, 4-dimethoxy-phenyl)-ethyl]-methyl-amino}-1-phenyl-butan-1-one (**6.4a**) (0.6 g, 1.77 mmol), 1 M heptylmagnesium bromide (2.7 mL, 2.7 mmol), Tol (10 mL), and 2 M HCl/EtOH (15 mL). The product was obtained as a light brown oil in 0.27 g, 37% yield. ¹H NMR (CDCl₃, 300 MHz) δ 7.30-7.22 (m, 5H), 6.77-6.74 (m, 2H), 6.66-6.65 (m, 1H), 5.70-5.66 (t, 0.33H, *J*=7.1), 5.58-5.54 (t, 0.67H, *J*=6.8), 3.85-3.83 (br s, 6H), 2.85-2.81 (m, 2H), 2.78-2.76 (m, 1H), 2.75-2.70 (m, 2H), 2.51-2.49 (m, 4H), 2.46-2.44 (m, 1H), 2.15 (s, 3H), 1.28-1.21 (br s, 10H), 0.88-0.81 (m, 3H); ¹³C NMR (CDCl₃, 75.5 MHz) δ 149.20, 147.82, 143.03, 142.79, 131.78, 130.86, 128.60, 128.41, 126.99, 126.53, 124.53, 120.77, 112.20, 111.55, 59.29, 58.43, 57.11, 56.13, 41.76, 41.26, 32.67, 32.03, 30.21, 29.80, 29.34, 28.92, 26.93, 25.83, 22.84, 14.31; ESIMS: 424 (M + H); HRMS calcd for C₂₈H₄₂N₂O₂: 424.3216; Found: 424.3222.



[2-(3,4-Dimethoxy-phenyl)-ethyl]-[4-(3,4-dimethoxy-phenyl)-undec-3-enyl]-methylamine. **(6.6)** Procedure A was carried out using 1-(3,4-dimethoxy-phenyl)-4-[[2-(3,4-dimethoxy-phenyl)-ethyl]-methyl-amino} butan-1-one (**(6.4b)**) (0.5 g, 1.25 mmol), 1 M heptylmagnesium bromide (1.88 mL, 1.88 mmol), CH₂Cl₂ (15 mL), and 7 M HCl/EtOH (20 mL). The product was obtained as a light brown oil in 0.35 g, 58% yield. ¹H NMR (CDCl₃, 300 MHz) δ 7.61-7.54 (m, 1H), 6.94-6.75 (m, 5H), 5.68-5.64 (m, 0.51H), 5.46-5.44 (m, 0.49H), 3.81-3.77 (br s, 12H), 2.79-2.75 (m, 4H), 2.68-2.61 (m, 2H), 2.42-2.39 (m, 4H), 2.07 (s, 2H), 1.98-1.94 (m, 1H), 1.30 (br s, 10H), 0.90-0.88 (m, 3H); ESIMS: 484 (M + H); HRMS calcd for C₃₀H₄₆N₂O₄: 484.3427; Found: 484.3418.



[4-(3-Chloro-phenyl)-4-phenyl-but-3-enyl]-[2-(3,4-dimethoxy-phenyl)-ethyl]-methylamine. **(6.7)** Procedure A was carried out using 4-[[2-(3, 4-dimethoxy-phenyl)-ethyl]-methyl-amino}-1-phenyl-butan-1-one (**(6.4a)**) (0.5 g, 1.47 mmol), 0.5 M 3-chlorophenylmagnesium bromide (4.4 mL, 2.2 mmol), Tol (10 mL), and 2 M HCl/EtOH (15 mL). The product was obtained as a yellow solid in 0.27 g, 42% yield. ¹H NMR (CDCl₃, 300 MHz) δ 7.61-7.59 (m, 2H), 7.25-7.22 (m, 2H), 7.13-7.10 (m, 2H), 6.47-6.44 (m, 3H), 5.87-5.81 (m, 1H), 3.53 (s, 3H), 3.49 (s, 3H), 2.81-2.79 (m, 2H), 2.74-2.72 (m, 4H), 2.42 (s, 3H), 1.88-1.85 (m, 2H); ¹³C NMR (CDCl₃, 75.5 MHz) δ 149.95, 149.87, 148.78, 148.70, 137.11, 134.28, 130.22, 130.17, 129.74, 129.53, 128.80, 121.50, 121.45,

112.77, 112.21, 58.48, 56.68, 56.25, 41.31, 36.06, 31.45, 19.53; ESIMS: 437 (M + 2H); HRMS calcd for C₂₇H₃₁N₂O₂Cl: 436.2043; Found: 436.2039.

6.5.2 Biology

Sarcoplasmic reticulum vesicles were prepared from canine ventricular tissue. Ca²⁺-ATPase activity was measured using an enzyme-linked continuous ATP assay at 37°C. 10 to 20 µg of CSR vesicles were added to 1 mL of 50 mM imidazole buffer (pH 7.2) containing 100 mM KCl, 5 mM MgCl₂, 0.4 mM EGTA, 2 mM phosphoenol pyruvate, 22U/mL lactate dehydrogenase, 10U/mL pyruvate kinase, 1.0 mM NADH, 0.1 mg/mL deoxycholate. The synthetic compounds were dissolved in DMSO, and stored at 4°C at a stock concentration of 10 mg/mL. The compounds were added to the vesicle suspension in assay mix and pre-equilibrated for 10-15 min. The reaction was started by the addition of 2.4 mM Tris-ATP (pH 7.0). The Ca-ATPase activity is expressed as µmoles ATP split per minute per mg total SR protein.

6.6 References

- 1) Endo, M. "Calcium release from the sarcoplasmic reticulum," *Physiol. Rev.* **1977**, *57*, 71-108.
- 2) East, J.M. "Sarco(endo)plasmic reticulum calcium pumps: recent advances in our understanding of structure and function," *Mol. Membrane Bio.* **2000**, *17*, 189-200.
- 3) Fabiato, A. "Calcium-induced release of calcium from the cardiac sarcoplasmic reticulum," *Am. J. Physiol.* **1983**, *245*, C1-C14.
- 4) Frank, K.F.; Bolck, B.; Erdmann, E.; Schwinger, R.H. "Sarcoplasmic reticulum Ca^{2+} -ATPase modulates cardiac contraction and relaxation," *Cardiovasc. Res.* **2003**, *57*, 20-27.
- 5) Moller, J.V.; Olesen, C.; Jensen, A.M.; Nissen, P. "The structural basis for coupling of Ca^{2+} transport to ATP Hydrolysis by the sarcoplasmic reticulum Ca^{2+} -ATPase," *J. Bioenerg. Biomembr.* 2005, *37*, 359-364.
- 6) Stokes, D.L.; Green, N.M. "Structure and function of the calcium pump," *Annu. Rev. Biophys. Biomol. Struct.* **2003**, *32*, 445-468.
- 7) Toyoshima, C.; Nomura, H. "Structural changes in the calcium pump accompanying the dissociation of calcium," *Nature.* **2002**, *418*, 605-611.
- 8) Kobayashi, M.; Shoji, N.; Ohizumi, Y. "Gingerol, a novel cardiotonic agent, activates the Ca^{2+} -pumping ATPase in skeletal and cardiac sarcoplasmic reticulum," *Biochim. Biophys. Acta.* **1987**, *903*, 96-102.

- 9) Antipenko, A.Y.; Spielman, A.I.; Kirchberger, M.A. "Interactions of 6-gingerol and ellagic acid with the cardiac sarcoplasmic reticulum Ca^{2+} -ATPase," *J. Pharmacol. Exp. Therap.* **1999**, *290*, 227-234.
- 10) Maier, L.S.; Schwan, C.; Schillinger, W.; Minami, K.; Schutt, U.; Pieske, B. "Gingerol, isoproterenol and ouabain normalize impaired post-rest behavior but not force-frequency relation in failing human myocardium," *Cardiovasc. Res.* **2000**, *45*, 913-924.